Effects of Multiple Metal Oxides on Properties of ZTA-5TiO_2-5MgO Composites

A Dissertation Submitted in Partial Fulfillments of the

Requirements for the Degree of

DOCTOR OF PHILOSOPHY

in

APPLIED CHEMISTRY AND CHEMICAL ENGINEERING

by

MD. AL-AMIN

(Reg. No: 68/2018-19)

DEPARTMENT OF APPLIED CHEMISTRY AND CHEMICAL ENGINEERING

UNIVERSITY OF DHAKA

NOVEMBER, 2022

VALIDATION

The research work, 'Effects of Multiple Metal Oxides on Properties of ZTA-5TiO_2-5MgO Composites' has been jointly supervised under-

Research supervisors:

1.

Dr. Md. Zahangir Alam
Professor
Department of Applied Chemistry and Chemical Engineering
University of Dhaka, Dhaka 1000, Bangladesh.

2.

Dr. Abdul Gafur
Principal Scientific Officer
Pilot Plant and Process Development Centre
Bangladesh Council of Scientific and Industrial Research
Dhanmondi, Dhaka-1205, Bangladesh.

CANDIDATE'S DECLARATION

I, Md. Al-Amin, hereby declare that no portion of the work referred to in the thesis has been submitted in support of an application for another degree or diploma or qualification of this or any other university or institute of learning.

Md. Al-Amin
Registration No: 68/2018-19
Department of Applied Chemistry and Chemical Engineering
University of Dhaka, Dhaka-1000.

DEDICATED

To

My all-respected teachers

CERTIFICATE OF APPROVAL

Concerning this thesis entitled 'Effects of Multiple Metal Oxides on Properties of ZTA-5TiO_2-5MgO Composites' being submitted by Md. Al-Amin, Reg. No 68/2018-19, Department of Applied Chemistry and Chemical Engineering, University of Dhaka, has been accepted for satisfactory submission in partial fulfilment of the requirement for the degree of Doctor of Philosophy (PhD) in Applied Chemistry and Chemical Engineering. I certify that this is an original work of the author and carried out under my supervision and guidance. No part of this thesis has been submitted before to any other academic institution or university for the award of any other degree or diploma.

_____

Dr. Md. Zahangir Alam
Professor
Department of Applied Chemistry and Chemical Engineering
University of Dhaka, Dhaka-1000.

ACKNOWLEDGEMENTS

First and foremost, in a humble manner, I would like to wish all the praise to Allah, the almighty, who has blessed me with the ability to do my thesis work and has given me the courage, strength and time to do so.

Once, a wise guy stated, “A PhD is like a child”. From a crying, defenseless infant in its first year, to a youngster in its second year who isn't completely independent, and was almost an adult at the time of submission. And no matter where your research is in the process, you are passionate about it with a motherly (or fatherly) devotion, despite whatever dissatisfaction or tiredness you may have.

I would like to offer my sincere admiration to Dr. Md. Zahangir Alam, Professor, Department of Applied Chemistry and Chemical Engineering, University of Dhaka, who oversaw my PhD and offered me the chance to develop my professional life. Words are unable to adequately express how valuable your counsel was to me throughout these years. Your kindness and support always gave me the motivation I needed to get through the challenges. You were the one who allowed me to feel the yell and scream of excitement with each achievement. I appreciate you being the best boss ever and setting a great example.

To my honored co-supervisor Dr. Abdul Gafur, principal scientific officer, PP & PDC, BCSIR, Dhaka, I would really convey to extend my warmest respects, genuine gratitude, and best regards for all that he has done to help me friendly with this research. At each step of the planning process, he significantly contributed. I am incredibly appreciative that he let me do the research at his lab. This endeavor would not have been feasible without his direction and encouragement.

I want to express my appreciation for the academic cooperation and official support received from the faculty and staff at the university of Dhaka's department of Applied Chemistry and Chemical Engineering.

In particular, I want to thank Md. Rakibul Qadir, Sajib Aninda Dhar, and Md. Arifur Rahman Khan for their assistance with my XRD analysis and peak quantification, as well as Md.

Shofiqul Islam, SO, PP & PDC, BCSIR, for his grateful willingness to help on the AFM analysis.

I choose to express my thankfulness to the management and employees of PP & PDC, BCSIR, Dhaka, for their remarkable cooperation in enabling me to make use of the lab's resources.

My sincere gratitude is extended to Dr. Tania Hossain, a scientist at the Center for Advanced Research in Sciences (CARS), University of Dhaka, who assisted me with a cell viability test; to Md. Shahriar Bashar, PSO, IFRD, and Dipa Islam, SSO, BTRI, BCSIR, who provided kind assistance with imaging using a FESEM with EDS; and to Mohammad Zahirul Islam Mollah, PSO, BAEC for his admiring willingness to help me use gamma ray sterilization technique.

I appreciate my colleagues Md. Mahboob Ali Siddiqui, Shihab Uddin and Md. Kabir Hossain, whose helpful advice made my time conducting this research quite pleasant.

I am really indebted to BCSIR authority for offering the funding support to carry out the research.

Last but not least, I convey my heartfelt gratitude to my beloved family members for their love and support over the years. And to everyone else that I might have forgotten.

ABSTRACT

The aim of this thesis is to investigate the effects of different oxides on the properties of zirconia toughened alumina (ZTA) composites, for structural (cutting tool) and biomedical (dental and orthopedic implants) applications, through a powder mixing route, which allows tailoring the properties as well as compositions and sintering temperatures.

Alumina (Al_2O_3) is the most widely used ceramic oxide. It has several inherent properties like high hardness, elastic modulus, thermal and chemical stability and excellent wear and corrosion resistivity. It also shows outstanding biocompatibility. But the major drawback of alumina is its brittleness due to its lower fracture toughness value and its sintering temperature also high. To overcome the limitations of alumina, zirconia reinforced for increasing the toughness of alumina through stress induced transformation toughening mechanism.

Zirconia toughened alumina (ZTA) is the most promising advanced structural ceramics due to its superior mechanical properties such as high hardness, strength, fracture toughness, thermal and chemical stability as well as wear and corrosion resistivity. It has been considered as a very high-performance ceramic tool due to its diverse applications in structural, mechanical, electrical, biomedical and some other advanced engineering fields. The resistance to failure of ZTA is a great technical challenge for the researchers.

Previous researches focus on the addition of different oxides to zirconia toughened alumina (ZTA) for the improvement of different physical, microstructural and mechanical properties. Addition of titania (TiO_2) increases density and reduces sintering temperature. Addition of magnesia (MgO) increases stability and hardness through pinning effect. Addition of ceria (CeO_2) also increases stability and fracture toughness by forming cerium aluminate ($CeAl_{11}O_{18}$). Addition of calcia (CaO) increases fracture through forming elongated platelet shape hibonite ($CaAl_{12}O_{19}$) phase.

Addition of an individual oxide increases the specific mechanical, microstructural and physical properties of zirconia toughened alumina (ZTA). But overall mechanical properties of zirconia toughened alumina (ZTA) may be improved by adding more than one or multiple oxides. So, we have in vision to add more than two oxides in ZTA (zirconia toughened alumina) for getting the best mechanical as well as thermal properties.

In this research, ZTA with 15 wt.% zirconia (ZrO_2) and combined with equal (5 wt.%) amount of titania (TiO_2) and magnesia (MgO) were prepared by conventional pressure less sintering technique through simultaneously addition of calcia (CaO) and ceria (CeO_2) from 0-5 wt.% consecutively at 1400-1650°C for 3 hours. The raw materials were nano grade alpha alumina (α-Al_2O_3), 3 mol% yttria stabilized zirconia (3YSZ), titania (TiO_2), magnesia (MgO), ceria (CeO_2) and calcia (CaO) powders of high purity. Density, Vickers microhardness, Diametral tensile strength, Fracture toughness, Crystallite size, Cytotoxicity and Antimicrobial susceptibility test of the samples were performed.

Almost 95% of the theoretical density was obtained by this process. The Vickers microhardness value of around 11.72 GPa was also found for ZTA-5TiO_2-5MgO with 5 wt.% CeO_2 very close to higher density. The diametral tensile strength and fracture toughness value of around 125 MPa and 13.34 MPa.$m^{1/2}$ were achieved for ZTA-5TiO_2-5MgO and ZTA-5TiO_2-5MgO containing 5 wt.% CeO_2 and 3 wt.% CaO combinedly. Phase contents and identification were done by using X-ray diffractometer with rietveld refinement analysis. Surface morphology with roughness properties were observed by following FESEM and AFM techniques. To ensure biocompatibility, cell viability and antimicrobial susceptibility tests were carried out. The variations in mechanical properties as well as biocompatibilities of the samples with sintering temperature and composition were studied during this research.

Contents

List of Figures

List of Tables

List of Abbreviations

AZ	Alumina-Zirconia
ZTA	Zirconia Toughened Alumina
α-Al_2O_3	α-Alumina
t-ZrO_2	Tetragonal Zirconia
m-ZrO_2	Monoclinic Zirconia/Baddeleyite
3YSZ	3 mol% Yttria Stabilized Zirconia
MgO	Magnesia
TiO_2	Titania
CeO_2	Ceria
CaO	Calcia
TSM/SSS	Traditional Sintering Method/Single Step Sintering
TSSM	Two Step Sintering Method
SPS	Spark Plasma Sintering
HP	Hot Pressing
HIP	Hot Isostatic Pressing
CIP	Cold Isostatic Pressing
AFM	Atomic Force Microscopy
PSZ	Partially Stabilized Zirconia
TZP	Tetragonal Zirconia Polycrystal
FSZ	Fully Stabilized Zirconia
CSZ	Cubic Stabilized Zirconia
8YSZ	8 mol% Yttria Stabilized Zirconia
9YSZ	9 mol% Yttria Stabilized Zirconia
YTZP	Yttria stabilized Tetragonal Zirconia Polycrystal
TMA	Thermo-Mechanical Analyzer
XRF	Xray Fluorescence
XRD	Xray Diffraction
FESEM	Field Emission Scanning Electron Spectroscope
EDS	Energy Dispersive Spectroscopy
TEM	Transmission Electron Microscope

DSC	Differential Scanning Calorimetry
TGA	Thermo Gravimetric Analysis
HDPE	High Density Poly Ethylene
EG	Ethylene Glycol
CTE	Coefficient of Thermal Expansion
$t \rightarrow m$	Tetragonal to Monoclinic
Ts	Sintering Temperature
wt.%	Weight Percentage
vol.%	Volume Percentage
PVA	Poly Vinyl Alcohol
MPa	Mega Pascal
GPa	Giga Pascal
Hv	Vickers hardness
K_{IC}	Fracture Toughness
ρ	Density
P	Porosity
E	Elastic Modulus
DTS	Diametral Tensile Strength
THR	Total Hip Replacement
DMEM	Dulbecco's Modified Eagles' Medium
ZOI	Zone Of Inhibition
GPLs	Graphene Platelets

INTRODUCTION

CHAPTER 1
INTRODUCTION

1.1 Background

Ceramics have been used in human history since an ancient period and has been provided a vital contribution for the improvement of human civilization. Generally, ceramics are solid crystalline inorganic materials containing different oxides, carbides, nitrides, borides having important physical, structural, mechanical, biomedical, thermal and electronic properties. Almost all the ceramic materials have covalent and ionic bonding which ensures improved high temperature properties like high melting point, thermal and chemical stability, strength and corrosion resistivity at high temperature, etc. The improved high temperature mechanical properties, coupled with high wear and chemical resistance makes it a material of choice for many advanced and engineering applications such as cutting tool inserts, ceramic bearings and grinding media, automobile parts (engine components), aerospace turbine blades, radomes for missiles, space shuttle tiles, ceramic armors (bullet resisting vest), orthopedic and dental implants, etc. [1]. However, low fracture toughness makes ceramics use limited for many advanced engineering applications [2, 3, 4]. Numerous research works and efforts have been done to reduce the brittleness of ceramics. Among these, composite materials have been found to be the most successful in overcoming the limitations of the ceramics.

Out of the oxide ceramic composites, zirconia toughened alumina ceramics have drawn the most attention because of their superior mechanical and thermal properties, including high strength, fracture toughness, chemical and thermal stability, hardness, and many others. Low fracture toughness and a high sintering temperature are the main limitations of alumina (Al_2O_3) based ceramics. Even though ZTA is frequently used in structural, mechanical, and biomedical applications, its lower fracture toughness causes an intriguing design challenge that was overcome by modifying the synthesis process, adding oxides, and other factors [5]. ZTA's properties can be improved to become a high-performance technical ceramic through proper engineering and modulation [6].

Zirconia grains are interspersed throughout the alumina-based ZTA matrix. To increase the matrix alumina fracture toughness and other mechanical properties, zirconia phase is added [7, 8]. For zirconia, there are three crystallographic phases: cubic, tetragonal, and monoclinic. Tetragonal zirconia has the best mechanical properties of all of them. But, at an ambient

temperature, t-ZrO_2 is unstable in nature [9]. For boosting the volume percentage of tetragonal zirconia on ZTA matrix, stabilizers are added. Yttria-stabilized zirconia (YSZ) is the most common stabilizer for ZTA ceramic composites. Additionally, MgO, CaO, or CeO_2 can be added to stabilize zirconia [10, 11, 12]. The lattice parameter or thermal characteristics of ceramic composites may also be modified by the presence of certain materials. The inclusion of specific materials in their ionic form might cause either a cation vacancy or an anion vacancy, which has the effect of the properties of ZTA.

By adding specific inclusions, some toughening mechanisms are triggered. Zirconia is capable of microcrack toughening and stress induced transformation toughening, which contribute to increasing ZTA's toughness [13, 14]. The crystal structures of strontium hexa-aluminate as well as calcium hexa-aluminate resemble each other and platelets in shape. Such materials can be added to provide crack deflection and crack bridging toughening mechanisms [15]. Hardness can also be increased by adding specific materials like Cr_2O_3 with ZTA matrix [16]. The capability to engineer the grain boundary is another notable effect of inclusions. Some oxides, such ZrO_2 and MgO, are capable of refining grains [17]. Additionally, the particle size and porosity are linked to the grain boundary effect as well. The pore growth may be decreased by some additives, and others may have unique morphologies that enable the blockage of cracks.

ZTA's surface hardness can also be modified using some additives. The inclusion of certain materials may improve the pinning effect, which contributes to value enhence [17]. The phases that are present because of the inclusions can be found using XRD and Rietveld analyses. Structural, mechanical and morphological properties of zirconia toughened alumina is significantly impacted by the existing phases in the composites. Some inclusions, when introduced in a specific amount, may boost or just decrease certain mechanical properties.

Compared to traditional ceramics, ZTA ceramics have superior mechanical properties, which give them a huge potential increase. ZTA is considered a great engineering choice when taking manufacturing costs into account due to availability of alumina which is the base element of ZTA and extremely cheap relative to other materials. Usually, the manufacturing processes used in ZTA ceramics, such as solid-state sintering, chemical methods like sol-gel, and co-precipitation, are comparatively more economic than the highly sophisticated sample processing techniques used for other technical

ceramic composites. ZTA enhances competitive fracture toughness in contrast to other advance ceramics in terms of mechanical properties. Despite it has an inherently lower Vickers Microhardness than other advance ceramics, yet it is still considered to support a wide range of applications.

Due to its diverse applications, ZTA is a particularly fascinating research topic. It can be used for conventional purposes like cutting tools and structural ceramic. It also has tremendous promise as a biomedical implant. Almost all of the ZTA ceramics are bioinert, although the addition of other oxides may alter this behavior. The lack of a thorough investigation of the effects of various additives and the resulting property upgrades is what led to the selection of this material. Different metallic oxides could be added for greatly improve the mechanical characteristics. Out of the superior properties, low fracture toughness of modern ZTA ceramics is one of their main flaws. The right selection of additives can considerably improve the ZTA toughness. But, to assess the perspective of this composite materials, a wholistically studied literature is needed specially in case of design problems.

The modification and trend of change in the mechanical properties of ZTA due to various oxide inclusions will be the main focus of this thesis. There is a lot of discussion about the effects of additives like MgO, TiO_2, CeO_2, and CaO. This study objectives are to determine how inclusions effect the ZTA, so that it can be developed for the optimal attributes.

1.2 Research objectives with specific aims

Research goals with specific aims are mentioned as follows:

- Fabrication of alumina-zirconia (AZ) ceramic composites using different wt.% of metal oxides such as TiO_2, MgO, CeO_2 and CaO.
- To investigate the properties of ZTA-5TiO_2-5MgO ceramic composites for the inclusion of CaO and CeO_2 simultaneously.
- To find out the optimum composition and sintering temperature for achieving best physical, mechanical, and microstructural properties.
- Correlate the microstructure with different mechanical properties like fracture toughness, strength, hardness, porosity and density etc.

- To study the morphology of the particles and its behavior with respect to composition and sintering temperature.
- To analyze the phase content and its crystallite size after sintering.
- To study the biocompatibility of the composites.
- To obtain coefficient of thermal expansion and variation with respect to composition and sintering temperature.

1.3 Chapter summary

The thesis is composed of five themed chapters which are shortly listed as following:

Chapter 1 of this thesis dealt with the background of the research, objectives, and outline of the thesis paper.

Chapter 2 discussed the literature review along with a brief summary of the recent development of alumina-based composites.

Chapter 3 described the sample preparation technique and different characterization techniques required for analyzing sintered composites.

Chapter 4 presented the results and discussion of the characterizations that were done on the sintered body as-prepared.

Chapter 5 revealed the significances of the concluding remarks and the recommendations for future work.

LITERATUTE REVIEW

CHAPTER 2
LITERATURE REVIEW

2.1 Introduction of Al_2O_3 and 3 mol% Yttria Stabilized Zirconia

Alumina (Al_2O_3): Aluminum oxide is also known as α-alumina or alumina or corundum in the crystalline form. Alumina that has Cr_2O_3 impurities in nature is known as Ruby, and alumina that has titanium impurities in nature is known as Sapphire [18]. A common explanation for the crystal structure is that the Al^{3+} cations fill two thirds of the octahedral interstices while the O^{2-} anions are arranged in an almost hexagonal close-packed pattern. These ions (Al^{3+}, O^{2-}) have comparatively increased mobility at the elevated temperatures [19]; so, alumina is easily sintered. **Figure 2.1** shows the crystal structure of corundum.

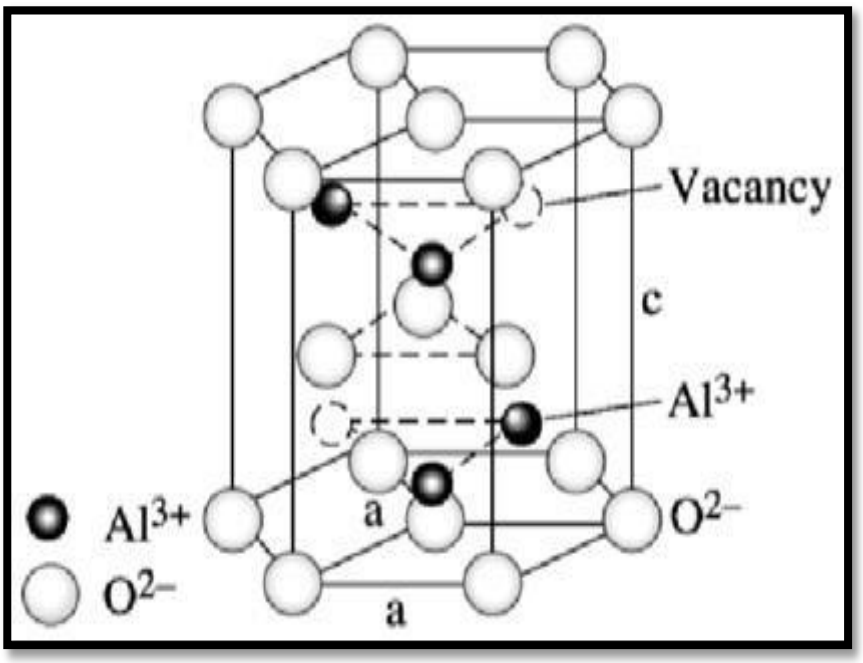

Figure 2.1 Crystal structure of corundum (α-Al_2O_3).

Alumina was initially used as a biomaterial in 1930 and was given a patent by Rock in Germany [20]. The first generation of alumina hip joint ceramics were introduced in 1970, and Professor Bautin in France started using ceramic components in joint replacement surgery by swapping out the conventional metal femoral heads with alumina. However, these early ceramics were more prone to fracture because of their low density and poor microstructure [20]. With time came second-generation alumina components that performed better than the previous

generation, because to advancements in material quality, processing methods, and ceramic design knowledge. Lastly, the third generation of alumina maintained the pattern of lowering particle size and raising density.

One of the most stable oxides, alumina can withstand harsh acidic or alkaline conditions under high temperatures [21]. Alumina has a high compressive strength but, like most ceramics, has a low tensile strength since it is naturally brittle, and once a crack begins to form, it spreads quickly (low toughness). Density and mechanical strength are tightly correlated, with higher density resulting in higher strength. By employing high-purity alumina, the mean grain size must be kept low and a glassy phase at the grain boundaries must be avoided. The femoral heads and cups are less likely to wear thanks to the high hardness of alumina, which also allows for better surface quality.

Despite the positive mechanical properties listed above, alumina has a poor fracture toughness (~ 4 $MPa.m^{1/2}$) and is susceptible to failure at stresses below the maximum fracture strength due to slow crack development [22]. As a result, alumina can only be used for a specific kind of prosthetic design. For instance, to reduce the probability of failure in vivo, alumina ball heads should have a diameter greater than 28 mm [22].

Dr. Sami Sandhaus, who discovered the application of polycrystalline alumina in complete medical devices, the CBS dental implant, was the one who first introduced alumina to the dental device industry [23]. Alumina has a number of design flaws, including stiffness, poor flexural strength, fracture toughness, and faults that occurred during surface grinding, in addition to the good benefits of aesthetics and biocompatibility, which have led to failures on these devices [23].

Yttria Stabilized Zirconia (YSZ):

Zirconia possesses good mechanical properties like high tensile strength, high fracture toughness, hardness and corrosion resistance. A zirconium oxide-based ceramic called yttria-stabilized zirconia which is stabilized at ambient temperature by the addition of yttrium oxide to a particular zirconium oxide crystal structure. Crystal structures of yttria, zirconia and yttria stabilized zirconia are presented in **Figure 2.2**.

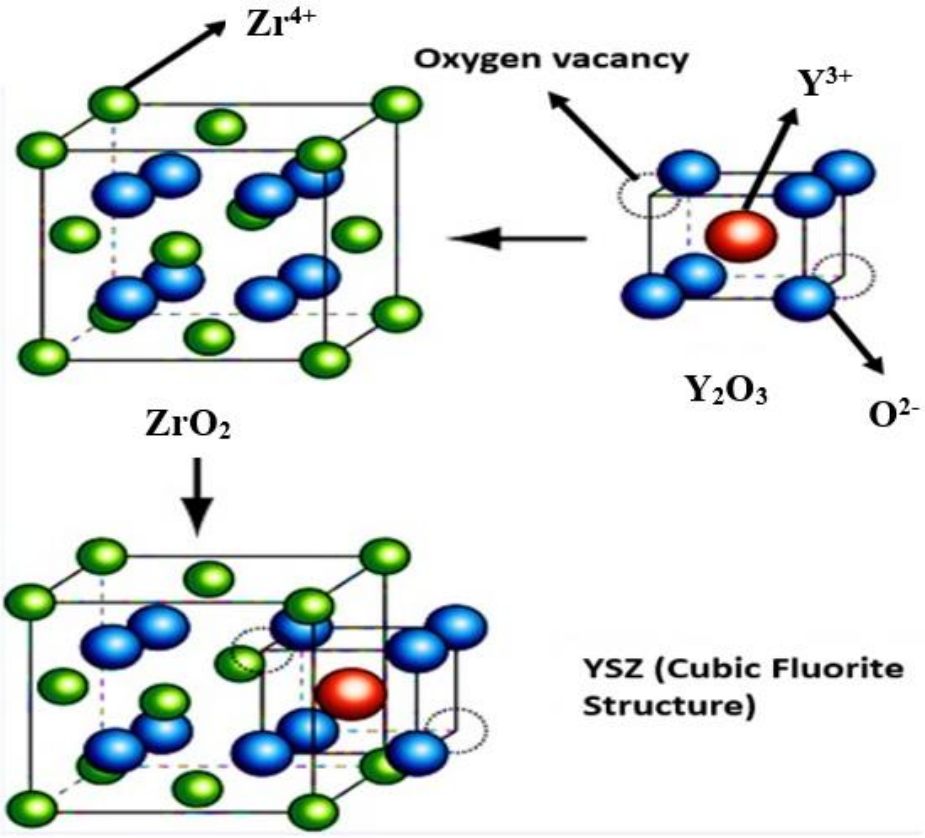

Figure 2.2 Crystal structures of yttria, zirconia and yttria stabilized zirconia.

With increasing temperature, pure zirconium oxide goes through a phase transition from monoclinic to tetragonal, subsequently to cubic which is shown in **Figure 2.3**.

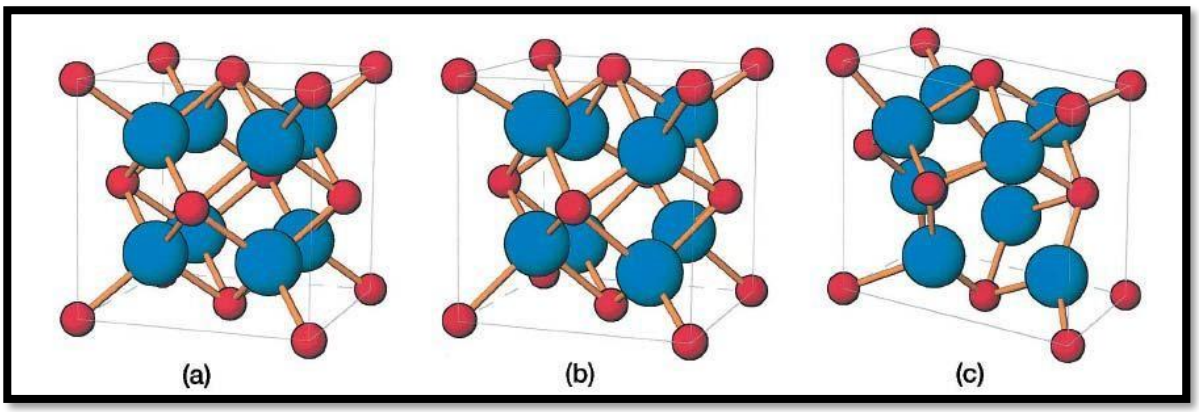

Figure 2.3 Zirconia crystal structure for (a) cubic, (b) tetragonal, and (c) monoclinic. The blue circles represent O atoms and red circles represent Zr atoms [24].

Because of the significant volume change that occurs when a material changes from tetragonal to monoclinic (approximately 3-5 percent), it is challenging to produce ceramic goods made of stable sintered zirconia [25, 26]. By replacing some of the Zr^{4+} ions (ionic radius of 0.82 Å) in the crystal lattice with slightly bigger ions, such as those of Y^{3+} (ionic radius of 0.96 Å), To stabilize the cubic polymorph of zirconia, a wide temperature range is required. Consequently, doped material made of zirconia is known as stabilized zirconia. The Y_2O_3-ZrO_2 phase diagram is depicted in **Figure 2.4**.

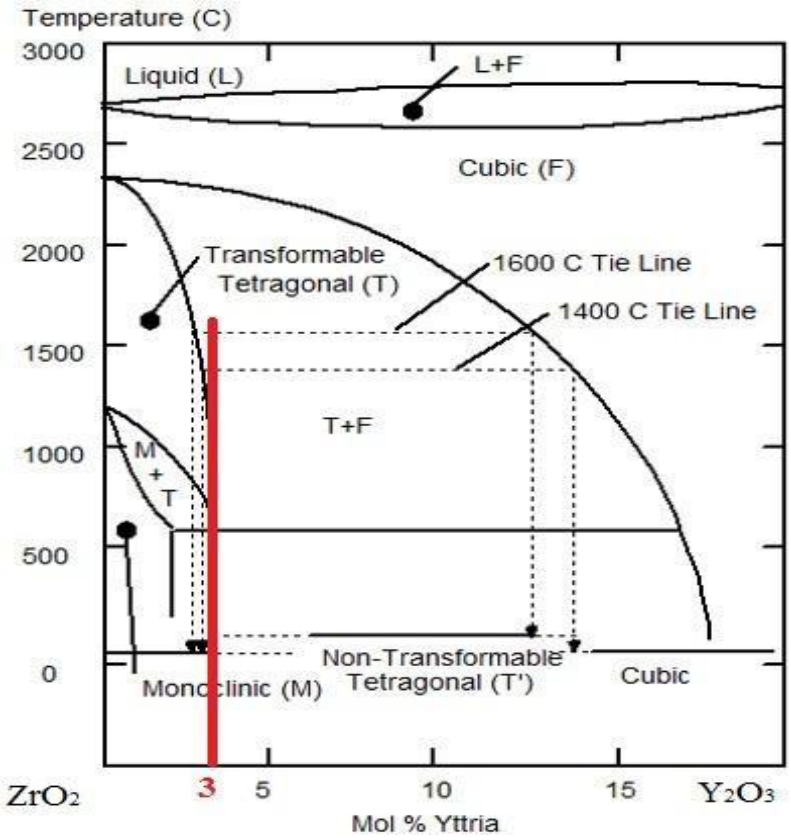

Figure 2.4 Phase transition graph of Y_2O_3-ZrO_2 [27, 28].

Zirconia can be modified with trivalent ions to stabilize it at high temperatures and at normal temperature. These modifications are significant enough to prevent the pure material from being used in applications that need a complete solid structure by correlating volume changes during cooling [29]. Full stabilization necessitates a considerable dose of dopant, 8 mol percent in the case of Y_2O_3, and depending on the necessary characteristics, partial stabilization occurs

at 2 to 5 percent [30, 31]. Combining fracture toughness and sintered compact density and the stabilizer content both affected the crucial tetragonal zirconia grain size. According to the amount of yttrium content in the sample, there is a critical granular size, must be reached for any spontaneous tetragonal to monoclinic grain transformation to take place, even though an overly fine structure or small particle size would prevent the transformation.

Due to its exceptional durability, tetragonal polymorph is employed as a high-performance structural ceramic in products like dental crowns and jet engines [32]. Because of the high oxygen vacancy content, which grows with temperature, cubic polymorph is able to conduct oxygen ions. Because of this property, cubic polymorph can be utilized for making solid oxide fuel cells as well as an Oxygen sensor [33]. **Figure 2.5** presents the Alumina-Zirconia (AZ) system's phase transition graph.

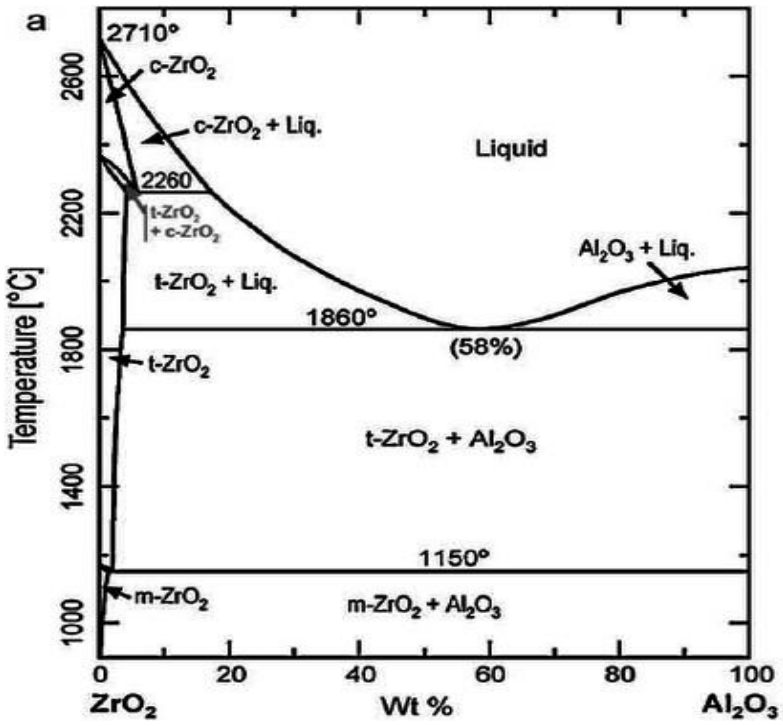

Figure 2.5 Alumina-Zirconia binary system phase transition graph [34].

The equilibrium phase diagram of the Al_2O_3-ZrO_2 system demonstrates that during the heating and cooling process, both ZrO_2's phase transformations (monoclinic, tetragonal, and cubic phase) and Al_2O_3-ZrO_2's eutectic transformation exist. Al_2O_3 has a lower density than that of ZrO_2 . The pure Al_2O_3 becomes denser when ZrO_2 is added. Additionally, the total miscibility

of ZrO_2 and Al_2O_3 in a liquid state helps to improve the density of the Al_2O_3-ZrO_2 composite. **Figure 2.5** demonstrates that a eutectic transition with a composition of roughly 58 percent alumina takes place at 1860°C. After cooling, at the eutectoid temperature of 2260°C, cubic zirconia transforms into the tetragonal zirconia crystal structure and followed into monoclinic zirconia crystal structure at 1150°C with alumina matrix as well [35]. Zirconia into solid alumina has an extremely low solubility limit (less than 2%), and alumina into solid zirconia is nearly nonexistent, but alumina and zirconia exhibit perfect miscibility in the liquid state. Considering the equilibrium phase diagrams shown in various previous works, the solubility of zirconia into solid alumina may reach 5% [36]. Amorphous phase development during rapid solidification is known to be maximized by such limited solubility in the solid state.

2.2 Physical Properties of Al_2O_3 and Zirconia Stabilized with Yttria at 3 mol% (3YSZ)

Typical mechanical and thermal properties of alumina (Al_2O_3) and 3 mol% yttria stabilized zirconia measured through powder compaction method by earlier researchers are summarized in **Table 2.1**.

Table 2.1 Typical physical properties of alumina (Al_2O_3) and 3 mol% yttria stabilized zirconia (3YSZ).

Physical Properties	**Al_2O_3**	**3YSZ**
Density (g/cm^3)	3.97	6.10
Melting Point (°C)	2054	2750
Hardness (GPa)	20.45	13.73
Tensile Strength (MPa)	300-900	210-1400
Modulus of Elasticity (GPa)	370	205
Flexural Strength (MPa)	400	800
Fracture Toughness ($MPam^{½}$)	3-4	9.5
Thermal Conductivity (W/mK)	30	2
CTE, 25-1000°C (~X 10^{-6}/°C)	8.2	10
Maximum Service Temperature (°C)	1750	1000
Thermal Shock Resistance (ΔT)	<300	250

2.3 Alumina Composites: A Literature Review

There is a lot of literature available about composites made of alumina (Al_2O_3). Each study has shown the formation of various opposing themes. The toughening mechanism of composites made of alumina is a topic that is addressed in a comparatively modest amount of literature. Over the past 20 years, a considerable data has become accessible about the toughening mechanism of composites made of Al_2O_3. To get superior qualities, researchers looked at the effects of various chemicals. This section's goal is to study current works on composites made of alumina. Few relevant reviews are noted as follows:

2.3.1 Yttria stabilized zirconia (YSZ) added Al_2O_3 composites

Among others, the first study on Alumina-Zirconia (AZ) system was done by Claussen N. [37]. The fracture toughness values of Claussen's hot-pressed composites, which contained 15 vol.% ZrO_2, were 10 $MN/m^{3/2}$, which was twice as high as the $A1_2O_3$ matrix. His research showed that adding small amount of monoclinic ZrO_2 particles significantly increases the fracture toughness of Al_2O_3. It was assumed that the final sample would have a high density of small matrix microcracks that would slowly propagate and absorb energy. The expansion of ZrO_2 during the tetragonal to monoclinic transformation produced the resulting microcracks.

According to Bronsnan et al. study, microwave sintering of Al_2O_3 ceramic specimens led to a reduction in processing time and sintering temperature [38]. At 1700°C for only 15 minutes, the Al_2O_3-ZrO_2 nanocomposite specimens were microwave sintered which obtained 99% of relative density as well as homogeneous microstructures with no discernible phase development.

In an experiment, Moraes et al. fabricated an alumina composite that contained 80% Al_2O_3 and 20% 3YSZ, and they found that the fracture toughness was around 7.4 $MPa.m^{1/2}$ [39]. The green sample was hot pressed after the air sintering took place for two hours at 1600°C in a muffle furnace. They discovered higher values of fracture toughness through thermal treatments of the composites resulting the expansion of grain sizes of zirconia particles and alumina matrix. They established that, when compared to pure alumina ceramics, a composite can improve about 90% of flexural strength as well as 29% of fracture resistance.

Sug Won et al. did an experiment using a new technique for the manufacture of nanostructured alumina with 3YSZ (20 vol.%) [40]. High-frequency induction heating was used to sinter composites. After sintering at 1370°C, the composites' relative density was increased to more than 99 percent of their theoretical density. The fracture toughness and hardness values were 5.05 $MPa.m^{1/2}$ and 17 GPa. The outcomes demonstrated that high-frequency induction heating sintering considered as promising technique that producing nanoceramic composites with very little amount of time as well as at a considerably reduced temperature.

Ahmad et al. provided an important investigation and debate on the Al_2O_3-YSZ composites [41]. They demonstrated how the weight percentage of YSZ additions affected the microstructures of Al_2O_3-YSZ for cutting inserts. The microstructures had a significant impact on the cutting inserts mechanical properties like Vickers hardness, wear resistance and fracture toughness. For 20 weight percent of YSZ added Alumina, the fracture toughness was 4.5 $MPa.m^{1/2}$, the minimal wear area was also demonstrated, and the maximum hardness was approximately 16 GPa. Although the cutting inserts fracture toughness increased up to 60 weight percent YSZ, the inserts Vickers hardness showed a tendency to decline as YSZ addition increased. They came to conclusion that, a polished samples microstructure began to show microcracks and create larger YSZ grain sizes above 60 wt. percent, which made it difficult for the transformation toughening mechanism to work properly.

Rejab et al. state that the microstructure that contains elongated grains force a crack to propagate in multiple planes before encircling the grain in an intergranular mode [42]. Furthermore, in the microstructure, more energy is needed for inter-granular fracture via the elongated grains than for trans-granular fracture over the flat platelets. They therefore demonstrated a correlation between the number of elongated grains and fracture toughness, with a higher quantity of elongated grains resulting in a higher fracture toughness property.

In a series of simulated experiments, Rittidech et al. investigated the effects of Y_2O_3 additions ranging from 1 to 8 wt.% on phase formation and fracture toughness of Al_2O_3-ZrO_2-Y_2O_3 (AZY) composites [43]. It was discovered that Y_2O_3 concentrations had little effect on the grain structure of Al_2O_3-ZrO_2-Y_2O_3 composites. Maximum fracture toughness of the composite was attained at 4.827 $MPa.m^{1/2}$ when the Y_2O_3 content was 4 wt.%. They demonstrated how more Y_2O_3 caused the t-ZrO_2 phase to entirely convert into the m-ZrO_2 phase, which was crucial in increasing fracture toughness.

According to S.M. Naga et al., nano-size Ta^{5+} ions improved cohesiveness of grains, that caused hardness property to increase [44]. On the other hand, internal tension was induced into the body due to variations of the body's components in terms of thermal expansion coefficients (CTE). This increases the composites Vickers hardness. The sample's ability to withstand fracture became more resilient as the Ta_2O_5 level rose. They stated that a tiny number of weak interfaces were produced as a result of the nano-sized Ta^{5+} ions that were present at surface boundaries of particles. From their experiment, they found that the mutual presence of interfaces (both strong and weak) caused the toughening methods of various types including crack bridging, crack branching, crack deflection, and micro cracking to interact synergistically. This, in turn, increased the transformability of t-ZrO_2 to m-ZrO_2 when Ta_2O_5 was added in the amount of 0.12 vol%. Zirconia particle transformability was lowered by additional Ta_2O_5 addition. When only 0.36 vol.% Ta_2O_5 was present, the fracture toughness value of ZTA was obtained at 7.19 $MPa.m^{1/2}$, which was 38.27% higher than that of undoped ZTA which was found in 5.2 $MPa.m^{1/2}$. The primary element that boosted the fracture toughness may be the plate-like structure of Al_2O_3.

Gafur et al. study on Al_2O_3-YSZ composites is the most recent [45]. For the composite that contained 5 vol.% ZrO_2, they were able to obtain a value 17.46 GPa as the maximum micro-hardness, and for the composite that contained 20 vol.% 3Y-ZrO_2, they were able to achieve a fracture toughness value of 10.33 $MPa.m^{1/2}$. As a sintering aid, they utilized a little quantity of MgO. The composites were fired at 1580°C in an ambient atmosphere for two hrs. A disagreement with the earlier findings from other authors because no one else was able to generate composites made of Al_2O_3 and YSZ with such high fracture toughness. They came to the conclusion that the stress necessary for transformation in the high stress region surrounding a crack tip may be larger than the fracture stress if the tetragonal phase is excessively stable. They came to the conclusion that the composite will have poor fracture toughness, similar to Al_2O_3.

High purity, low-temperature sinter enable Al_2O_3 powder combined with precipitated $Zr(OH)_4$ gel has been examined by Rao et al. [46]. The resulting gel combination underwent a two-hour calcination at 600°C. The composites of Al_2O_3 and ZrO_2 were sintered for two hours at normal atmosphere and temperature between 1350 and 1500°C. Al_2O_3-15 wt.% ZrO_2 composites sintered at 1425°C achieved about full densifications as well as maximum flexural strength of

932 MPa, whilst the best fracture toughness of 8.5 $MPa.m^{1/2}$ was obtained after sintering at 1475°C.

Al_2O_3-ZrO_2 composites made from sol-gel method have been subjected to pressureless sintering research by Jayaseelan et al. [47]. By using the sol-gel method, composites of Al_2O_3 and ZrO_2 (pure ZrO_2, ZrO_2 stabilized by ceria at 12 mol%, and ZrO_2 stabilized by yttria at 3 mol%) containing 5-25 vol% ZrO_2 maintained consecutively interval 5 vol% have been prepared. Applying pressureless sintering, at 1530°C, all the samples were fired for 3 hours, producing up to 99.8% of the composite's theoretical density.

The impact of sintering time on several ZrO_2 based ZTA composites has been researched by Daguano et al. [48]. In their research, the effect of sintering time on the characteristics of a composite ZrO_2-Al_2O_3 material comprising 20 wt.% Al_2O_3 was examined. The ceramic composites were fabricated by sintering in the air at 1600°C for 0 to 1440 minutes. With hardness values between 1500 HV (120 min) and 1310 HV (1440 min) and a fracture toughness of 8 $MPa.m^{1/2}$ after sintering at 1600°C, the material proved to depend on sintering duration, making it ideal for biological applications like dental implants.

A non-destructive method called impedance spectroscopy that showed to be sensitive to the microstructure of the composite, was used by Fortulan et al. to study the Al_2O_3-ZrO_2 composite [49]. The observed decrease in the conductivities of ZrO_2 grains along with grain borders indicates compression of ZrO_2 grains by the alumina matrix. With a drop in ZrO_2 content in the composite, this effect grew stronger. Composites that were over percolation limit were measured through vacancy conduction of ZrO_2 particles. On that composite conduction, the impact of densification and grain growth was measured. It was discovered that the variations in the specific conductivities of the ZrO_2 grain and grain boundaries were connected.

Cecilia et al. examined the mechanical characteristics of Al_2O_3-ZrO_2 composites with varying ZrO_2 contents (5-80 wt.%) [50]. When compared to pure Al_2O_3 ceramics, these systems have an increase in fracture toughness of 29% and a 93% increase in flexural strength. These findings demonstrated that ceramic abutments components might be made ready for dental implants-based prosthetic rehabilitations.

According to Sarkar et al., a wet interaction procedure using sol-gel method was applied for preparing an Al_2O_3-ZrO_2 composite containing 5 mol percent ZrO_2 [51]. The hydrogel was made, aged at room temperature for optimal development and orientation, and then to lessen agglomeration, low temperature drying was used. The precursor powder of sol-gel was accurately described by measuring the surface area, particle size, and performing a thermal analysis. Cold isostatic pressing was used to produce the nano powder, with a maximum densification of 98.4% reached at 1550°C, in which the sintering behavior was examined. The t-ZrO_2 to m-ZrO_2 transformation was related with cracks propagating along the grain boundaries during Vickers indentation with a 5 kg load, which shattered the ZrO_2 particles.

2.3.2 TiO_2, Nb_2O_5, and La_2O_3 added Al_2O_3 composites

According to Wang et al., Al_2TiO_5 phase was found in the grain boundaries or at the triple junctions, as well as their availability was confirmed through x-ray diffractometer (XRD) examination [52]. The growth of elongated Al_2TiO_5 grains was facilitated by the presence of TiO_2. Despite lowering the hardness value, the development of the elongated grains had a significant impact on the material's fracture toughness. According to a study by Chen et al., the trend of microstructure traits was slightly different [53]. In that study, they established that as TiO_2 concentrations increased from 1-8 wt.%, respectively, grain size increased as well as elongated alumina grains declined. However, since spark plasma-sintering have employed this work, it could have an impact on the behavior of grain development.

By using microwave sintering techniques, Yun-Long AI et al. fabricated an alumina composite with Nb_2O_5 and La_2O_3 [54]. The fracture toughness of that alumina ceramic composite was about 70% greater compared to monolithic alumina ceramic, according to their report. The composite with the outstanding mechanical characteristics having hardness of 12.6 GPa and fracture toughness of 6.3 $MPa.m^{1/2}$ at 1500°C was made using 5% Nb_2O_5, 7.5 wt.% La_2O_3, and 82.5 wt.% Al_2O_3. They indicated that the domain switching of $LaNbO_4$ and plate-like $LaAl_{11}O_{18}$ grains increased the fracture resistance and flexural strength of Al_2O_3 up to a certain limit and thereafter declined. However, as $LaNbO_4$ volume friction increased, the composite of $5Nb_2O_7$-$7.5La_2O_3$-Al_2O_3 fracture toughness decreased.

Changhong and Yunlong took a broader viewpoint; they claimed and demonstrated that the fracture toughness was attained 6.48 $MPa.m^{1/2}$ for 15% Nb_2O_5, which was marginally higher

than previous experiment [55]. They synthesized an Al_2O_3 composite with 15% Nb_2O_5 and 7.5% La_2O_3 (vol.%) applying microwave sintering type in half an hour as well as maintained firing temperature just 1550°C. During the analysis of the $15Nb_2O_7$-$7.5La_2O_3$-Al_2O_3 composite, they came to the conclusion that the Nb_2O_5 that was left over after the reaction had turned to liquid, aiding for enhancement of Al_2O_3 columnar grains and densification for firing. In place of equiaxial Al_2O_3 grains, more and more columnar grains began to grow as the sintering temperature increased. As a result of the growth of the grains in columnar shape, and declined length fracture toughness.

Hassan et al. on the contemporary period, used pressure-less sintering technique at 1650°C to create a composite of Al_2O_3 with 5 wt.% ZrO_2 and 0.6 wt.% Nb_2O_5 [56]. They came to an accord with Kim et al. after discovering that the hardness and fracture toughness values were 17.92 GPa and 6.19 $MPa.m^{1/2}$, respectively [57]. According to their justification, the inclusion of pentavalent oxides, such as Nb_2O_5 and Ta_2O_5, increases the transformability of t→m and m→t ZrO_2 phase transitions, which is why the augmentation in fracture toughness with the rise in Nb_2O_5 content happened. Another factor contributing to the greater fracture toughness may be the stabilized ZrO_2 powder utilized, which contains 5 mol% Y_2O_3.

Report obtained from Y. WU et al. that, Al_2O_3 with 25 vol.% $LaAl_{11}O_{18}$ composites were made by pressure-less sintering at 1550°C using composite powders formed by coprecipitated technique, provided an important study and discussion on the topic [58]. The composites fracture toughness was 4.3 $MPa.m^{1/2}$, and the results demonstrated that $LaAl_{11}O_{18}$ grains inhibited the growth of Al_2O_3 grains while the rodlike grains enhanced the composite Al_2O_3-$LaAl_{11}O_{18}$ fracture toughness. Both Kern and Negahdari et al. expressed agreement with the earlier findings [59, 60]. They demonstrated how at low sintering temperatures, the existence of the cylindrical shaped particles improves the process of sintering. The composites, according to their claims, demonstrated excellent bending and fracture strengths as well as great resistance to subcritical cracks growth. They also came to the conclusion that $LaAl_{11}O_{18}$ boosts the fracture toughness and lowers the temperature for firing of ZTA composites. The preparation of pure $LaAl_{11}O_{18}$ phase at lower temperatures by the calcinations of La_2O_3 and Al_2O_3 or the reaction of $Al(OH)_3$ and $La(NO_3)_3.6H_2O$, however, has been reported to be challenging by numerous authors. According to Negahdari et al., the reason why the hardness of Al_2O_3-$LaAl_{11}O_{18}$ composites was raised up to 20 vol percent $LaAl_{11}O_{18}$ is because $LaAl_{11}O_{18}$

inhibits the formation of alumina grains [60]. The further increase in $LaAl_{11}O_{18}$ can be explained to the apparent porosity rises and relative density declines. The behavior described above was comparable to that of Kern's 12Ce-TZP composites reinforced with in situ produced Lanthanum hexa-aluminate [59].

To make monolithic alumina more resistant to fracture, Ceylan and Fuierer pointed out some of the methods for creating a multilayer composite of lanthanum titanate ($La_2Ti_2O_7$) and α-Alumina (α-Al_2O_3) [61]. The composites were made using two diametrically opposed processing techniques. First, stacks of individually pre-sintered $La_2Ti_2O_7$ and α-Al_2O_3 pellets were hot-forged together. Second, dense α-Al_2O_3 and tape cast molten salt $La_2Ti_2O_7$ were assembled and hot forged. An interphase of Aluminum Titanate (Al_2TiO_5) was discovered to occur during the hot-forging process as a result of the reaction between α-Al_2O_3 and $La_2Ti_2O_7$. The resulting laminate composites flexural strength and fracture toughness were determined to be 320 MPa and 7.1 MPa.$m^{1/2}$, respectively.

With TiO_2 as an addition, S. A. Dhar et al. changed the structural as well as mechanical properties for ZTA ceramic, that have made via a solid-sintering method. Samples were sintered at 1600°C for 1 hour in a pressure less environment for different wt.% of TiO_2 (i.e., 0 wt.%, 2 wt.%, 3 wt.%, 4 wt.%, 6 wt.%, and 8 wt.%) [62]. Flexural strength, fracture toughness, and hardness were discovered to have steadily grown with the addition of TiO_2, reaching their maximum value at 4 wt.%, before decreasing with the addition of TiO_2. Adding 4 wt.% TiO_2 greatly slowed down the growth of Al_2O_3 grains, but adding more TiO_2 caused the grains to grow larger, according to scanning electron microscopy. Due to the fine microstructure, hardness and bulk density have also increased from 0 to 4 wt.%, improving the materials characteristics.

2.3.3 MgO added Al_2O_3 composites

Rejab et al. evaluated the impact of MgO addition on ZTA-CeO_2 ceramic composite parameters such as density, firing shrinkage, microstructure, Vickers hardness, and fracture toughness [63]. MgO was added in varying amounts, ranging from 0 to 2 wt.%. The Vickers indentation method was used to determine the Vickers hardness and fracture toughness of the sintered samples. According to the SEM microstructures, the $MgAl_{11}CeO_{19}$ elongated secondary phase began to form at 0.5 wt.% magnesia. This elongated phase was played vital role for increased fracture resistance of ceramic composites. Similar to this, an additional

secondary phase spinel ($MgAl_2O_4$) was formed when more than 0.5 wt.% of MgO was added, as shown by XRD. It has been established that this phase has poor intrinsic fracture toughness. As a result, the sample with 0.5 wt.% MgO showed the best qualities with the highest Vickers hardness as well as fracture toughness properties.

Similar tests were conducted by Wang et al. in the 1980s to demonstrate the ceramic system contained Al_2O_3-MgO has greater the typical values of Vickers hardness than the traditional ceramic system of Al_2O_3, since alumina's capacity to sinter and reduce particle size are both improved by MgO [64]. Nearly 20 years later, Chakravarty et al. prepared a composite system made of Alumina-Magnesia (Al_2O_3-MgO) using a non-conventional sintering technique (spark plasma) and the findings showed a result that was 25 GPa of hardness and 4.5 $MPa.m^{1/2}$ of fracture toughness [65]. In a series of experiments, Azhar et al. combined MgO particles with various concentrations of Al_2O_3 [66]. Even though the hardness increased, the fracture toughness reduced because of MgO content increased. It was a small grain that was primarily related to sharp decline of fracture toughness. Casellas et al. asserted that, decreased grain size led to poorer inherent toughness because of lower load bridging capabilities of smaller grain bridges, are in agreement with this point of view [67]. According to Azhar et al., adding more MgO than 0.7 wt.% led to a slow decline in fracture toughness. Due to MgO's inherent low fracture toughness, depending on the MgO composition, the fracture toughness result for samples containing MgO more than 1.0 wt.% progressively declined. As a result, it was established that the ZTA system can also benefit from MgO's effectiveness as an additive, in addition to monolithic Al_2O_3 systems. Similar to this, Rittidech et al. reported in their study that adding small amounts of MgO (0.25 wt.%) to the alumina matrix significantly changes the mechanical properties of bulk alumina and makes it possible for the alumina to sinter to almost theoretical density [68]. **Figure 2.6** displayed the phase diagram of Al_2O_3-MgO combination.

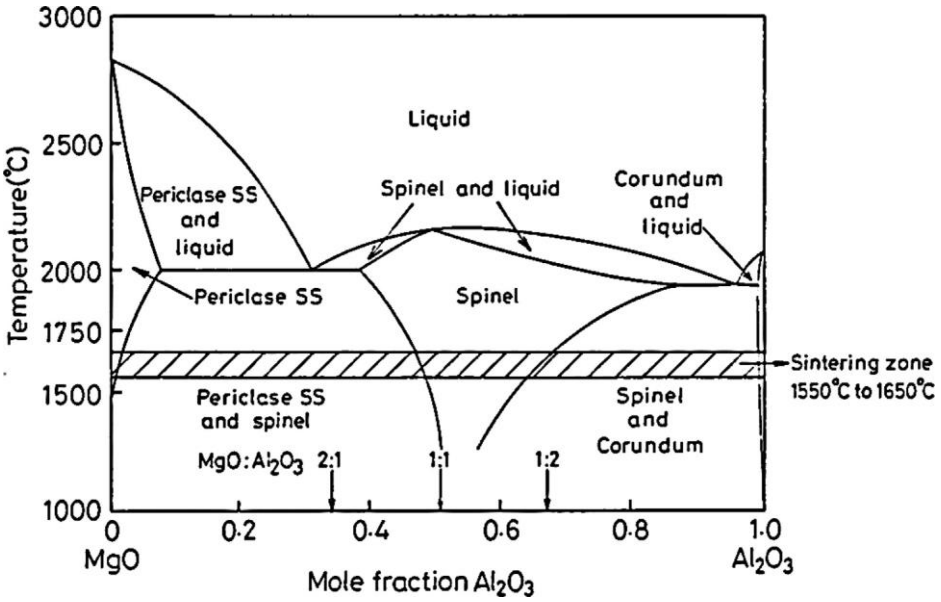

Figure 2.6 Phase diagram for the system Al_2O_3-MgO [69].

The phase diagram of MgO and alumina binary combination was displayed in **Figure 2.6**. From that, we can observe that at the operational temperature range, they have essentially little solubility. The alumina phase often gets a little amount of MgO added to it. Thus, the phase that is most likely to be present in the matrix is corundum. For the addition of MgO, the solubility limit is roughly 0.04 mol percent. Spinel can be discovered in the matrix because MgO is added there at a higher concentration. Spinel's glassy phase will cause it to lose mechanical qualities such flexural strength, Vickers microhardness, and fracture toughness. That explains why adding MgO at a high-level result in poor mechanical properties. The development of spinel is the fundamental cause. Corundum is the only feasible phase that can be identified, however, and this results in the improvement of some mechanical properties for small degree additions. We can also get periclase for spinel that is MgO rich. However, with the minor addition of MgO on ZTA, that won't be common.

2.3.4 CeO_2 added Al_2O_3 composites

By including ceria to the alumina matrix, Kumar et al. fabricated a cutting tool made of alumina ceramic composite [70]. In comparison to pure alumina ceramic cutting tool inserts, the Al_2O_3-CeO_2 ceramic composite cutting tool insert demonstrated better mechanical qualities, including hardness and fracture toughness. The resulting insert's machining

capabilities were superior to those of pure alumina inserts and on par with those of commercial zirconia toughened alumina inserts. Sintered the insert at high temperature, yielding hardness of 16.8 GPa as well as of 4.7 $MPa.m^{1/2}$ for fracture toughness.

R.V. Mangalaraja et al. conducted a study to examine an impact of cerium on the Al_2O_3-YSZ composite [71]. The fracture toughness values in their experiment were discovered to have fallen from 8.309 to 3.875 $MPa.m^{1/2}$. At 1650°C, the samples were sintered. The larger apparent porosity, which may have been caused by the addition of 5 wt.% ceria, was revealed to be the cause of the lower mechanical characteristics (CeO_2). No indication of ceria-related X-ray intensity peaks were visible. However, a microcrack density that is too high can reduce fracture toughness rather than give toughening, which reduces fracture strength [72]. The increased apparent porosity may have resulted from particles being mixed in a solid state. Zirconia particles distribution and morphology determines how tough an Alumina-Zirconia (AZ) composite is to fracture. Moreover, the shape, size and position of zirconia particles within the alumina matrix as well as their size distribution also associated with the property of fracture toughness. All of these factors are significantly influenced by the processing method according to J.B. Watchman (for instance, mixing and milling, consolidating and sintering) [73].

I. Akin et al findings were similar to the earlier trial [74]. They initially looked at Al_2O_3-YSZ composites devoid of CeO_2 and discovered that they had better hardness compare to single crystal alumina sintered bodies. Composite Al_2O_3-YSZ showed a declining trend of hardness when ZrO_2 content was raised from 10 to 30 vol%. For Al_2O_3 with 10 vol.% YSZ, the fracture toughness increased from 2.8 $MPa.m^{1/2}$ to 5.6 $MPa.m^{1/2}$, and further addition led to greater fracture toughness values. The additive's level of 30 vol% YSZ was determined to have the highest value of fracture toughness, 6.2 $MPa.m^{1/2}$. Then, applying sintering temperature of 1400°C for 5 minutes through SPS (spark plasma sintering) and a pressure of 40 MPa, they created Al_2O_3-YSZ composites that had 3 and 5 mass% of ceria (CeO_2). The XRD peak and SEM were used to identify and detect the formation of elongated $CeAl_{11}O_{18}$ grains, although for containing 3 & 5 mass% CeO_2, the fracture resistance of Al_2O_3-YSZ ceramics were found to be 5.2 and 4.9 $MPa.m^{1/2}$, respectively, less than that of composites without CeO_2. One drawback of this work is that the authors failed to explain why CeO_2 declined the resistance to fracture despite the relative density being extremely close (99.3%) to theoretical density.

At the contemporary time, Azhar et al. demonstrated that the least wear area was obtained by adding 0.6 wt.% of Cr_2O_3 [75]. With the addition of a modest amount of Cr_2O_3 (0.6 wt.%), the ZTA composite was considerably changed in microstructure, growing grains larger and taking on a platelet shape. The outcome was found as fracture toughness enhanced from 4.41 MPa.$m^{1/2}$ to 4.73 MPa.$m^{1/2}$. In comparison to ZTA cutting inserts containing 0 wt.% Cr_2O_3, ZTA cutting insert with 0.6 wt.% Cr_2O_3 had the lowest wear area of 0.0165 mm^2, an improvement of 26.70%.

Rejab et al. suggest from a broader perspective that CeO_2 increased the fracture toughness of yttria stabilized zirconia toughened alumina [76]. Up to 15 wt.% of CeO_2 was added to the powder mixes. Under no pressure, the samples were sintered at 1600°C for 4 hours. Vickers indentation was used to test the fracture toughness of the sintered samples under a 30 kg-f stress. According to XRD examination, where shift in position of the zirconia peaks were also seen due to the CeO_2 addition, only corundum and yttria doped zirconia phases were present. Microstructural analysis revealed that the addition of more CeO_2 increased the grain sizes of both corundum and yttria-doped zirconia. The sample with 5 wt.% CeO_2 additions had the maximum fracture toughness (8.38 MPa.$m^{1/2}$) and hardness value (1688 HV). When compared to ZTA without additives, the sample made with CeO_2 additives had a 30% higher fracture toughness. In complete contrast to the earlier results, this result. The high fracture toughness value of such composite may be due to the 5.4 mol% yttria stabilized ZTA powder. It was shown by Tsukuma and Shimada in 1986 that the amount of cerium oxide added to Tetragonal Zirconia Polycrystals (TZP) had a notable effect on the fracture resistance as well as hardness [77].

2.3.5 CaO/SrO added Al_2O_3 composites

The effects of in-situ formation of $CaAl_{12}O_{19}$ (hibonite) on the microstructure and mechanical characteristics of zirconia toughened alumina were studied by Sktani et al. [78]. Samples were sintered at 800°C for 4 hours to obtain CaO, and then at 1600°C for 4 hours to form elongated $CaAl_{12}O_{19}$ grains, in order to study the disintegration of $CaCO_3$. The investigations revealed that $CaAl_{12}O_{19}$ and pore quantities increased in direct proportion to the amount of $CaCO_3$ added. They demonstrated that the toughness value increased with the addition of $CaAl_{12}O_{19}$ for a critical range and thereafter reduced, whereas the hardness and

density data revealed the opposite pattern. The sample with 0.5 wt.% $CaCO_3$ added had a reasonable hardness value 1568 HV and the highest toughness value 6.3 MPa.$m^{1/2}$.

Figure 2.7 shows the phase diagram of the CaO and Alumina system. There may be the steps of reaction that finally result in the formation of CA_6. The name of this mineral CA_6 is hibonite. Hibonite has the highest melting point among the phases and is the one that contains the most alumina [79]. It is a gem mineral with a Mohs hardness of 7.5-8 and a specific gravity of 3.84 [80]. It has similar characteristics with alumina. Additionally, it's thermal expansion coefficient is equivalent to alumina. However, due to its anisotropy, the expansion is not uniform, and as a result, thermal shock can cause the ceramics matrix to disintegrate [81].

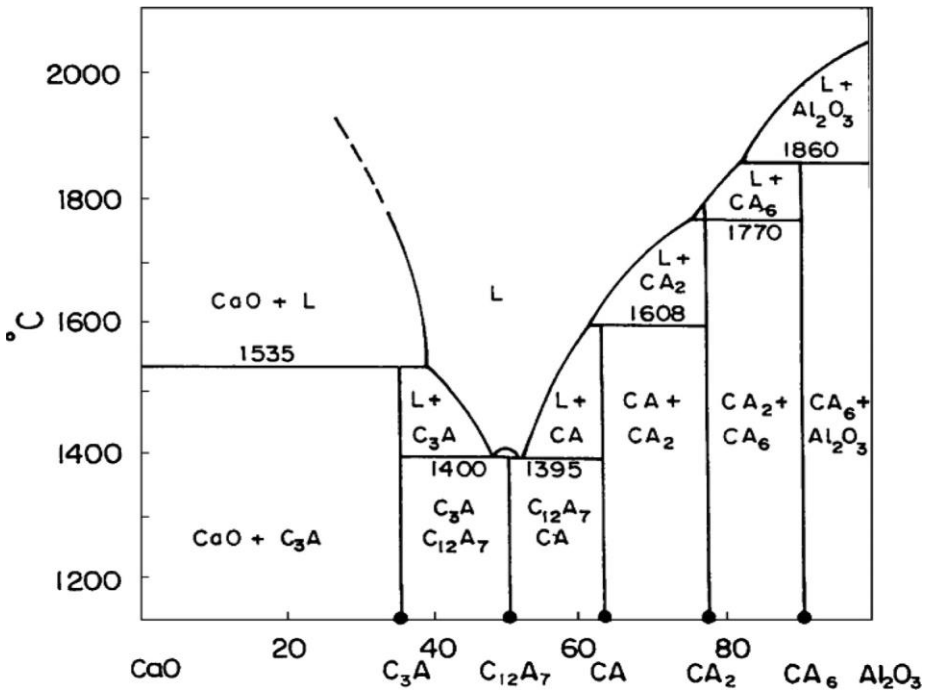

Figure 2.7 A phase diagram for Al_2O_3-CaO system.

Lovleen Kumar Bhalla showed his thesis, how the production of elongated grains by strontium oxide enhanced the hardness and fracture toughness of alumina by absorbing the energy of crack propagation [82]. The highest recorded hardness value was 1658 HV, while the highest recorded fracture toughness value was 4.7 MPa.$m^{1/2}$. The alumina-based composite forms hexa-aluminate when alkali earth oxides like SrO are present, and if particular preparation

techniques are used, the hexa-aluminate develops plate-like or elongated grains through which increases toughness following crack deflection and crack bridging mechanisms.

2.3.6 SiC added Al_2O_3 composites

Al_2O_3 with 5% SiC nanocomposites were fabricated in a study by Jeong et al. applying pressure-less sintering at 1800°C for 2 hours with 0.1% MgO as a sintering aid, followed by post hot isostatic pressing (HIP) at 1600°C for 1 hour [83]. They showed that MgO was able to facilitate the densification of the composites but was unable to induce the growth of Al_2O_3 matrix grains due to SiC nanoparticles inhibition of grain growth. Al_2O_3-SiC nanocomposites were fully densified after HIP treatment, and a high fracture strength of 1 GPa was attained for the materials using pressure less sintering and post HIP processing. Al_2O_3 and SiC were used to made a composite in 2013 by Parchoviansk et al for mechanical application [84]. They determined that 10% SiC with Al_2O_3 had a fracture toughness value of 6.0 $MPa.m^{1/2}$ and a hardness value of 20 GPa for 20% SiC. The powder combinations were hot pressed for 1 hour at 1740°C under 30 MPa of pressure in an environment of argon gas. While monolithic Al_2O_3 had a hardness of 18.4 GPa after being hot pressed for 1 hour at 1350°C in vacuum. In a recently released publication, Klement et al. reported results for a composite of polymer-derived Al_2O_3 with 8% SiC via HIP at 1800°C with hardness values of 21.1 GPa and toughness values of 4.4 $MPa.m^{1/2}$ [85]. SiC requires a higher sintering temperature than other additions to increase Al_2O_3's fracture toughness, which is not very advantageous for industrial manufacturing.

2.3.7 Graphene added Al_2O_3 composites

A different composite was made by J. Liu et al. in a different way. They used Spark Plasma Sintering (SPS) at a temperature of 1550°C to produce completely densed alumina ceramics reinforced by graphene platelets [86]. They showed that the fracture toughness of ZTA composites increased by 40% with the addition of only 0.81 vol% GPLs. The pull-out of GPLs, crack bridging, and crack deflection behaviors increased the toughness of the composites. The fracture toughness and hardness were 4.4 $MPa.m^{1/2}$ and 17 GPa respectively. According to Porwal, adding only 0.8 vol% graphene boosted the material's fracture toughness by 40% [87]. By applying Spark plasma sintering (SPS), they made composites of graphene-Al_2O_3 containing near 5 vol% graphene and observed that the improvement in fracture toughness was only limited for higher graphene levels. For the Alumina matrix, graphene

changed the crack expansion process in between trans and inter-granular alteration. Easy fracturing for concentration up to 2 vol% was encouraged by the formation of an interconnecting graphene network. Due to the development of the interconnecting graphene network, elastic modulus was remained constant for the first 2 vol% and then considerably dropped for the remaining 5 vol%. Although more research is needed to confirm this behavior, graphene up to 5 vol% did not appreciably change the nano-composites' densification behavior. Bocanegra-Bernal et al. investigated how carbon nanotubes affected the characteristics of zirconia toughened alumina composites and found that they increased fracture toughness over pure ZTA by 44% [88].

2.3.8 Al_2O_3 Carbide composites

Acchar and Segades showed in 2005 that using NbC added Al_2O_3 in place of WC-Co materials for cutting tool applications [89]. They made an Al_2O_3 composite containing 30% NbC. In an inert atmosphere, samples were hot-pressed at 1650°C. They found a fracture toughness of 4.4 $MPa.m^{1/2}$ and a hardness of 20 GPa, and the results were in good agreement with those of alumina reinforced with TiC and TiN (4.5-5.0 $MPa.m^{1/2}$). They argue that the measured values were low in comparison to the more prevalent Tungsten Carbide and Zirconia reinforcements in another literature published in 2009 [90]. However, compared to other Alumina-Carbide systems, the Alumina-NbC composites shown a good combination of hardness, fracture toughness, and other mechanical parameters.

On the other hand, Yu Cheng developed a composite for cutting hard steel, super alloy, or cast iron at high speeds [91]. The experimental findings demonstrated that the Al_2O_3-TiC composite, which was sintered at 1700°C in argon for 10 minutes, had 99.2% theoretical density, a fracture toughness value of 5.18 $MPa.m^{1/2}$, a Vickers hardness of 21.2 GPa, and excellent mechanical properties. Due to quick microwave sintering, a homogenous microstructure was produced. Yu Cheng evaluates the effect of Graphene platelets (GPLs) on Alumina composite in a significant study [92]. They conducted an experiment using an Al_2O_3-TiC composite material that was produced using microwave sintering and reinforced with graphene platelets (GPLs). They emphasized the effects of GPLs content on the Al_2O_3-TiC-GPLs composites microstructure, mechanical characteristics, and toughness mechanisms. With the addition of GPLs, the composite's microstructure got finer, and the best mechanical properties were attained with as little as 0.2 wt.% of Graphene Platelets. Percentage of bulk

density in compare to theoretical measurement was 97.7%, the Vickers hardness was 18.5 GPa, the fracture toughness was 8.7 MPa.$m^{1/2}$. Vickers hardness was 12.7% lower compared to Al_2O_3-TiC composites, whereas fracture toughness was 67.3% higher. The toughening mechanisms of crack deflection, crack bridging, crack branching, and pull-out of GPLs produced good agreement with the results. Similar to this, Z. Yin et al. conducted an experiment using an Al_2O_3-Ti(C, N) composite that was microwave-sintered at 1550°C for 10 min [93]. It had a relative density of 98.4%, a fracture toughness of 6.72 MPa.$m^{1/2}$, and a Vickers hardness of 18.4 GPa, respectively. They claim in their study that a 14% and an 89% reduction in soaking duration as well as sintering temperature, respectively, will help the industrial manufacturing of Alumina-Ti(C, N) tools. They provided an explanation for their choice of Ti(C, N), stating that the presence of TiN in solid solution with TiC gives it significantly better mechanical properties than TiC alone. Therefore, Ti(C, N) has a both high hardness of TiC and toughness of TiN. However, the weakness of this paper is that, it does not adequately explain why they chose to produce that composite with 9% Ni and Mo.

According to data from multiple investigations, high temperatures and long sintering times were needed to produce exceptionally dense and durable composites using carbide materials as reinforcement in an alumina matrix [90, 94, 95, 96].

2.4 Toughening Mechanism with 3YSZ Addition

The densification of alumina-based composites has long been accomplished by zirconia addition in alpha alumina just for sintering aid. Nevertheless, Recently, the concept of toughening alumina ceramics by dispersing zirconia particles throughout alumina matrix has gained recognition. Claussen asserts that a second phase dispersion can increase the fracture toughness energy of a ceramic [97]. The energy absorbing mechanisms include crack blunting, crack deviation, and crack front elongation. As a result, the fracture energy rises, which is typically asserted to the crack front's contact with the second phase. Microcracking is shown by adding ZrO_2 particles inside the ceramic's base material, such as Al_2O_3. The ZrO_2 particles associated with volume growth, which ranges from 3 to 5%, upon cooling through the transformation temperature (T_{t-m}) is sufficient to create a microcrack. But for stabilized zirconia, phase change toughening takes place. According to Tang et al., "The toughness enhancement is proportional to the amount of transformable zirconia" [98]. They observed from the study that in contrast to samples having only a phase, YSZ samples with both m-ZrO_2

and t-ZrO_2 can get the maximum fracture toughness values. Each tetragonal zirconia precipitate is known to be under stress and to contain energy that needs to be released.

Stress Induced Phase Transformation Toughening

When zirconia undergoes phase transformation, the volume of its crystal's changes, which increases the material's resistance to crack propagation. This phenomenon is known to as stress induced phase transformation. At the crack tip, this stress induced change involves the transformation of zirconia from metastable tetragonal phase to the monoclinic phase. Compressive stress develops in zirconia particles owing to volume expansion, allowing it to bear heavy loads that is called phase transformation toughening. In **Figure 2.8**, Phase transformation toughening is the term which shows fine tetragonal zirconia phases dispersed in a matrix, can be helpful in understanding the phenomena.

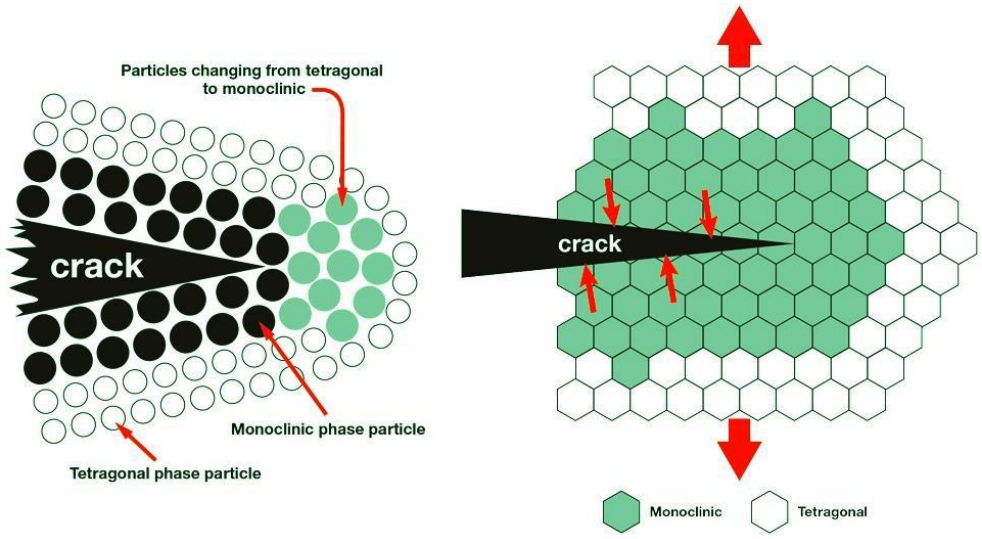

Figure 2.8 Schematic diagram of suppression of crack propagation [99, 100].

Upon cooling from the processing temperature of stabilized zirconia, the surrounding matrix can resist it from undergoing transformation, allowing it to remain stable in a metastable tetragonal phase. When the matrix's pressure on these metastable tetragonal particles is released, i.e., when a crack propagates in the material, they can change into the monoclinic zirconia (m-ZrO_2) phase, that causes a considerable volume enlargement (3-5%). The stress field connected to the phase change expansion acts against the stress field which stimulates the fracture propagation. The

resisting compressive stress brought on by volume expansion and the transformation from t→m phase both disperse the potential related with the crack growth, which boosts the material's toughness and strength. In case of zirconia, a certain particle size range where t-ZrO_2 particles may undergo stress-induced transformation. If the particles are less than the critical size, a spontaneous transformation will occur. The matrix constraint and the system's composition affect this critical size limit. With an increase in stabilizing oxides, the chemical free energy related to the phase transition reduces. Therefore, larger particles can be remained to maintain their metastable tetragonal state.

Microcrack Toughening

The baddeleyite or monoclinic zirconia is involved for toughening of ZTA through microcracking. The volume expansion of the ZrO_2 particles of 3-5% that takes place when they are cooled through the transformation temperature (T_{t-m}) results in a crack (**Figure 2.9 and 2.10**). Around the transformed particle, tangential stresses are generated that cause the matrix to microcracks. The ability of the cracks to extend in the stress field for propagating cracks or to deflect the propagating crack, which can absorb or dissipate the crack's energy, increases the ceramic's toughness. The optimum condition is when the particles are big enough to transform but small in size to form limited microcracks.

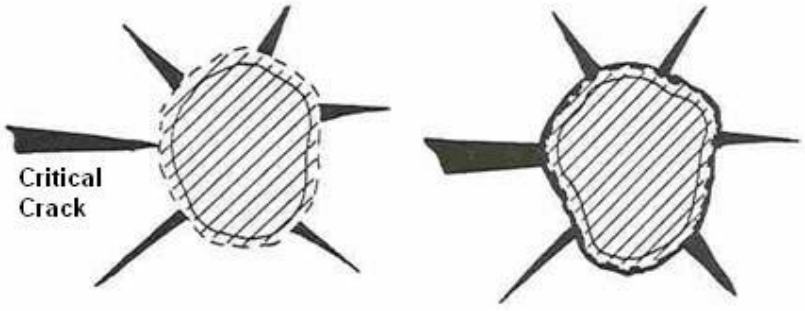

(a) (b)

Figure 2.9 The martensitic transformation in ZrO_2 (t→m, at 900-1100°C) with its 3-5% volume expansion, develop microcracks around the ZrO_2 particles (a) A crack propagating into the particle is deviated and becomes bifurcated (b) Thus, increasing the measured fracture resistance [101].

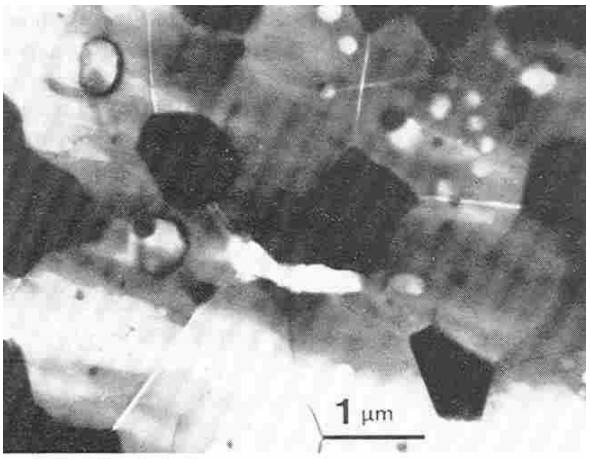

Figure 2.10 TEM of Al_2O_3-ZrO_2 showing the zirconia particles at the dark phase. The transformation develops high strains in the Al_2O_3 matrix which can be accommodated by microcracking [101].

Typically, milling time before sintering or ageing conditions after sintering can be used to control ZrO_2 particle size for getting desired size. The volume fraction of ZrO_2 inclusions must be at an optimum level in order to achieve maximum toughness [102]. It has been shown that toughness has a limit above which microcracks produced by the ZrO_2 particles would interact with one another and decreases the strength of the composite material.

Subcritical Crack Growth (SCG)

It is widely known that ceramic materials are susceptible to subcritical crack growth (SCG), which is characterized by a slow propagation of cracks. This phenomenon generally happens when the stress intensity factor K_I is less than fracture toughness K_{IC}. Temperature and other environmental variables, as well as the applied load, have an impact on the subcritical crack growth [104]. The corrosive action in the stressed zone near the crack tip under constant load or a pre-existing defect in material are related to SCG in bio-ceramics [103].

2.5 Toughening Mechanism by Platelet Reinforcement

Alumina, a well-known material for structural applications, has a low fracture toughness or brittleness. Alumina-based composites have been produced with the addition of zirconia particles [104, 105], SiC whiskers [106], and metallic [107] or ceramics particles [108]

for the purpose of increasing the low resistance to fracture of alumina. Tetragonal zirconia stabilized with yttria (3Y-TZP) was used as the reinforcing component for the alumina matrix. The stability of the tetragonal phase of zirconia has some limitations in regard to mechanical characteristics of ZTA (zirconia toughened alumina) ceramics.

In other words, at low temperatures of roughly 100°C, environmental factors like moisture may cause the change of yttria stabilized zirconia grains into m-ZrO_2 (monoclinic) from t-ZrO_2 (tetragonal) phase. Since tetragonal phase is stable, zirconia does not exhibit toughening behavior beyond the martensitic initiation temperature [109, 110]. Despite the presence of the stable tetragonal phase in the composite, the mechanical characteristics cannot be improved because the zirconia grains do not react well to crack propagation since there is not enough tetragonal-monoclinic transformation.

To keep the fracture toughness at a reasonable level, it is therefore of great interest to incorporate further toughening elements. Strontium is one of the key options that fits the criteria for incorporating the Alumina matrix and assisting the toughening process. The alumina-based composite forms hexa-aluminate when alkali earth oxides like SrO are present, and if particular preparation techniques are used, the hexa-aluminate develops plate-like or elongated grains through which increases toughness following crack deflection and crack bridging mechanisms. **Figure 2.11** demonstrates how a platelet particle (elongated grain) deflects a crack's path in a composite to increase the fracture toughness.

According to Cutler et al., strontium hexa-aluminate can have a plate-like crystal structure, which increases flexural strength and fracture toughness, when $SrZrO_3$ is added in small quantities to Ce-TZP-Al_2O_3 matrices [112]. This outcome is completely compatible with findings from Masichio et al., where show that Al_2O_3-Cr_2O_3/ZrO_2 matrixes have higher fracture toughness [113]. Incorporating calcium and strontium hexa-aluminate improved the mechanical properties of zirconia toughened alumina, as shown by Balmonte et al. and Maity et al. [114, 115]. Therefore, the addition of such additives can be used to reinforce as well as improve the structural characteristics of alumina-based composites.

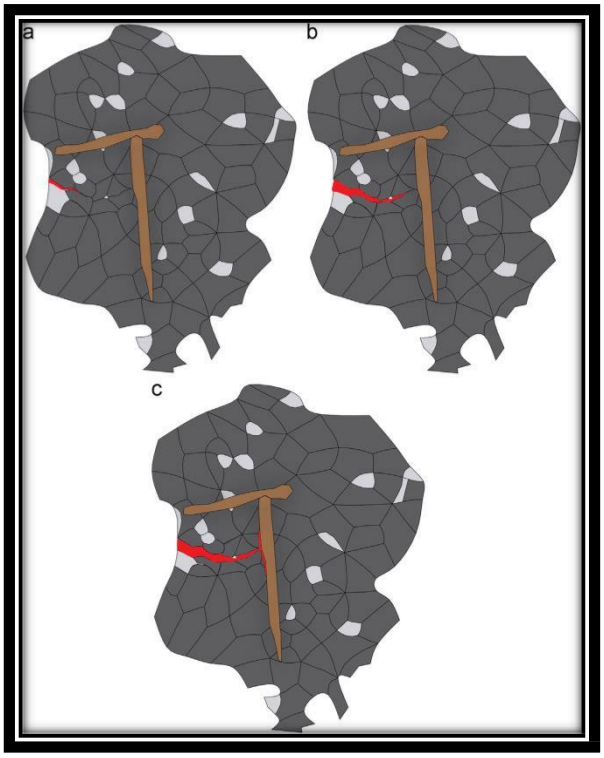

Figure 2.11 Schematic illustration of a crack that reaches a platelet particle in ZTA composite and gets deflected by an elongated grain [111].

2.6 Applications of Alumina-Zirconia (AZ) Composites

Historically, the alumina-zirconia alloy's original use was as toughened abrasive grain for industrial graining wheels. Alumina-zirconia composites are already well known to material scientists. This might provide a new approach to implants because both materials are biocompatible. A phase-stabilized zirconia matrix reinforced with alumina particles, alumina toughened zirconia (ATZ), or an alumina matrix reinforced with zirconia particles, zirconia toughened alumina (ZTA), can be fabricated in this system. Higher toughness values than with monophase ceramics can be achieved with both materials, although higher values are expected for ZTA composites. ZTA is a high purity combination of zirconia's high strength and alumina's low cost. ZTA is a ceramic-ceramic composite that has good mechanical properties. Due to the combination of ZrO_2 and Al_2O_3 characteristics, ZTA ceramics are desirable materials. Strength and, more importantly, toughness have significantly improved with ZTA. Compared to high purity alumina, it is three to four times more abrasion resistant.

Different engineering tools are made using alumina and alumina-based composites. Electronics applications is predominantly centered in making substrate in hybrid circuit, piezo-ceramic sensor and next generation computer memory [116]. In the biomedical industry, alumina and alumina-based composites are widely utilized to make parts such prosthetic joints, bones, and teeth [117, 118]. Owing to their high thermal and chemical stability, composites are also frequently employed in aerospace batteries, hot gas filters, electrolysis diaphragms, thermal barrier coatings, solidified, super alloy turbine blades, furnace heating elements, oxygen sensors, fuel cells, and catalytic membrane, to name a few other applications of alumina-based ceramics [119, 120].

Excellent mechanical properties, along with biocompatibility, wear resistance, and high chemical resistance, make the material a promising candidate for a number of applications. Few are represented in **Figures 2.12**.

(a) Advanced structural ceramic

(b) Ceramic components for medical equipment

(c) Ceramic shaft

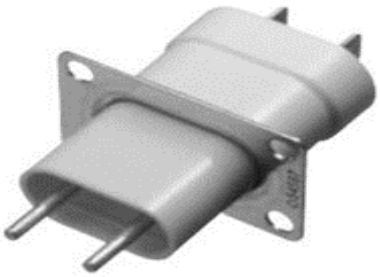

(d) Ceramic capacitor

(e) Dental implant

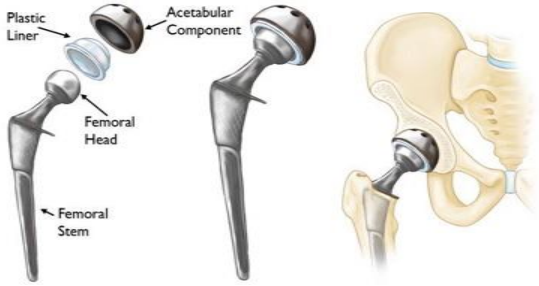

(f) Orthopedic implant

Figure 2.12 Different advanced ceramics: (a) Advanced structural ceramic (b) Ceramic components for medical equipment (c) Ceramic shaft (d) Ceramic capacitor (e) Dental implant (f) Orthopedic implant.

Traditional refractories provide some of their inherent strength for a useful level of thermal shock resistance. Only the microstructure, which is porous and contains numerous coarse grains, allows these materials to work. During thermal shock, these materials do not store a significant amount of elastic energy. They can, however, be more easily attacked by slag and subject to erosion from flowing molten metal. An appropriate size and amount of m-ZrO_2 dispersion in the suitable matrix phase significantly improves this scenario. Refractories that are dense, strong, and resistant to thermal shock can now be designed.

2.7 Scope of the Research

The desire for materials that can provide modern standards and applications has motivated the modification of technology for the manufacture of novel materials that are biocompatible. Advanced ceramics have been used as biomaterials since the 1970s, and then, these materials have continued to improve in a variety of applications. Ceramics materials have made it possible to make a significant improvement.

Zirconia Toughened Alumina (ZTA) refers to the Al_2O_3-based composite material that contains ZrO_2. The use of MgO, CaO, TiO_2 and CeO_2 additives can additionally toughen Al_2O_3. These strengthened materials are suitable for biomedical, dental, structural, and other applications because they have better physical and mechanical properties. These materials are used in sensitive applications because they need to have good surface characteristics.

There have been numerous studies conducted on the addition of various additives to Al_2O_3 to improve its mechanical and physical properties. The majority of them followed zirconia-toughened alumina (ZTA) with MgO or TiO_2 or CaO or CeO_2 individually. MgO was used in amounts of 0 to 3 wt.%, TiO_2 of 0 to 10 wt.%, CaO and CeO_2 from 0 to 15 wt.% and ZrO_2 from 10 to 20 weight percent. All the ingredient were used to modify the characteristics of Al_2O_3. Researchers applied a variety of pressure ranges between 150 and 400 MPa to manufacture ZTA using different methods. MgO and TiO_2 were both used as additives in this study in fixed amount of 5 wt.%. ZrO_2 content was also fixed at 15% by weight. Under a pressure of 254.6 MPa, the samples were shaped using a hydraulic press.

The goal of this research is to investigate the effects of two additives, CaO and CeO_2, varies from 0-5 wt.% on ZTA-5TiO_2-5MgO composites simultaneously.

MATERIALS AND METHOD

CHAPTER 3
MATERIALS AND METHOD

In this chapter, initially the essential steps for the fabrication of zirconia toughened alumina (ZTA) composites with the inclusion of different metal oxides for instance TiO_2, MgO, CeO_2 as well as CaO using powder compaction method are presented. Later on, the experimental techniques to investigate the physical, structural, mechanical, morphological, and biomedical properties have been discussed.

3.1 Selection of Raw Materials

Nanosized α-Al_2O_3 and yttria stabilized ZrO_2 powders were utilized to fabricate zirconia toughened alumina (ZTA) ceramics. Due to transformation property with increasing temperature up to certain stage, yttria stabilized ZrO_2 was utilized in this method. As Al_2O_3 is the strong matrix phase, some of the t-ZrO_2 partially transformed into the monoclinic phase after cooling but a complete transformation is not occurred. As a result, the final material includes the matrix Al_2O_3 and a combination of monoclinic and tetragonal ZrO_2 phases, which can improve certain mechanical properties like fracture toughness, strength etc. For availability of monoclinic and tetragonal ZrO_2 phases, the material is capable of being strengthened through a variety of mechanisms, including transformation toughening, microcracking and crack deflection toughening. These methods for toughening work together with one another.

Impurities that might be added to raw materials during powder processing can occasionally be formed some glassy phases in the grain boundaries of composite materials. The material ages and loses mechanical strength as a result of formation glassy phases. As a result, yttria stabilized ZrO_2 and nanosized α-Al_2O_3 were utilized in this study. Besides, for tailoring the properties of ZTA, additives like TiO_2, MgO, CaO and CeO_2 were also used in this study. In **Table 3.1**, the overall characteristics of nanosized α-Al_2O_3, yttria stabilized ZrO_2, MgO, TiO_2, CaO and CeO_2 used in the current work are listed below.

Table 3.1 Characteristics of the raw materials used in this research (All specifications are collected from the product catalogue)

Properties	α-Al_2O_3	ZrO_2	TiO_2	MgO	CeO_2	CaO
Purity	99.8%	99.9%	99.9%	>97%	99.95%	99%
Density(g/cm^3)	3.97	6.1	3.89	3.58	7.13	3.3
Av. particle size (nm)	150	30-60	40	<50	-	-
Origin	Advanced materials, USA	Advanced materials, USA	Advanced materials, USA	RCL Labean ltd., Thailand	Loba Chemie, India	Qualikems, India

3.2 Compositions of Composites or Samples

Powders of Al_2O_3, ZrO_2, MgO, TiO_2, CaO and CeO_2 were mixed to prepare a number of composites. While the percentages of CaO and CeO_2 were varied from 0-5 wt.%, and the ZrO_2 was fixed at 15 wt.%, MgO and TiO_2 powders were also fixed at 5 wt.%. Alumina (α-Al_2O_3) was used as matrix substance. According to **Table 3.2**, seven various types of samples were prepared for the experiment.

Table 3.2 Compositions of samples prepared for the experiments.

Sample Categories	Sample ID	Wt.%				
		ZTA	TiO_2	MgO	CeO_2	CaO
ZTA-TiO_2-MgO	Z15	90	5	5	0	0
ZTA-TiO_2-MgO-CeO_2	Z15Ce5	85	5	5	5	0
ZTA-TiO_2-MgO-CeO_2-1CaO	Z15Ce5Ca1	84	5	5	5	1
ZTA-TiO_2-MgO-CeO_2-2CaO	Z15Ce5Ca2	83	5	5	5	2
ZTA-TiO_2-MgO-CeO_2-3CaO	Z15Ce5Ca3	82	5	5	5	3
ZTA-TiO_2-MgO-CeO_2-4CaO	Z15Ce5Ca4	81	5	5	5	4
ZTA-TiO_2-MgO-CeO_2-5CaO	Z15Ce5Ca5	80	5	5	5	5

3.3 Sample Preparation

Initially, a motor-driven pot mill was used to mix and mill the powders in pure ethanol media over a 24 hours period. After mixing, a strainer was used to remove the powder mixture and dried at 100°C in a vacuum oven (Memmert) for 24 hours in the following steps. To prepare a uniform mixture, hand milling was done by a mortar pestle for an hour. By using a uniaxial compaction method, a green body (bulk sample) is formed or shaped in the pellet form of diameter 10 mm. In order to provide the pellets some green strength for subsequent handling polyvinyl alcohol (PVA) binder was added with it before compaction of the processed powder. The proper amount of pressure as well as binder added during the fabrication of green sample were important; otherwise, the sample's edge would break or complications might be shown during green sample ejection from mold. Regarding current study, each sample was subjected to 254.6 MPa of pressure and 1(one) drop of PVA binder was added for each 0.8 gram of processed powder. For each sample, two minutes of pressing time was used to maintain thickness uniformity. The die was thoroughly cleaned after each sample was prepared because any powder that remained inside the die could cause resistance during the subsequent pressing and uneven load distribution, which could breakdown the sample. The sample preparation flow sheet is presented in **Figure 3.1**.

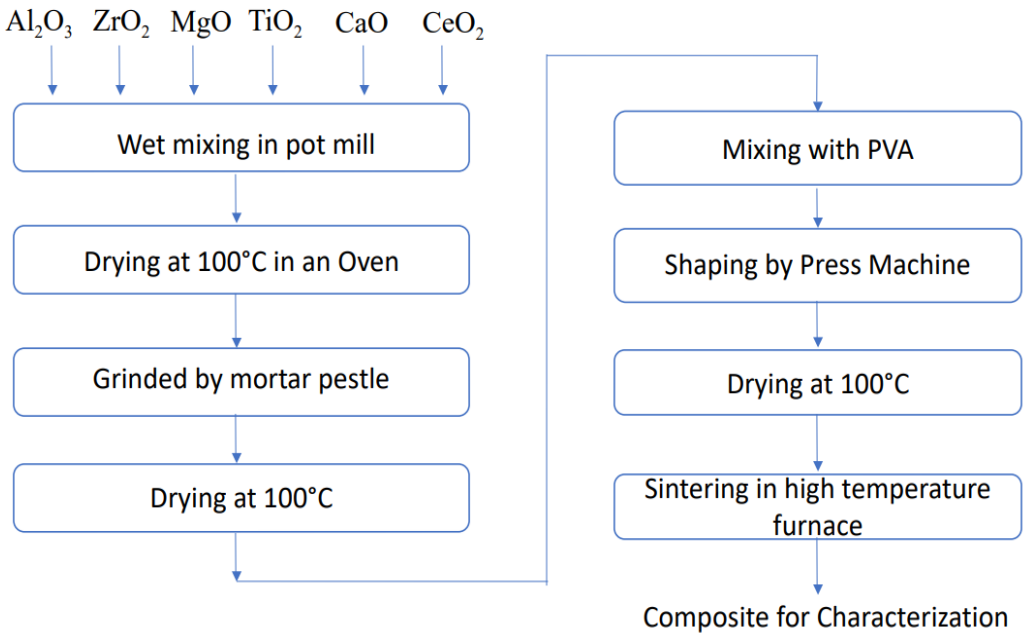

Figure 3.1 Flowchart of alumina-zirconia (AZ) composite fabrication.

Figure 3.2 Pot milling.

Figure 3.3 Mortar pestle.

Figure 3.4 Die and its parts.

Figure 3.5 A Press Machine (P/O/WEBER GmbH).

Figure 3.6 Prepared composite materials.

3.4 Sintering of the Green Body

Sintering (firing) method is applied for consolidating ceramic powder particles by thermally treating a green sample to a high temperature below the melting point, when the material from the separate powder particles diffuses to the neighboring powder particles. Sintering is the final step in the process of preparing ceramic products. Densification from high-temperature sintering gives ceramic products their strength and other advantageous properties. Throughout this process, the pores are eliminated and the individual ceramic particles mix to form a continuous solid network. The sintered product typically has dense grains with a microstructure made up of various starting particles.

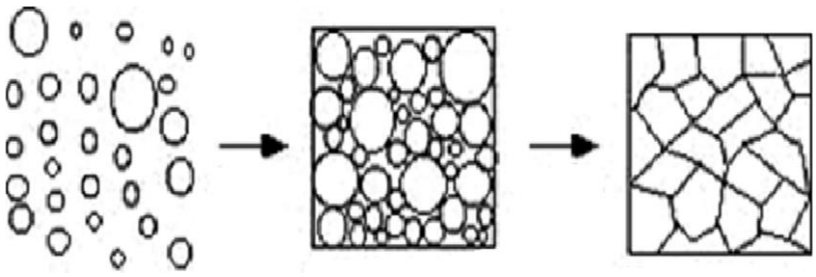

(a) Raw powder (b) Formed body (c) Sintered product.

Figure 3.7 Schematic illustration of microstructure (a) raw powder, (b) green formed, and (c) sintered ceramic product [121].

Generally, firing controls both grain growth and densification simultaneously. Densification is the process of making a sample denser by decreasing its porosity. The process of grain boundary motion to increase the average grain size is known as grain growth. Both a high relative density and a small grain size are advantageous for a variety of properties, including mechanical strength and electrical breakdown strength. Controlling these properties throughout processing is, therefore, extremely important from a technological standpoint. Grain growth naturally takes place during sintering because high temperatures are needed for densifying powders.

The following steps are involved in the process of making ceramic products by sintering powders:

- Mixing a binder to the processed powder for providing green strength.
- Putting the dried powder into a die or mold and pressing it to form a green body.
- Low-temperature heating of green body to burn off the binder completely.
- High temperature sintering, which fuses the ceramic particles each other.

In the present work, the samples were sintered at 1450°C, 1500°C, 1600°C and 1650°C in a high temperature electric furnace (**Figure 3.8**) controlled by a microprocessor. The following **Figure 3.9** depicts a typical sintering cycle.

Figure 3.8 A high temperature furnace (MHI Corp., BPAN-2010, USA).

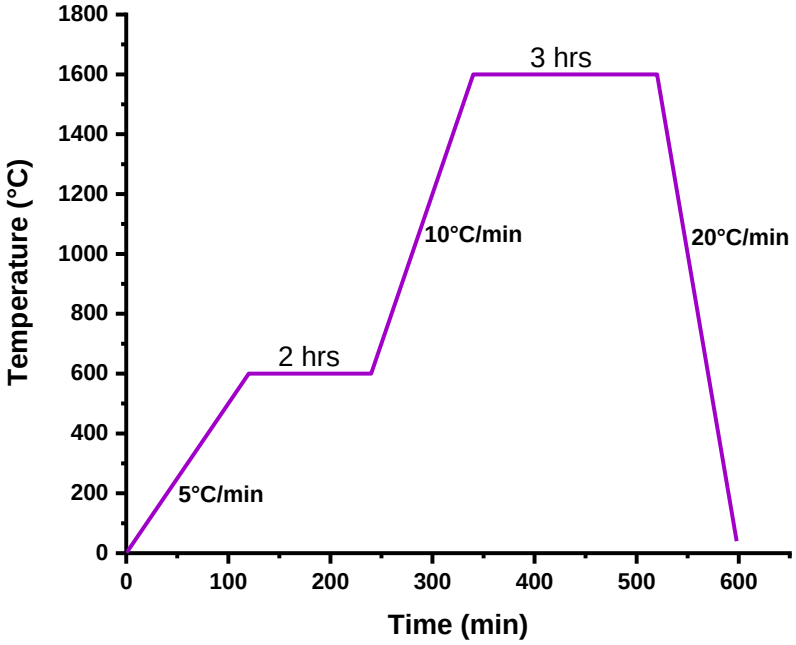

Figure 3.9 A typical sintering cycle at 1600°C.

3.5 Characterization of Composites

3.5.1 Density Measurement

By immersing the sintered body in distilled water and applying Archimedes' principle, the density of the sample was measured. Density was measured using a minimum of six samples, and the variation in density was found to be within ±1%. The density of the sintered sample is determined using the standard Archimedes formula as follows:

$$\rho_s = \frac{m_s \rho_w}{m_s - m_w} \qquad \ldots\ldots\ldots\ldots\ldots\ldots\ldots\ldots\ldots (3.1)$$

Where, ρ_s is the density of the sintered sample, ρ_w is the density of the water, m_s is the mass of the sintered disc, m_w is the mass of the disc in water.

3.5.2 Porosity Measurement

During sintering of oxide materials, porosity is a characteristic that is unavoidable. Notably, the studied samples porosity has a significant effect on their physical and mechanical

properties. For a better comprehension of different characteristics of the investigated bodies and to correlate the microstructural features and property relationships of the samples under investigation, it is therefore necessary to have an accurate concept of the proportion of pores in a studied sample. According to the grain size, shape, and degree of storage and packing of the grains, a material porosity will vary.

Using the standard formula [122], the percentage of total porosity (φ) was calculated from the sintered density (ρ) and theoretical density (ρ_o).

$$\varphi = \left(1 - \frac{\rho}{\rho_o}\right) \times 100 \quad \ldots\ \ldots\ \ldots\ \ldots \ldots \ldots \ldots \ldots (3.2)$$

where, φ is the total porosity of the sample, ρ is density of sintered pellet and ρ_o is the theoretical density of samples.
Using the rule of mixtures, the theoretical density of the sample was calculated from the actual density of the starting powders and their weight percentages.

3.5.3 Microhardness Measurement

Hardness is one of the most often measured characteristics of ceramic materials. The microhardness of a material, which is an important characteristic for ceramic materials, is correlated to its capability to resist indentation of the surface by a simultaneous effect of brittle fracture and plastic flow. Its value contributes to define of resistance to fracture, densification, and deformation.

Typically, a Vickers microhardness test is used to determine the hardness of technical ceramics. According to the Vickers microhardness test method, the test material is indented using a diamond indenter in the shape of a right pyramid with a square base and an angle of 136 degrees between opposite faces under a load of 1 to 2 kg-f. Normally, 6 to 15 seconds of the entire load are applied. A microscope is used to measure and average two diagonals of indentation remaining on the material surface following removal of load. Calculations are made regarding the indentation's sloped surface area. Vickers microhardness is calculated through dividing the amount of applied load by the square mm area of the indentation.

Usually, the applied load in a Vickers microhardness test is indicated by the notation HV10 or HV20 (in this case 10 or 20 kg, respectively). Vickers' microhardness tester, model “HMV-2 Series”, Shimadzu Corporation, Japan is shown in **Figure 3.10** and was used in this study to measure microhardness. The specimen could indent utilizing 2 kg force holding 10 seconds using the Vickers microhardness tester.

Figure. 3.10 A microhardness tester (HMV-2, SHIMADZU Corp., Japan).

Vickers microhardness was determined employing the equation given below [123, 124]:

$$H_v = 0.01819\ (\frac{P}{d^2}) \quad \ldots\ldots\ldots\ldots\ldots\ldots\ (3.3)$$

Where, H_v is the Vickers microhardness (GPa), P is the applied load (N), d is the average length of two diagonals of the indentations (mm). The amount of surface porosity, the size of the microstructure's grains, and the effects of grain boundary phases need to be taken into consideration when evaluating microhardness data for ceramic materials.

3.5.4 Fracture Toughness Measurement

Fracture toughness, or the ability to resist fracture by crack propagation when a crack is already present, is another important property of ceramic materials. The indentation fracture test is a common technique for determining the fracture toughness using indentation data. It offers some advantages, including simple geometry, a few numbers of specimens, simple measurement methods, and equipment [125]. The formula for calculating fracture toughness (Casellas Equation) is shown below [126]:

$$K_{IC} = 0.024 \left(\frac{E}{Hv}\right)^{½} \left(\frac{P}{C^{\frac{3}{2}}}\right) \qquad \ldots\ldots\ldots\ldots\ldots (3.4)$$

where, K_{IC}, Hv, E, P and C stand for the fracture toughness ($MPam^{½}$), Vickers hardness (GPa), elastic modulus (GPa), indentation load (MN) and radial crack length (m), respectively.

(a)

Figure. 3.11(a) A Hardness Tester (DVK-2, Matsuzawa Co., Ltd., Japan).

(b)

Figure. 3.11(b) An Optical Microscope (NMM-800TRF, MTI Corp. Ltd.).

An applied load of 50 kg was used by a hardness tester machine (DVK-2, Matsuzawa Co. Ltd., Japan) to measure the fracture toughness. An optical microscope (NMM-800TRF, MTI Corp., USA) was used to observe all fracture surfaces which is shown in **Figure 3.11**.

Prior to indentation, the specimen surface was successively ground using SiC discs with 1200 and 4000 grit, respectively. The samples were then polished on a texmet cloth with 6 m and 1 m diamond paste. The reported values were the average of the measuring data from six indentation tests. **Figure 3.12** illustrates the crack formation by Vickers indentation.

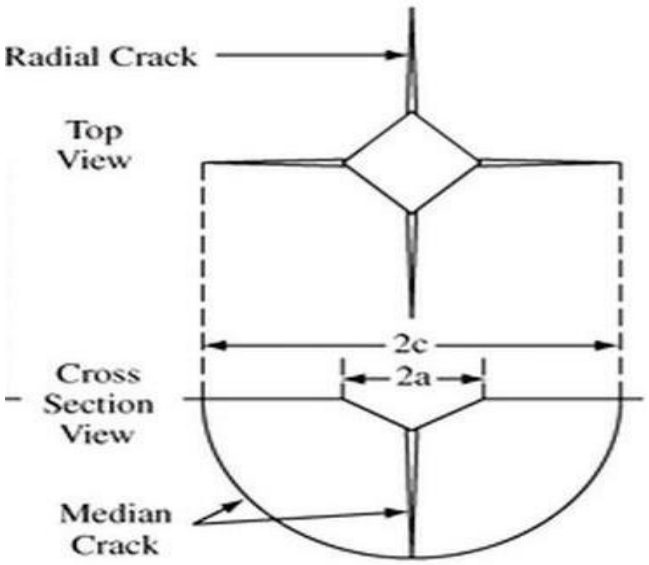

Figure 3.12 Schematic illustration of crack formed by Vickers indentation [127].

Dewey-Mackenzie relationship can also be used to measure the elastic modulus that depends on porosity [128]:

$$E = E_o (1\text{-}2\,\varphi) \quad \ldots\ldots\ldots\ldots\ldots\ldots\ldots\ldots (3.5)$$

where, E is the effective elastic modulus of porous composites. E_o is the elastic modulus of the dense composite and φ is the porosity of the sample.

3.5.5 Diametral Tensile Strength Measurement

A Universal Testing Machine (UTM) in **Figure 3.13** is used to test the mechanical property like diametral tensile strength of a material. A specimen in the shape of a dumbbell, rod, or wire is loaded to measure its tensile strength (a uniaxial tension test). Due to alignment and gripping problems, brittle materials make it difficult to conduct this type of test, hence an alternative test is now widely used to determine this property which is known as the diametral

compression test, and it is illustrated schematically in **Figure 3.14**. Only the materials with predominantly elastic deformation and little to no plastic deformation should be subjected to this type of test.

Figure. 3.13 A Universal Testing Machine (Hounsfield).

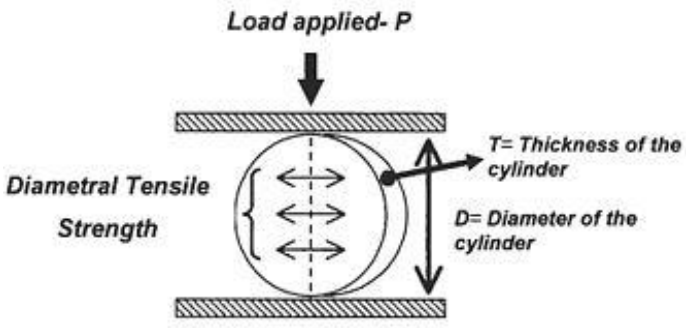

Figure 3.14 Schematic illustration of diametral tensile strength test [129].

According to this procedure, a short cylindrical specimen (disk) is subjected to a compressive load by a flat plate against its side, as shown in **Figure 3.14**. A tensile stress that is perpendicular to the vertical plane and passes through the center of the disk is produced by the vertical compressive force along the side of the disc. Along this vertical plane, fracture occurs (the disk's dotted vertical line). The tensile stress in this case is proportionate to the compressive force being applied. The following formula is used to calculate it [129, 130]:

$$Diametral\ tensile\ Strength\ (DTS) = \frac{2P}{\pi.(diameter).(thickness)} \quad \ldots\ldots\ldots\ldots\ldots\ldots\ldots\ldots (3.6)$$

Where, P represents the applied load. The results of this test are highly reproducible and the procedure is very simple. But when this test is used on materials that show noticeable plastic deformation prior to fracture resulting erroneously high tensile strengths. An unreliable test result may have been obtained because the material was broken into several fragments rather than the optimal two segments fragmentation.

3.5.6 X-ray Diffraction for Phase Analysis

X-ray Diffraction (XRD) technique is an effective nondestructive approach for crystalline material characterization. It gives details about the researched material's crystal structure, including details on phases, structures, preferred crystal orientations (texture), and more. Electromagnetic waves with wavelengths in the range of 1Å are known as X-rays. Because of its wavelength, which is of the same order of magnitude as crystal lattice constant, X-rays are extremely useful for studying the structural properties of crystals. The photons initially interact with the electrons of atoms when an X-ray beam incident on a substance and scattering them. The intensity distribution that results from the interference of diffracted waves from various atoms is significantly influenced by the contact. If the atoms are organized regularly or periodically throughout, as in crystals, the diffracted waves will have sharp interference maxima (peaks) with the same symmetry as the atom distributed. Thus, we may deduce the distribution of atoms in a substance by measuring the diffraction pattern. It should be noted that X-rays diffracted through elastic scattering only are measured in diffraction experiments. The atomic distance is directly correlated with the peaks in an XRD pattern.

Let us consider the interaction of an incident X-ray beam with periodic atoms, as depicted in the following **Figure 3.15**. The atoms, which are shown in the figure as spheres, can be seen forming several sets of planes inside the crystal. The condition for a diffraction (peak) to occur for a specific set of lattice planes having an inter-plane distance of d can be expressed mathematically as:

$2d\sin\theta = n\lambda$, which is Bragg's law.

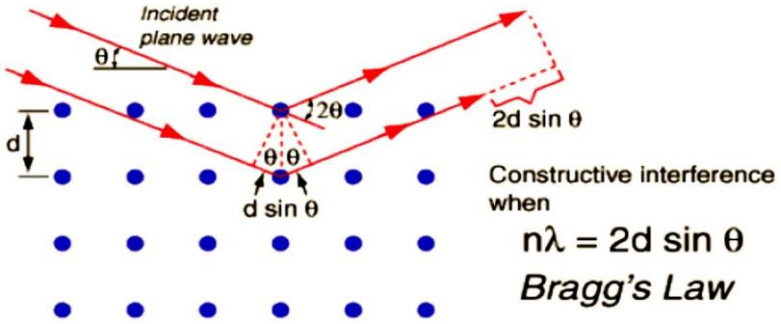

Figure 3.15 Schematic illustration for determining Bragg's law [121].

Where, the scattering angle is θ, the X-ray wavelength is λ, and the diffraction peak order is represented by the number n. One of the most important law, which is used to understand the X-ray diffraction data is the Bragg's Law. According to the law, the only way diffraction is possible when $\lambda<2d$.

Therefore, X-ray diffraction pattern represents a material's unique fingerprint for its periodic atomic arrangements. For a wide range of crystalline materials, fast phase identification is possible by doing an online search for X-ray powder diffraction patterns in a standard or common database.

The following are some uses for XRD:

- Measurement of the effects of strain, micro-strain, or average crystallite size in thin-film as well as bulk samples.
- Measurement of the preferred orientation (texture) in manufactured parts, thin films, and multi-layer stacks.
- Lattice parameter calculation to measure alloy content.
- Crystalline phase identification and measurement.

X-ray diffractometer (D8 Advance, BRUKER, Germany) (**Figure 3.16**) located at Bangladesh Council of Scientific and Industrial Research, Dhaka was used to identify the phases of the sintered sample of this study.

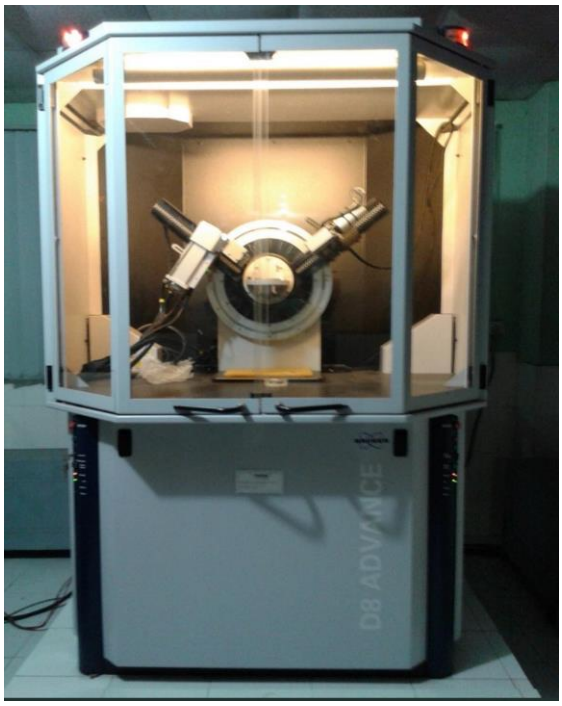

Figure 3.16 X-ray Diffractometer (D8 Advance, BRUKER, Germany).

The data was collected with a step size of 0.02 and an exposure time of each location was 0.6 seconds on the 2θ range from 10° to 90°. The samples were investigated in bulk form. Because of grinding up the bulk sample would result in some tetragonal to monoclinic phase transformation of zirconia at the new fracture surface, powdered samples weren't used. To confirm the presence of the tetragonal zirconia phase, the obtained XRD patterns were then compared with some standard spectra. According to the following equation, the volume fraction of monoclinic zirconia (V_m) was calculated [131].

$$V_m = \frac{I_{(\bar{1}11)m} + I_{(111)m}}{I_{(\bar{1}11)m} + I_{(111)m} + I_{(111)t}} \quad \ldots\ldots\ldots\ldots\ldots\ldots\ldots\ldots \quad (3.7)$$

Where, *I* refer to the integral intensity and the subscripts m and t represent the monoclinic and tetragonal phase, respectively.

"Rietveld profile refinement" is the standard technique used to analyze powder XRD patterns and neutron diffraction data. The technique involves fitting a model's parameters to the measured "whole-profile", which is the intensity measured as a function of scattering angle.

The Rietveld refinement model parameters can be categorized into three general groups and describe various aspects of the profile. First, the parameters that are used to calculate the space group of a crystal, unit cell characteristics, atomic locations, site occupancy, and displacements. The parameters that describe the background come next. The background might come from a variety of sources, including electronic noise, incoherent or inelastic scattering from the sample and its surroundings, and other undesired sources. Because the background scattering changes relatively slowly with scattering angle, the Bragg peaks can usually be separated from the background. The third set of parameters describes how Bragg peaks are shaped. By using the TOPAS software to refine Rietveld the powder XRD patterns, the crystallographic parameters and phase of the composites were quantitatively analyzed in this experiment.

3.5.7 Field Emission Scanning Electron Microscopy (FESEM)

The technique of FESEM imaging is widely used to obtain topographical features, surface morphology, crystal structure, crystal orientation, the presence and position of defects, particle density, etc. In scanning electron microscopy, a field-emission cathode in the electron gun provides narrower probing beams at low and high electron energy, improving spatial resolution and minimizing sample charging and damage. **Figure 3.17** depicts the FESEM that was used to determine the surface morphology of the sintered composites.

During FESEM imaging, electrons are released out from a source and are propelled in a strong electrical field gradient inside a high vacuum column ($10^{-4} \sim 10^{-10}$ torr). Primary electrons are an accelerated beam of monoenergetic electrons with energy between a few hundred eV to tens of keV. An electromagnetic lens is used to focus this beam into a narrow scan beam that bombards the target. Secondary electrons are emitted from every spot of the object. They are detected to generate an electrical signal. A portion of the sample's surface is scanned. The signal that was obtained conveys information details about the sample's morphology. A few of these electrons are elastically scattered from the nucleus Coulomb field.

Figure 3.17 Field Emission Scanning Electron Microscope (Model: JEOL JSM-7610F).

In contrast, some auger or secondary electrons are produced when electrons from host atoms are inelastically scattered. The element from which these auger electrons are emitted can be seen in their characteristics. An electronic signal is generated by a detector when it captures the secondary electrons. An image of this signal that is found from a video scan may be viewed on the display is amplified and transformed. For morphological examinations of the material, the image produced by the FESEM analysis was used. **Figure 3.18** provides a schematic representation of a FESEM's parts.

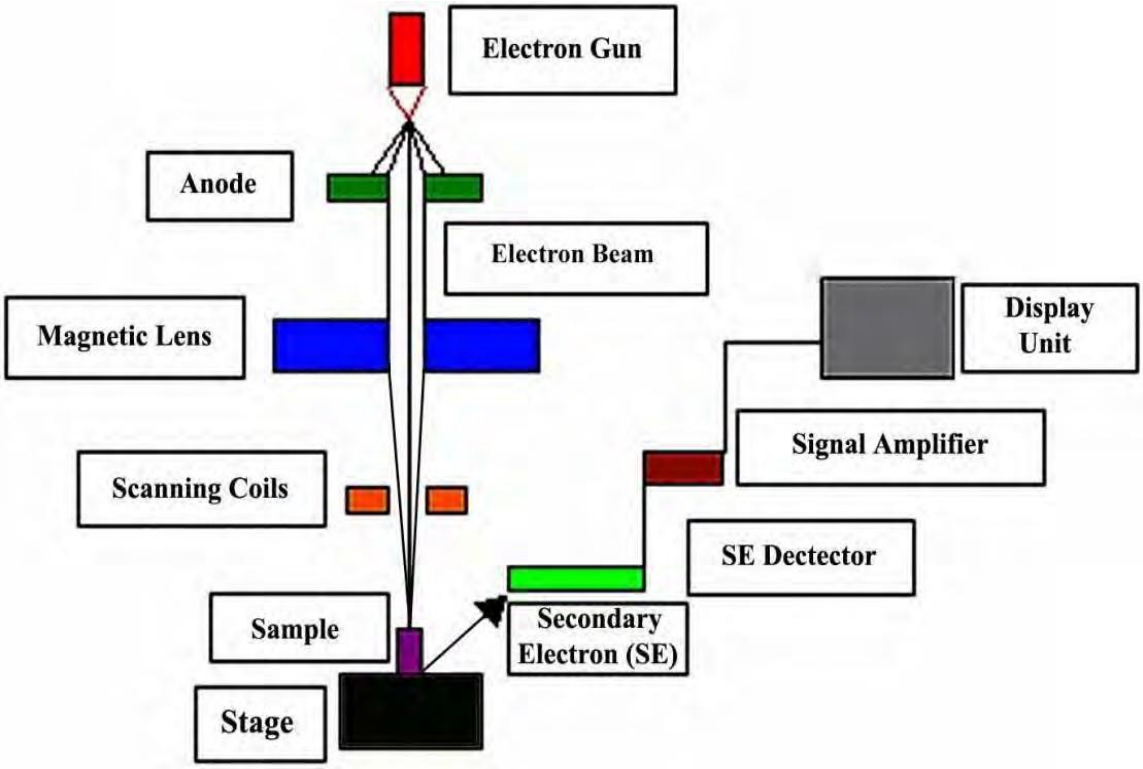

Figure 3.18 Schematic illustration of the parts of an FESEM [132].

3.5.8 Atomic Force Microscopy (AFM)

At the nanoscale, where traditional optical microscopy cannot operate, atomic force microscopy (**Figure 3.19**) can provide 3D images of the specimens. Utilizing a Dimension 3100 scanning probe microscope in contact mode, the topography and friction data of the surface and the wear scar are obtained in this study.

When scanning in contact mode, **Figure 3.20**, constant surface contact is maintained by the probe. When a surface is contacted by the tip, it deflects in a manner that is directly proportional to the normal load on the probe. In this study, a silicon nitride probe with the cantilever specified resonance frequency 17 kHz and force constant 0.08 N/m was used.

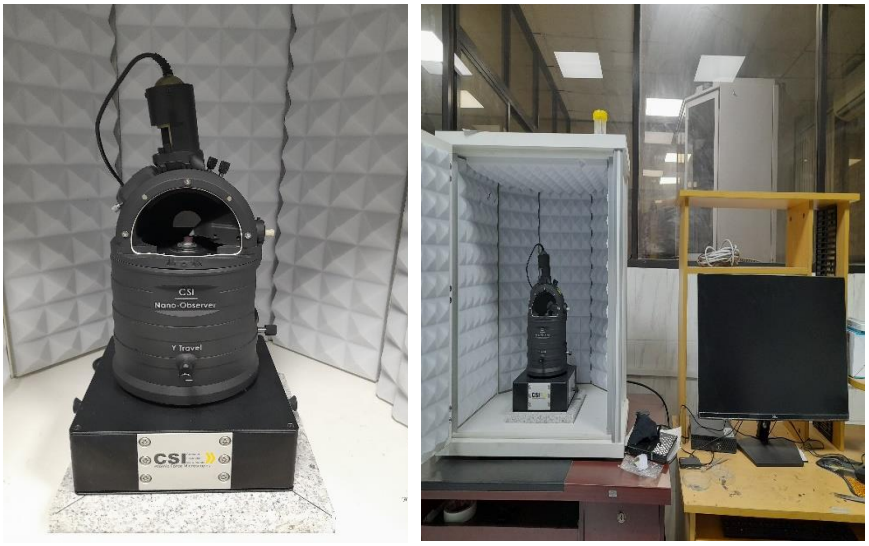

Figure 3.19 Atomic Force Microscopy (CSI-France).

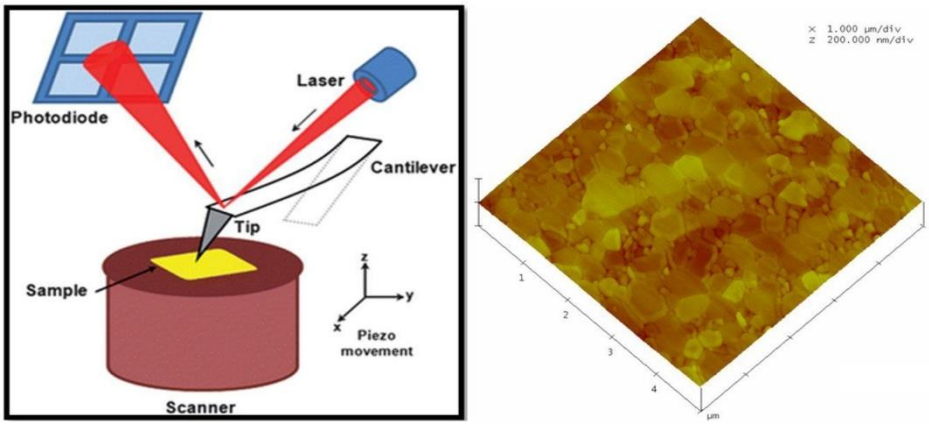

Figure 3.20 Schematic illustration of AFM in contact mode and a 3D image [133].

Cantilevers made of silicon nitride deflect at small loads because of their low spring constant. Through variations in the laser light that are reflected back to a detector in photodiode quadrants, the probe's deflection may be measured. A Z-feedback circuit is used to maintain the cantilever's bending invariable. This circuit's role is to adjust the scanner's vertical position (z) in response to changes in the surface's topography as they occur during scanning.

3.5.9 Thermal Expansion Coefficient

Thermal expansion is an important property that provides an information regarding dimensional change of material with change in temperature. The coefficient of thermal expansion (CTE) describes how a material's length changes with a unit change in temperature. Using a Thermo-Mechanical Analyzer (TMA) in **Figure 3.21** (SII, TMA/SS6300), a thermal expansion analysis of the examined sample is conducted. The co-efficient of thermal expansion (CTE) of the sintered alumina composite materials were measured from room temperature to 500°C at 10°C/min. Each material has a unique thermal expansion value. Thermal expansion study has been conducted for getting the optimum composition in order to observe how the additives influences the characteristics of base material.

Figure 3.21 Schematic illustration of TMA machine (SII, TMA/SS6300).

3.5.10 Electrometer for Electrical Conductivity

In scientific fields like physics, optics, and material science, electrometer/high resistance meter (Model: 6517B, China) (**Figure 3.22**) is used for the measurement of very low current, charge, resistance and voltage. Due to its extremely low voltage burden and simplicity

of use, it is particularly appropriate as a component for solar cell applications. It also has an internally power supply and minimal current sensitivity. Voltage reversal techniques used in the electrometer (Model 6517B) enhance measurements of volume and surface resistivity on nonconductive materials.

Figure. 3.22 Schematic illustration of electrometer/high resistance meter (6517B).

3.5.11 Antimicrobial Susceptibility Test

Antibacterial susceptibility test of the samples was conducted through Kirby-Bauer disk diffusion test and the corresponding zone of inhibition (ZOI) was observed. For the control test parameter, gram negative (Escherichia coli) as well as gram positive (Staphylococcus aureus) bacterial sample of concentration $1.5X10^5$ CFU/ml were taken. Following is the flow chart containing all the specific steps of this test.

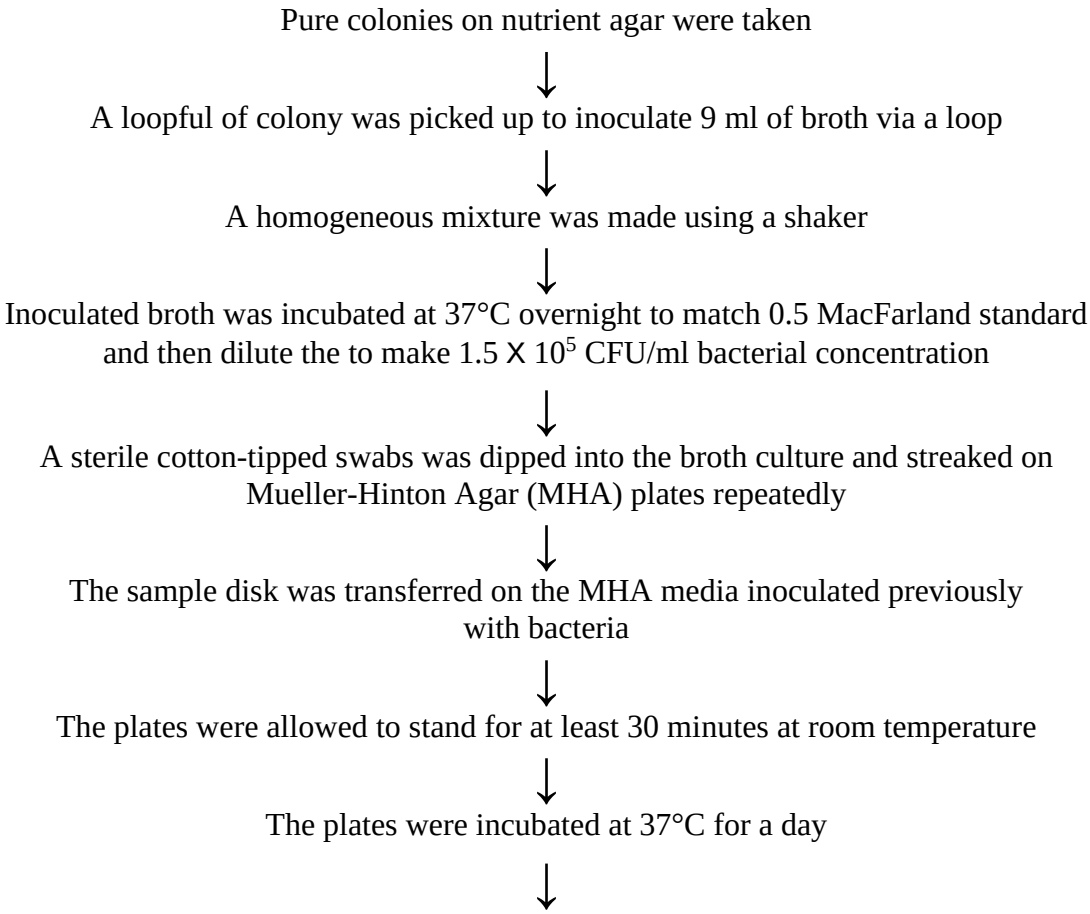

Figure 3.23 The workflow of antimicrobial test.

3.5.12 Cytotoxicity Test/Cell Viability Test

Cytotoxicity test was conducted utilizing Biological Bio safety cabinet (model: NU-400E, Nuaire, USA), CO_2 Incubator (Nuaire, USA), Trinocular microscope with camera (Optika, Italy), Hemocytometer. In brief BHK-21, a baby hamster kidney fibroblast cell line, was maintained in DMEM (Dulbecco's Modified Eagles' medium) with 1% penicillin-streptomycin (1:1) and 0.2% gentamycin and 10% fetal bovine serum (FBS). BHK-21 cells ($3x10^4$/200 µl) were seeded into 48-well plate and incubated at 37°C with 5% CO_2. After 24 hours, 50 µl specimen (sterilized) was further included every single well. After the sample had been incubated for 48 hours, its cytotoxicity effect was examined using an inverted light

microscope. For each sample, duplicate wells were used. The significance of negative control is that it boosts up a situation in which a cell has the full potential for growth and colony formation whereas positive control creates an environment which is completely adverse to the development of cell.

RESULTS AND DISCUSSION

CHAPTER 4
RESULTS AND DISCUSSION

This chapter analyses the research findings and discussions carried out in the experimental work.

4.1 X-ray Diffraction (XRD) Analysis

4.1.1 Phase analysis of the raw materials

The XRD examination was conducted for identifying phases as well as purity verification related to raw materials those were used during this experiment which were: α-Al_2O_3, 3YSZ (3 mol% yttria stabilized zirconia), TiO_2, MgO, CeO_2 and CaO. The following (**Figures 4.1-4.6**) showed the XRD diffraction patterns of these raw powders and ensure their corresponding phases presence in it respectively.

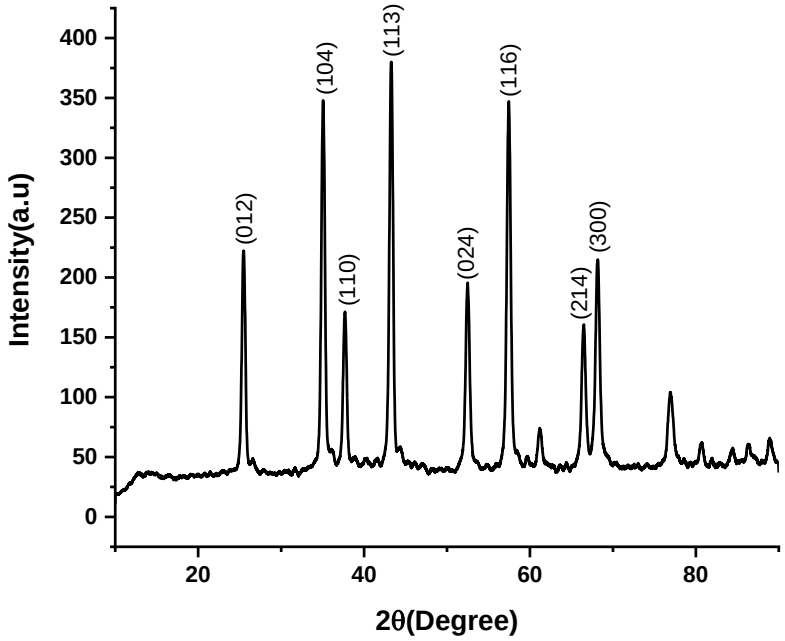

Figure 4.1 XRD diffraction pattern of raw α-Al_2O_3 powder.

Figure 4.1 demonstrates the XRD diffraction pattern of raw alumina that ensures the existence of aluminum oxide or alpha alumina (α-Al_2O_3) in the structure through the ICDD (International Centre for Diffraction Data) Card No. 01-076-8057. The crystalline form with rhombohedral structure is the most stable form of alumina which is called α-Al_2O_3 or corundum. Major characteristics peaks of α-Al_2O_3 were found from three different planes (104), (113), and (116) at different diffraction angles (2θ) of 35.13°, 43.33° and 57.47°, respectively. Its crystallite size was measured to be 23.39 nm as well.

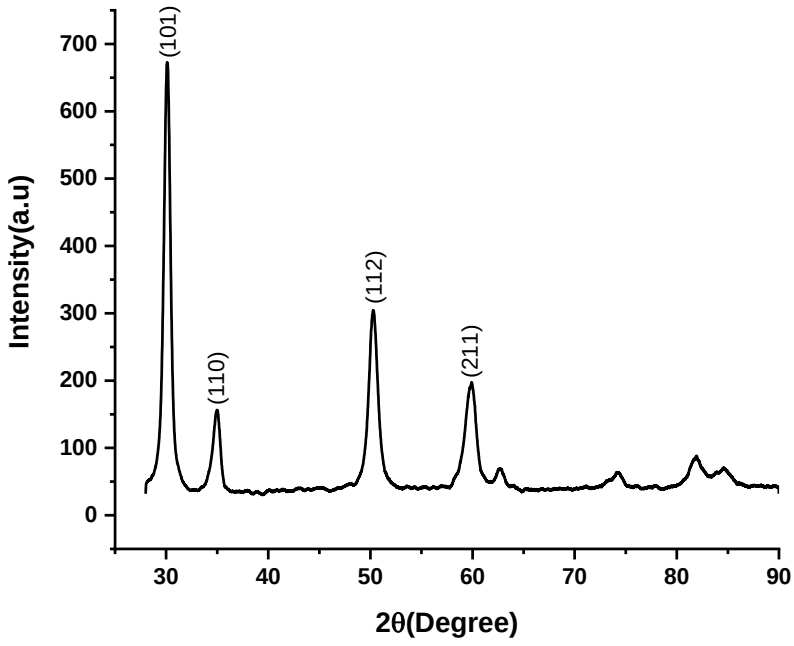

Figure 4.2 An X-ray diffraction graph for raw 3YSZ powder.

Figure 4.2 exhibits an X-ray diffraction curve for raw 3 mol% YSZ that ensures the presence of tetragonal zirconia (t-ZrO_2) in the structure through ICDD Card No. 01-070-4435. The crystalline form consisting monoclinic ZrO_2 is stable with an ambient condition that referred as baddeleyite (m-ZrO_2) and up to 1170°C it is stable in terms of crystal structure. Upon addition more than at 1170°C temperature it transforms crystal structure from monoclinic (m-ZrO_2) to tetragonal (t-ZrO_2) zirconia which is associated with volume change (~5%) up to 2370°C, then t-ZrO_2 transforms into c-ZrO_2 up to 2680°C. Strong characteristic peaks of 3YSZ (t-ZrO_2) were found from three different planes (101), (112), and (211) at different diffraction angles (2θ) of 30.09°, 50.16° and 59.64°, respectively.

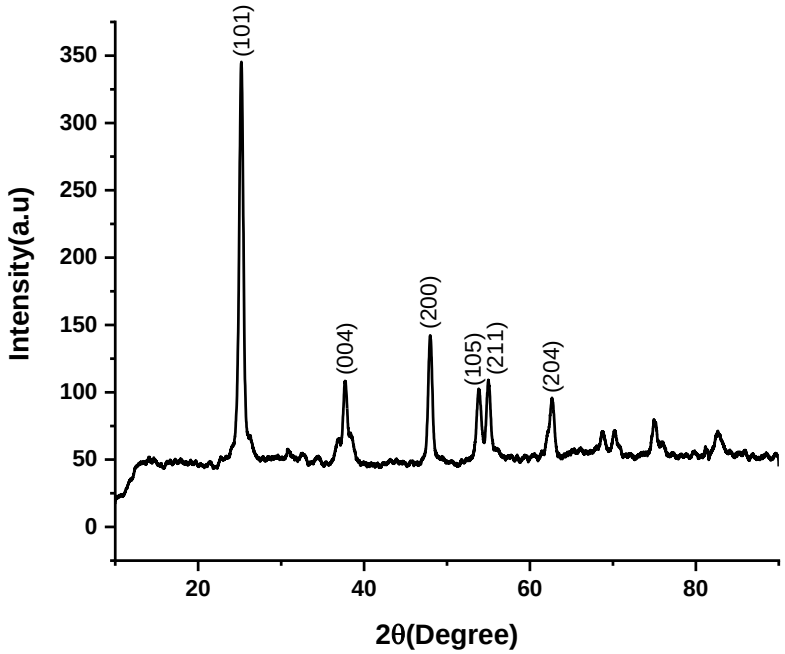

Figure 4.3 An X-ray diffraction curve for raw TiO_2 powder.

Figure 4.3 illustrates an X-ray diffraction graph for raw titanium dioxide or titania that confirms the existence of anatase phase of titania (TiO_2) in the structure through ICDD Card No. 00-021-1272. The crystalline anatase form with tetragonal structure is the stable phase of titanium dioxide at lower temperature. Major characteristics peaks of TiO_2 were indicated from three different planes (101), (200), and (004) at different diffraction angles (2θ) of 25.28°, 48.05° and 37.80°, respectively.

Figure 4.4 exhibits the XRD diffraction pattern of raw magnesium oxide or magnesia that confirms the presence of cubic phase of magnesia (MgO) in the structure through matching with ICDD Card No. 01-071-1176. The diffraction pattern also indicated MgO by the three sharp and strong diffraction peaks appeared at diffraction angles (2θ) of 42.85°, 62.21°, and 78.51° which also correspond to (200), (220), and (222) planes of ceria phases, respectively.

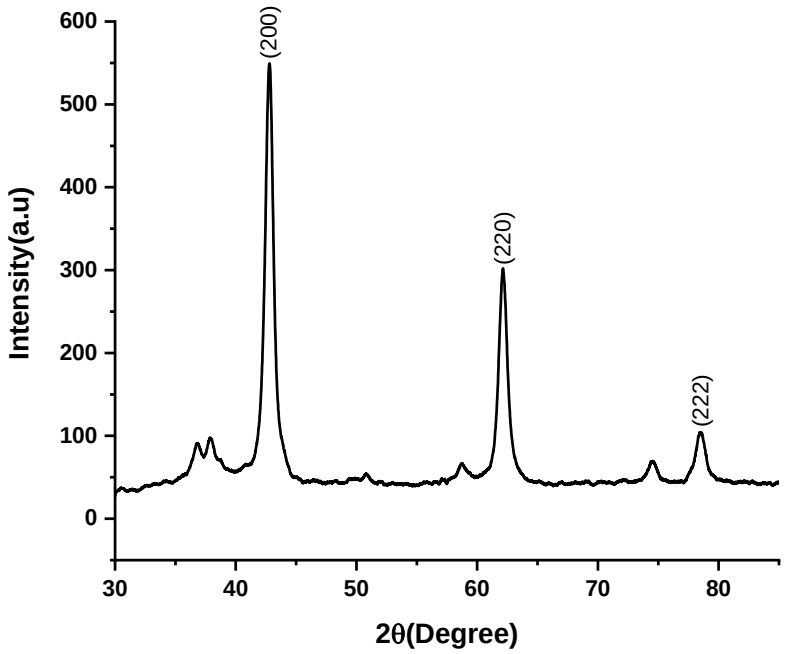

Figure 4.4 XRD diffraction pattern of raw MgO powder.

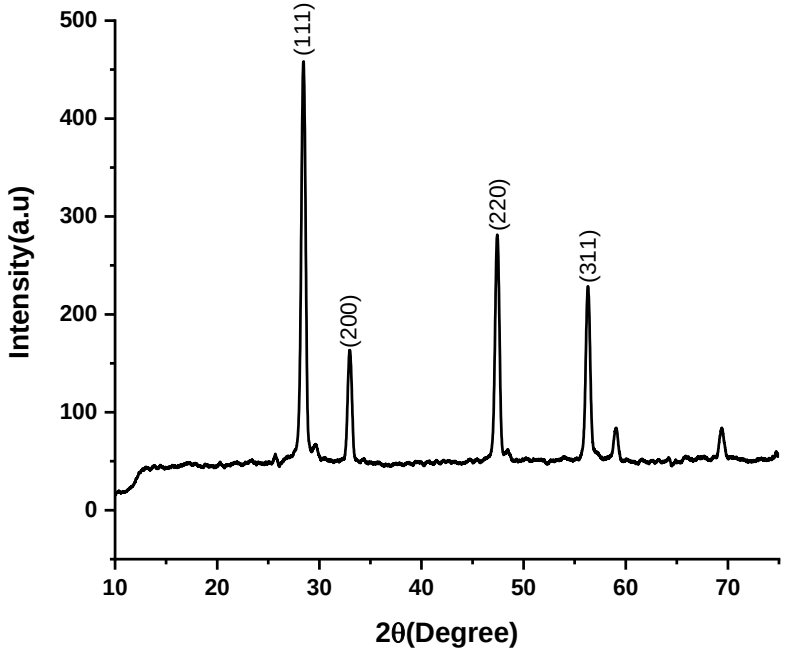

Figure 4.5 XRD diffraction pattern of raw CeO_2 powder.

Figure 4.5 displays XRD pattern of raw cerium oxide or ceria which confirms the presence of cubic ceria (CeO_2) phase in the structure by matching with ICDD File No. 01-075-9470. The diffraction pattern also indicated CeO_2 by the three sharp and strong diffraction peaks showed at diffraction angles (2θ) of 28.54°, 47.48°, and 56.34° which correspond to (111), (220), and (311) planes, respectively.

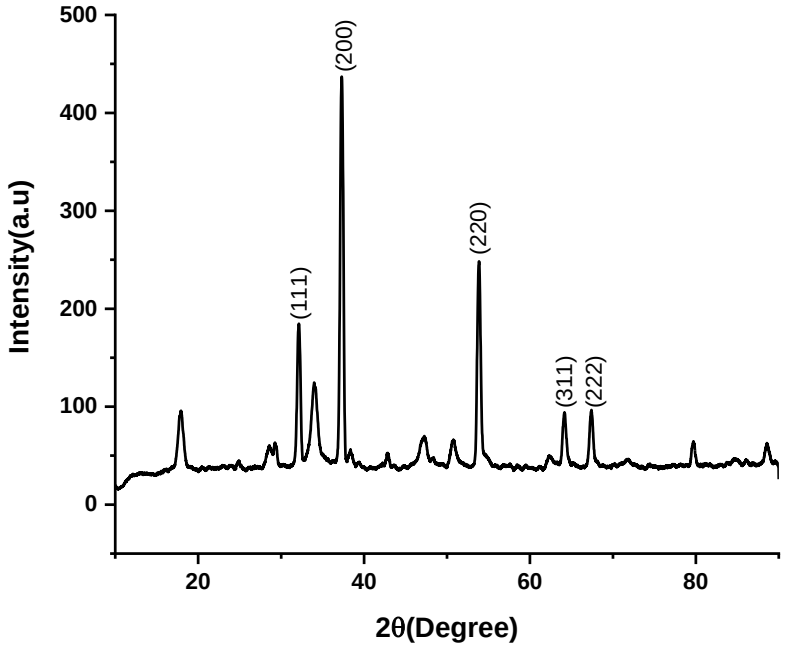

Figure 4.6 An X-ray diffraction pattern for raw CaO powder.

Figure 4.6 reveals X-ray diffraction pattern for raw calcium oxide or calcia which confirms the presence of cubic calcia (CaO) phase in the structure by matching with ICDD File No. 01-070-5490. The diffraction pattern also indicated CaO by three sharp and strong diffraction peaks appeared at diffraction angles (2θ) of 37.31°, 53.80°, and 32.17° which are also assigned to (200), (220), and (111) planes of calcia phase, respectively.

From XRD pattern analysis, the crystal properties of raw materials and their semi quantitative data are summarized in **Table 4.1**.

Table 4.1 Crystal properties and semi quantitative data of the raw materials.

Sl. No	Compd. name	Crystal structure	Space group	Lattice parameter	M.W	Vol.	Major peaks		
							2θ (°)	plane	d-spacing (Å)
01	α-Al_2O_3	Rhombohedral/ Trigonal	R-3c (167)	a- 4.7597 c-12.9935	101.96	254.93	35.132	104	2.55229
							43.333	113	2.08637
							57.470	116	1.60227
02	YSZ	Tetragonal	P42/nmc (137)	a- 3.6286 c-5.1371	121.46	67.64	30.096	101	2.96698
							50.161	112	1.81722
							59.639	211	1.54905
03	TiO_2	Tetragonal	141/amd (141)	a- 3.7852 c-9.5139	79.90	136.31	25.281	101	3.52
							48.05	200	1.89
							37.801	004	2.378
04	MgO	Cubic(fcc)	Fm-3m (225)	a- 4.217	40.30	74.99	42.856	200	2.1085
							62.217	220	1.49093
							78.51	222	1.21734
05	CaO	Cubic(fcc)	Fm-3m (225)	a- 4.8152	56.08	111.65	28.548	111	3.12422
							47.485	220	1.91318
							56.344	311	1.63157
06	CeO_2	Cubic(fcc)	Fm-3m (225)	a- 5.4113	172.12	158.45	37.319	200	2.4076
							53.805	220	1.70243
							32.172	111	2.78006

4.1.2 Phase and structural analysis of the sintered composite materials with variation of CaO content

The X-ray diffraction graphs of sintered ceramics adding 5 wt.% CeO_2 and (1-5 wt.%) CaO which also sintered at 1450°C, 1500°C, 1600°C and 1650°C are presented in the following **Figures (4.7-4.11)**, respectively.

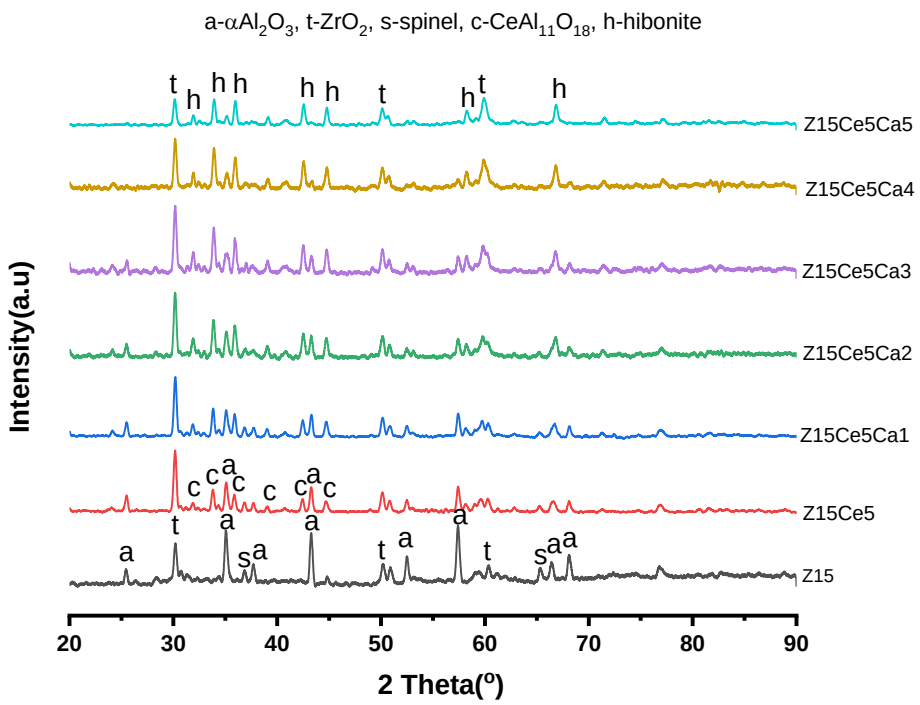

Figure 4.7 XRD diffractograms of Z15 (ZTA-TiO_2-MgO) sintered ceramic composite containing CeO_2 (5 wt.%) and CaO (1-5 wt.%) at 1450°C.

The XRD diffractograms of the Z15 (ZTA-TiO_2-MgO) sintered ceramic composite with CeO_2 (5 wt.%) and CaO (1-5 wt.%) at 1450°C are shown in **Figure 4.7**. The major diffraction peaks might be indexed as α-Al_2O_3 (designated as 'a', ICDD card number: 01-076-8057) and yttria stabilized zirconia or YSZ (designated as 't', ICDD card number: 01-070-4435), according to XRD patterns. Additionally, three secondary phases have been identified as hibonite ($CaAl_{12}O_{19}$) (marked as 'h', ICDD card No. 00-038-0470), cerium aluminate ($CeAl_{11}O_{18}$) (designated as 'c', ICDD Card No. 00-048-0055), and spinel ($MgAl_2O_4$) (designated as 's', ICDD Card No: 01-070-6979).

The analysis revealed that XRD pattern for ZTA-TiO_2-MgO without CeO_2 and CaO showed prominent diffraction peaks for alpha alumina (corundum) as well as t-ZrO_2 (YSZ) phases with spinel ($MgAl_2O_4$) as secondary phase. Cerium aluminate ($CeAl_{11}O_{18}$), a new phase formed by the addition of 5 wt.% CeO_2 to ZTA ceramics. With the formation of $CeAl_{11}O_{18}$, the peak strength of α-Al_2O_3 declined. Then, after addition of 1 wt.% CaO, another new phase known

as hibonite ($CaAl_{12}O_{19}$) is formed. In case of ZTA composites, peak intensity of hibonite ($CaAl_{12}O_{19}$) phase increased proportionately with the gradual addition of CaO from 1 to 5 wt.%. Conversely, as hibonite ($CaAl_{12}O_{19}$) phase increased with CaO, the peak intensity of α-Al_2O_3 decreased. Additionally, it was also found that as the CaO content increased, the cerium aluminate ($CeAl_{11}O_{18}$) phase decreased. Similar findings were revealed by SKtani et al. whose XRD results demonstrated that the peak intensity of α-Al_2O_3 decreased as a result of the development of the hibonite ($CaAl_{12}O_{19}$) phase in ZTA ceramics [134].

It was noted that 1 mole of Ca^{2+} ions and 12 moles of Al^{3+} ions are needed for the formation of 1 mole of the hibonite ($CaAl_{12}O_{19}$) compound. Therefore, the concentration of alpha alumina (Al_2O_3) decreases noticeably until there is no longer any α-Al_2O_3 in the peak of ZTA-TiO_2-MgO ceramics as demonstrated by the addition of 5 wt.% of CaO (**Table 4.2**). Other secondary phases like spinel ($MgAl_2O_4$) and cerium aluminate ($CeAl_{11}O_{18}$) also contained Al^{3+} ions which directly attributed to the lower concentration of ceramic composites. In all samples, the overall concentration of YSZ phase is almost constant. Full Pattern Matching (FPM) quantitative measurement, as shown in **Table 4.2**, was used to obtain these observations.

The expanded diffraction pattern between 31.5° to 34.5° of 2θ angles that illustrates peak shifting is shown in the **Figure 4.8**. The peak, $CeAl_{11}O_{18}$, was initially denoted by the 'c' since it could be seen in the sample with CeO_2 (5 wt.%) and CaO concentration at 1 wt.%. The gradual reduction of CeO_2 to Ce_2O_3 in the ZTA-TiO_2-MgO ceramics was used to explain the existence of the $CeAl_{11}O_{18}$ phase [135]. This phenomenon happens when Ce^{4+} ions having ionic radius of 0.97Å change into Ce^{3+} ions which have an ionic radius of 1.143Å [136]. The $CeAl_{11}O_{18}$ phase was gradually replaced by the $CaAl_{12}O_{19}$ phase as the concentration of CaO reached 3 wt.%. Ce^{4+} ions are replaced by Ca^{2+} ions, as evidenced by a significant transformation to $CaAl_{12}O_{19}$ from $CeAl_{11}O_{18}$ phase. The incorporation of Ca^{2+} ions into $CeAl_{11}O_{18}$'s lattice structure would increase the materials lattice parameters and cause a minor peak shift to the high 2θ angles. The peaks (110) and (107) changed its 2θ angles from 31.878°, 33.929° (at 0 wt.% CaO) to 32.185°, 34.156° (at 5 wt.% CaO) as a result of the phase transition.

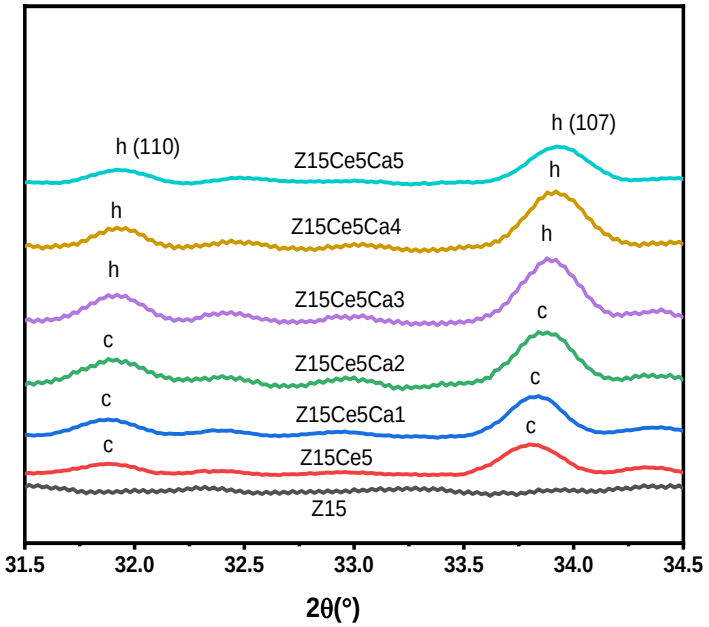

Figure 4.8 Expanded XRD diffractograms of **Figure 4.7** at 2θ angles from 31.5° to 34.5°.

The Bragg's law states that this lattice parameter slight increase indicates that the Ce^{3+} ion formed a solid solution in ZTA-TiO_2-MgO ceramics, particularly for the $CaAl_{12}O_{19}$ phase because ionic radius of Ce^{3+} is relatively close to Ca^{2+} (Ce^{3+}: 1.143Å and Ca^{2+}: 1.12Å), suggesting that this solid solution specifically formed in the $CaAl_{12}O_{19}$ phase. Yin et al. [137] state that the space surrounding the Ce^{3+} ion in the lattice is sufficiently large to permit ionic substitution by doping with other metal cations that have a larger radius. In order to balance the charges during this substitution reaction, oxygen is released resulting in a solid solution of substitution between CeO_2 and CaO [138].

Besides, the full pattern matching (FPM) from EVA and TOPAS softwares were used to perform the comprehensive phase quantification at 2θ angles from 10° to 90° and the results were recorded (**Table 4.2**). Phase percentages (%) are used to indicate the presence of phases formed from ZTA-TiO_2-MgO ceramics with varying CaO content (wt.%). According to the quantification results, the addition of 1 wt.% CaO critically decreased the $CeAl_{11}O_{18}$ phase percentage from 35.30% to 24.10%. A significant percentage (19.40%) of a new phase of $CaAl_{12}O_{19}$ was also formed at the same time. The transition from $CeAl_{11}O_{18}$ to $CaAl_{12}O_{19}$ phases was demonstrated by the addition of 3 wt.% CaO. The $CeAl_{11}O_{18}$ phase was seen to decrease from 0.9% to 0.1% and then with CaO additions (3 wt.% to 5 wt.%).

The phase percentage of α-Al_2O_3 was correspondingly decreased with further CaO addition. The α-Al_2O_3 phase was no longer present in the ceramics at the highest amount of CaO (5 wt.%) due to the complete consumption of Al^{3+} ion for the formation of $CaAl_{12}O_{19}$.

On the other hand, addition of CaO also decreased the phase percentages of spinel as formation of hibonite phases require more Al^{3+} ions than spinel. Basically, hibonite is a multiple oxide mineral with chemical formula (Ca, Ce) (Al, Ti, $Mg)_{12}O_{19}$ which has mainly calcium aluminate ($CaAl_{12}O_{19}$) with small amount of calcium (Ca) replaced by cerium (Ce) and aluminum replaced by titania (Ti) or magnesium (Mg). Moreover, TiO_2 works as a sintering aid and stabilizing agent, it prevents baddeleyite (m-ZrO_2) formation from YSZ (t-ZrO_2) and the abnormal grain growth of α-Al_2O_3. It was indicated from the slightly change in the phase % of the YSZ phase that the addition of CaO had no effect on this phase.

Table 4.2 Phase quantification of ZTA-TiO_2-MgO ceramic composites with CeO_2 (5 wt.%) and (1-5 wt.%) of CaO.

CaO	CeO_2	Phase percentages (%)				
Wt.%	Wt.%	α-Al_2O_3	YSZ	$MgAl_2O_4$	$CeAl_{11}O_{18}$	Hibonite
0	0	79.60	5.08	15.30	0.00	0.00
0	5	49.60	5.58	9.60	35.30	0.00
1	5	43.40	3.58	9.30	24.10	19.40
2	5	30.80	5.05	1.0	15.90	48.20
3	5	22.70	4.83	0.8	0.9	70.70
4	5	14.00	5.24	0.5	0.4	79.80
5	5	0.00	6.65	0.2	0.1	93.05

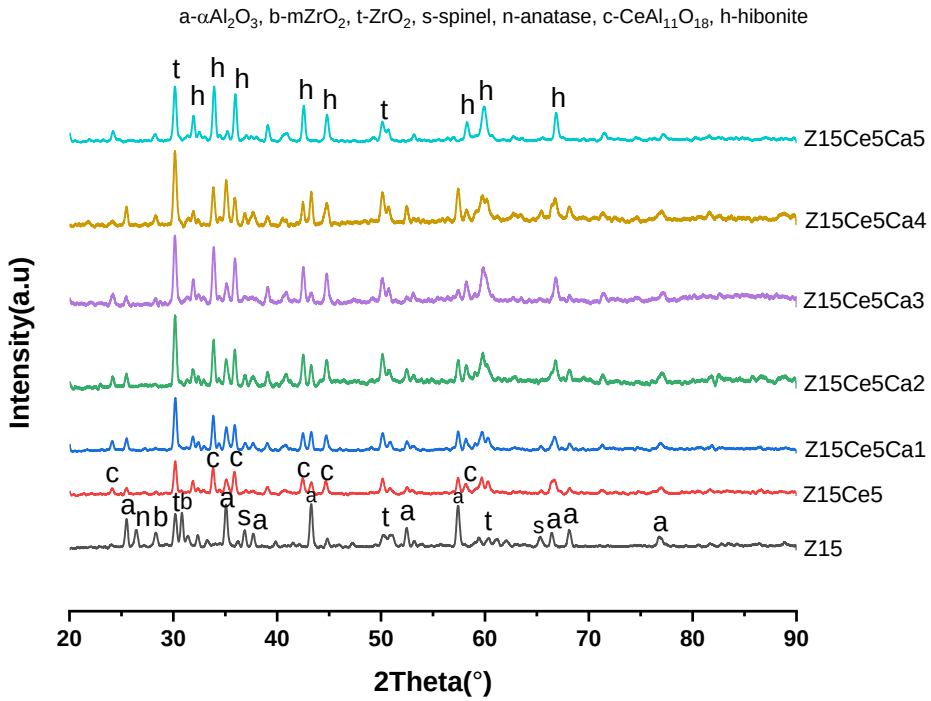

Figure 4.9 XRD diffractograms of Z15 (ZTA-TiO_2-MgO) composite containing CeO_2 (5 wt.%) and CaO (1-5 wt.%) at 1500°C.

Figure 4.9 shows the effect of CeO_2 and CaO content on ZTA-TiO_2-MgO ceramic composite at 1500°C. It can be found from that the major diffraction peaks can be marked as α-Al_2O_3, YSZ (t-ZrO_2), baddeleyite (m-ZrO_2), spinel ($MgAl_2O_4$), and anatase (TiO_2) from ZTA-TiO_2-MgO composites. Moreover, with the addition of CeO_2 (5 wt.%) formed a new phase cerium aluminate ($CeAl_{11}O_{18}$). Then gradual addition of CaO (1-5 wt.%) formed another new phase hibonite ($CaAl_{12}O_{19}$). As the phase percentages of hibonite increases with CaO, the phase percentages of α-Al_2O_3, m-ZrO_2, and spinel decreases simultaneously. All alumina (α-Al_2O_3) transformed into hibonite phases for the addition of maximum amount of CaO (5 wt.%) to ZTA-TiO_2-MgO ceramics. Besides, the phase percentage of YSZ (t-ZrO_2) remain almost same.

Many researchers suggest that the availability of YSZ (tetragonal zirconia) in ceramics ascertained to increase fracture toughness property through applying transformation toughening mechanism [139, 140, 141, 142].

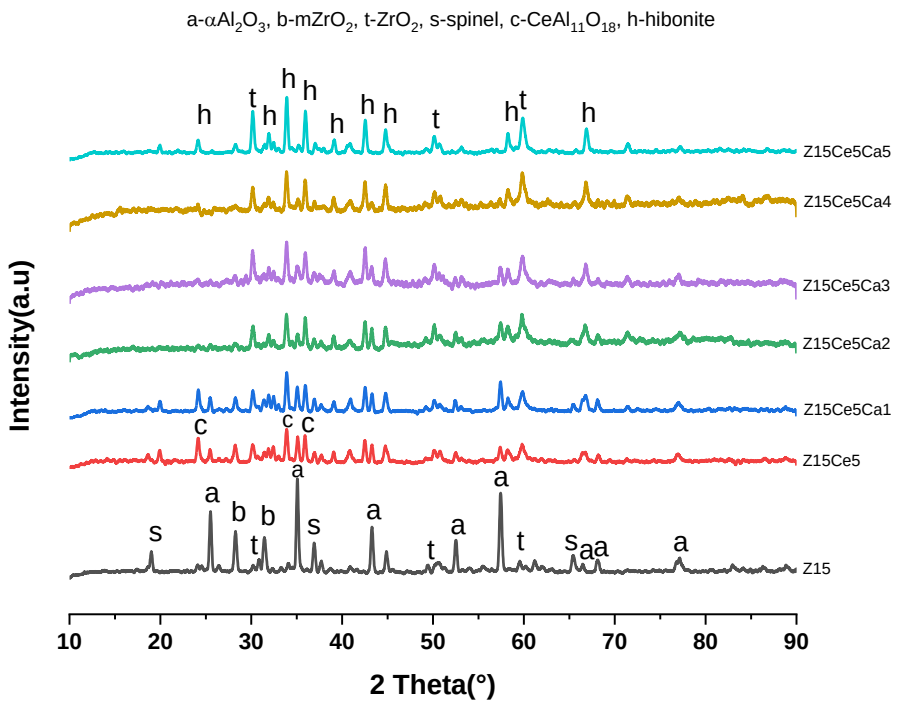

Figure 4.10 XRD diffractograms of Z15 (ZTA-TiO_2-MgO) composite containing CeO_2 (5 wt.%) and CaO (1-5 wt.%) at 1600°C.

Figure 4.10 exhibits the effect of CeO_2 and CaO content on ZTA-TiO_2-MgO ceramic composite at 1600°C. It can be found from that the major diffraction peaks can be identified as α-Al_2O_3, YSZ (t-ZrO_2), baddeleyite (m-ZrO_2), and spinel ($MgAl_2O_4$) in ZTA-TiO_2-MgO ceramics. Addition of CeO_2 (5 wt.%) formed cerium aluminate ($CeAl_{11}O_{18}$) phase. Then gradual addition of CaO (1-5 wt.%) formed another new phase hibonite ($CaAl_{12}O_{19}$). As the phase percentages of hibonite increases with CaO, the phase percentages of α-Al_2O_3, m-ZrO_2, and spinel decreases simultaneously. All alumina (α-Al_2O_3) transformed into hibonite phases for the addition of maximum amount of CaO (5 wt.%) to ZTA-TiO_2-MgO ceramics. Besides, at 1600°C, the peak intensity and phase quantities of YSZ (tetragonal zirconia) decreases as well as of baddeleyite (monoclinic zirconia) increases compared to lower sintering temperatures like 1450°C and 1500°C. This is due to the longer cooling rate pattern and formation of glassy phases of sintering cycle.

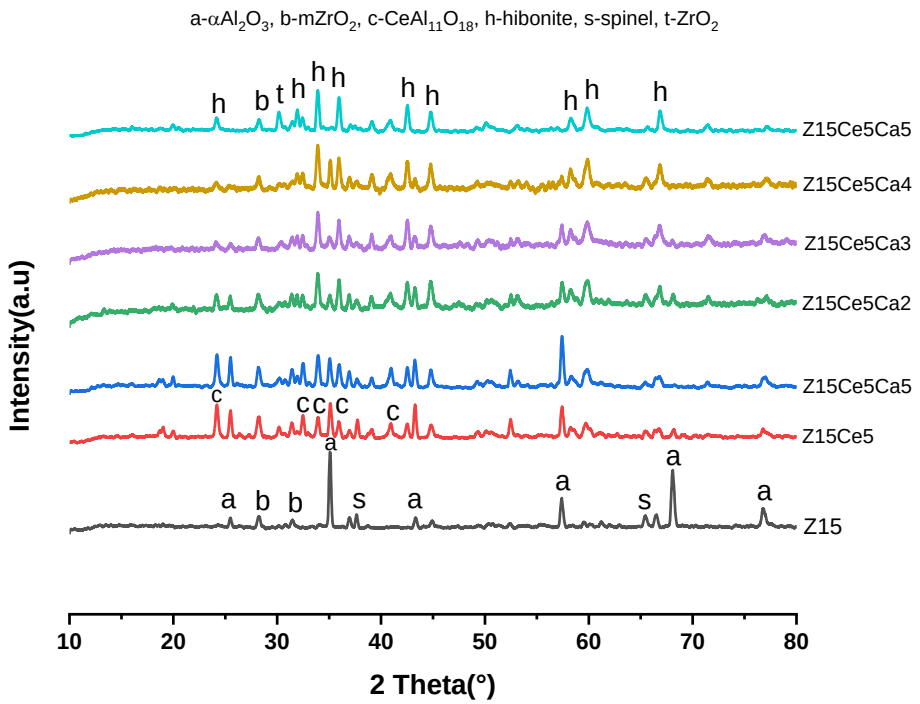

Figure 4.11 XRD diffractograms of Z15 (ZTA-TiO_2-MgO) composite containing CeO_2 (5 wt.%) and CaO (1-5 wt.%) at 1650°C.

Figure 4.11 represents the effect of CeO_2 and CaO content on ZTA-TiO_2-MgO ceramic composite at 1650°C. It can be observed from that the major diffraction peaks can be identified as α-Al_2O_3, baddeleyite (m-ZrO_2), and spinel ($MgAl_2O_4$) in ZTA-TiO_2-MgO ceramics. Addition of CeO_2 (5 wt.%) formed cerium aluminate ($CeAl_{11}O_{18}$) phase. Then gradual addition of CaO (1-5 wt.%) formed another new phase hibonite ($CaAl_{12}O_{19}$). As the phase percentages of hibonite increases with CaO, the phase percentages of α-Al_2O_3, and spinel decreases simultaneously. All alumina (α-Al_2O_3) transformed into hibonite phases for the addition of maximum amount of CaO (5 wt.%) to ZTA-TiO_2-MgO ceramics. Besides, the phase percentage of m-ZrO_2 remain almost same. On the other hand, at 1650°C the peak intensity and phase percentages of YSZ (t-ZrO_2) decreases and of m-ZrO_2 increases compared to lower sintering temperatures like 1450°C and 1500°C as well. This is due to the longer cooling rate pattern and formation of glassy phases of sintering cycle.

4.1.3 Phase analysis of the composite materials with variation of sintering temperature

In the following **Figures** (**4.12-4.15**), the XRD patterns show the effect of sintering temperature on ZTA-TiO_2-MgO ceramics and with the addition of CeO_2 (5 wt.%) and CaO (1-5 wt.%) to it.

It was found that for the same amount of YSZ (t-ZrO_2), TiO_2 (5 wt.%) and MgO (5 wt.%) in ZTA-TiO_2-MgO ceramics shown in **Figure 4.12**, the peak intensity and phase percentage of baddeleyite (monoclinic zirconia) increased as well as tetragonal zirconia decreased with an increase in sintering temperature. From the microstructure analysis, it was observed that the grain size of ZrO_2 is increased with sintering temperature [143]. Therefore, the increase in m-ZrO_2 phase and simultaneously decrease in t-ZrO_2 phase may be explained by a rapid increase in grain size of ZrO_2 phase and long cooling rate pattern of sintering cycle.

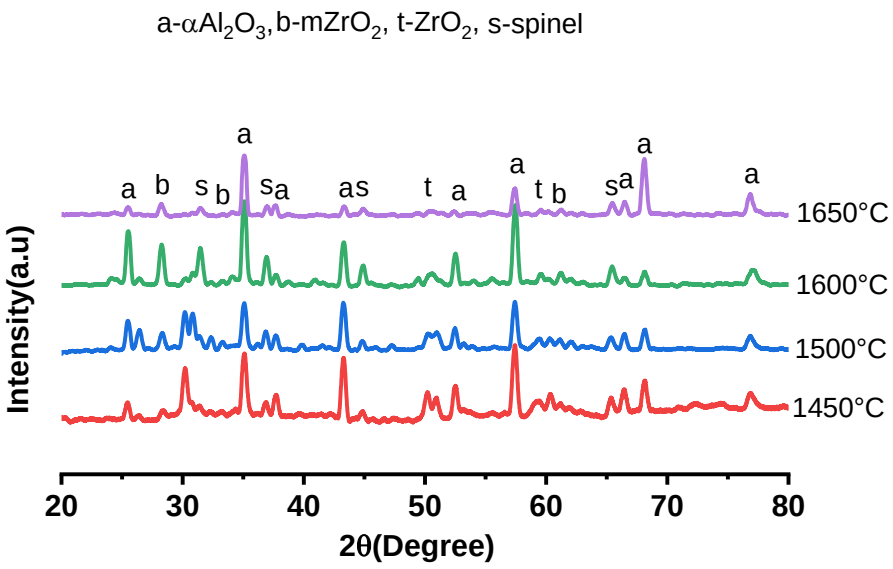

Figure 4.12 XRD diffractograms of Z15 (ZTA-TiO_2-MgO) composite at different sintering temperatures.

a-αAl_2O_3, t-ZrO_2, b-mZrO_2, s-spinel, c-$CeAl_{11}O_{18}$.

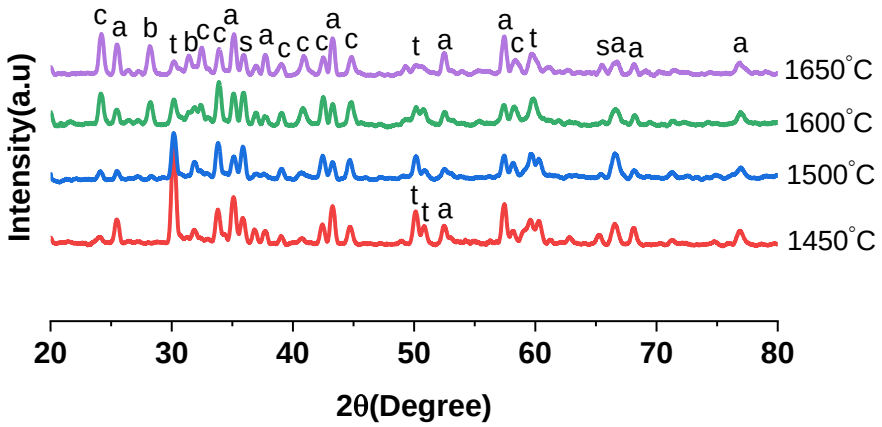

Figure 4.13 XRD diffractograms of Z15Ce5 (ZTA-TiO_2-MgO-CeO_2) composite at different sintering temperatures.

a-αAl_2O_3, t-ZrO_2, b-mZrO_2, s-spinel, h-hibonite,c-$CeAl_{11}O_{18}$.

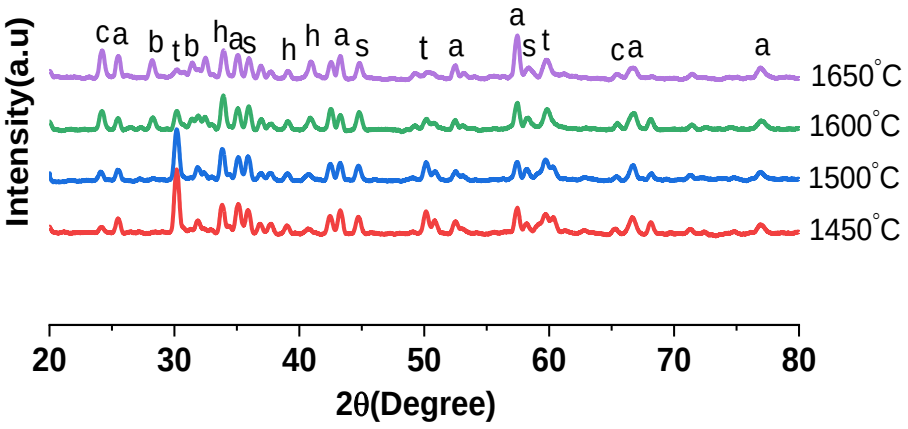

Figure 4.14 XRD diffractograms of Z15Ce5Ca1 (ZTA-TiO_2-MgO-CeO_2-CaO) composite at different sintering temperatures.

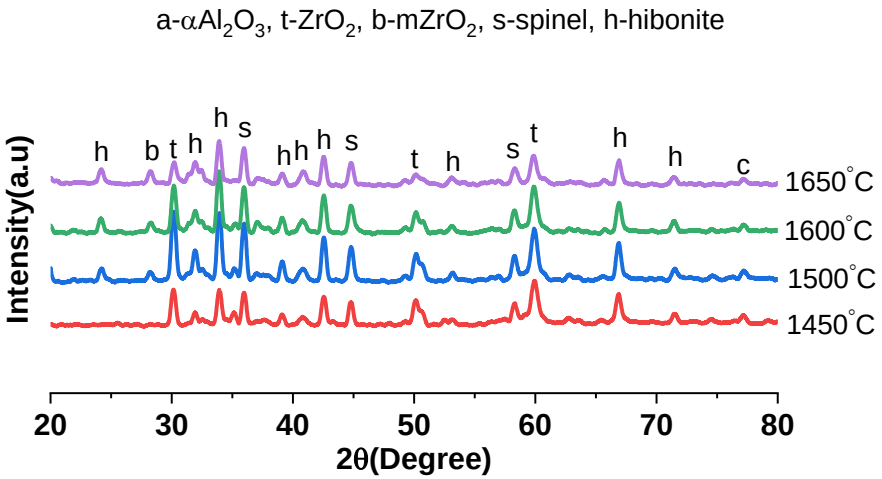

Figure 4.15 XRD diffractograms of Z15Ce5Ca5 (ZTA-TiO_2-MgO-CeO_2-CaO) composite at several sintering temperatures.

A secondary phase spinel ($MgAl_2O_4$) with cubic structure was also increased with sintering temperature up to 1650°C. Previous research conducted by Podzorova et al. observed the formation of secondary phase spinel in ZTA-CeO_2-MgO ceramic composites [144]. Addition of CeO_2 and CaO in ZTA-TiO_2-MgO ceramics formed another two secondary phases like cerium aluminate ($CeAl_{11}O_{18}$) and hibonite ($CaAl_{12}O_{19}$), those are increases with increasing sintering temperature up to 1500°C then decreases for further increase in temperature, that have been shown in **Figures 4.13, 4.14,** and **4.15**.

Using XRD data there have been determined the semi quantitative analysis (SQA), crystallite size and lattice parameters presented in the following **Tables 4.3-4.5**.

Table 4.3: Semi quantitative analysis (SQA) found from XRD data analysis through Rietveld analysis using EVA and TOPAS softwares.

Ts (°C)	Phases	Z15	Z15Ce5	Z15Ce5Ca1	Z15Ce5Ca2	Z15Ce5Ca3	Z15Ce5Ca4	Z15Ce5Ca5
	Al_2O_3	79.6	49.6	43.4	30.8	22.7	14	0
	t-ZrO_2	5.08	5.58	3.58	5.05	4.83	5.24	6.65
1450	s	15.3	9.6	9.3	0	0	0	0
	c	0	35.3	0	0	0	0	0
	h	0	0	43.5	64.1	72.4	80.7	93.35
	Al_2O_3	67.2	27.2	33.5	30	10.7	38.7	0
	tZrO_2	3.03	4.06	4.75	5.01	5.11	4.28	4.47
	m-ZrO_2	8.78	0	0	0	2.3	4.4	0
1500	s	13.7	0	0	0	0	7.1	4.8
	n	7.27	0	3.26	3.7	1.8	0	2.6
	c	0	68.7	0	0	0	0	0
	h	0	0	58.5	61.3	80.1	45.5	88.1
	Al_2O_3	68.2	27.6	31.2	22.2	24	7.7	0
	t-ZrO_2	0.77	1.96	1.68	2.50	3.61	2.74	3.38
	m-ZrO_2	10.24	8.5	6.61	5.2	0	0	4.69
1600	s	20.80	6.2	6.8	5.1	5.7	0	7.8
	n	0	6.6	4.35	0	0	0	0
	c	0	49.1	0	0	0	0	0
	h	0	0	49.4	65.1	66	89.6	84.1
	Al_2O_3	69.4	56.1	35.3	26.5	20.8	13	6.8
	t-ZrO_2	0.50	1.24	0	0.58	0.40	0	1.77
	m-ZrO_2	8.0	8.5	7.27	5.6	7.0	7.9	8.3
1650	s	22.1	11.1	8.9	11.1	9.4	0	0
	n	0	1.0	6.6	3.4	0	0	3.6
	c	0	22	0	0	0	0	0
	h	0	0	39.4	52.8	62.5	79	79.5

Table 4.4: Crystallite size of α-Al_2O_3 estimated from XRD data analysis.

CaO (wt.%)	CeO_2 (wt.%)	Crystallite size, nm			
		1450°C	1500°C	1600°C	1650°C
0	0	41.5	45.8	54.0	51.6
0	5	46.4	49.2	52.0	64.0
1	5	51.9	54.0	51.0	54.2
2	5	54.9	51.0	49.0	50.2
3	5	95.0	110	42.4	44.0
4	5	120	43.1	41.0	40.2
5	5	-	-	-	60.0

Table 4.5 Lattice parameters of α-Al_2O_3/hibonite estimated from XRD data analysis.

CaO (wt.%)	CeO_2 (wt.%)	Lattice parameters, α-Al_2O_3/hibonite	
		a [Å]	c [Å]
0	0	4.7597	12.9947
0	5	4.7590	12.9980
1	5	4.7600	12.9910
2	5	4.7617	13.0030
3	5	4.7634	12.9890
4	5	4.7600	13.0170
5	5	5.5880	22.0260

4.2 Mechanical Properties

The presence of three different secondary phases ($MgAl_2O_4$, $CeAl_{11}O_{18}$, and $CaAl_{12}O_{19}$), as revealed by XRD analysis, is mainly responsible for the changes in ZTA ceramics properties when four different additives (TiO_2, MgO, CeO_2, and CaO) were introduced simultaneously. The amount and grain morphologies of these secondary phases

gradually changed with the addition of CaO, as shown in the microstructure (**Figure 4.25-4.28**). Due to the presence of these three secondary phases, properties of bulk density, porosity, relative density, volume shrinkage, Vickers microhardness, fracture toughness, and diametral tensile strength varied.

4.2.1 Density

Powdered particle densification is a thermally assisted phenomena which carried out through sintering at various temperatures. Thermal energy helps the atoms in diffusion that leads to the development of bonds between nearby particles. More and more contact sites between the particles are formed owing to continuous heat energy supply, and the porosity in between diffuses away from the contact region. As a result, there is a significant increase in density. In the interim, the current grains within the particle have a chance to expand in order to reduce the system's overall energy. As a result, densification and grain growth happen at the same time. The phase transition of tetragonal to monoclinic zirconia near 950°C during cooling has an effect on ZTA ceramics' density as well. The density of the composite increases as more of the tetragonal phase is retained in the structure.

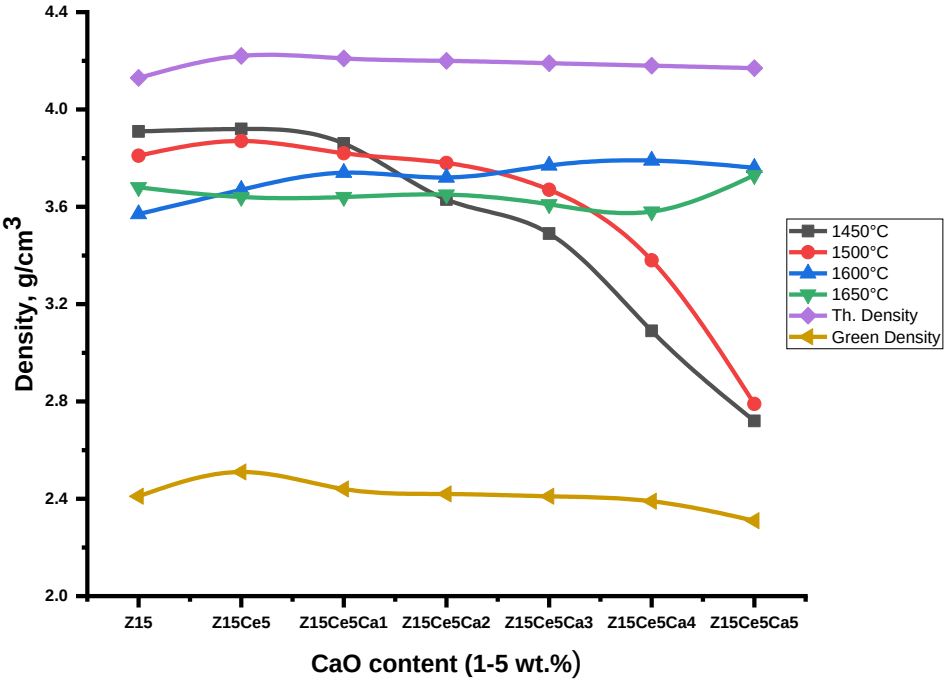

Figure 4.16 Bulk densities of Z15 (ZTA-TiO_2-MgO), Z15Ce5 with various contents of CaO.

Figure 4.16 shows the bulk density curves of ZTA-TiO_2-MgO ceramics with addition of CeO_2 (5 wt.%) and CaO (1-5 wt.%) gradually. The upper curve represents the theoretical density and the lower curve represents the green density of the ceramic composites. The curves between the theoretical and green densities represent bulk density for those ceramics. Initially, bulk density of ceramic composites increases with addition of CeO_2, as its density (7.13 g/cm^3) is higher than the base material α-Al_2O_3 (3.97 g/cm^3). It also decreases porosity. Among them, the sample with 5 wt.% CeO_2 had the highest bulk density value (3.92 g/cm^3) when the sintering temperature was 1450°C. However, addition of CeO_2 (5 wt.%) formed secondary phase cerium aluminate ($CeAl_{11}O_{18}$), which has the elongated platelet shaped grains and confirmed through XRD phase analysis. Further, gradual addition of CaO from 1-5 wt.% decreases the bulk density and increases the porosity of the ceramics due to low density of CaO (3.30 g/cm^3) which is confirmed by SEM images. Additionally, CaO formed another secondary phase 'hibonite' which contains mainly calcium aluminate ($CaAl_{12}O_{19}$) phase and with part of Ca may be replaced by Ce as well as Al replaced by Ti or Mg. Hibonite phases also have lower density (3.79 g/cm^3) [145] and contain elongated platelet shape grains and hexagonal structures. As the number of elongated platelet shaped grain increased with gradual addition of CaO, the microstructure become less uniform and forming a greater ratio between the elongated and spherical shaped grains. Hence the grains were unable to closely pack each together and tend to interlock each other [134], resulting in high percentage of porosity. A sample containing both CeO_2 as well as CaO (5 wt.%), sintered at 1450°C had the lowest bulk density value of 2.72 g/cm^3 and the highest percentage of porosity of 34.77% shown in **Figure 4.18**.

At higher sintering temperature (like 1600 & 1650°C), bulk density of ceramics slightly increases upon addition by CaO gradually due to the fast and more elimination of pores at higher sintering temperature and enhanced more compaction resulting sintering effects. However, for the compositional effects, the bulk density at 1650°C is lower than 1600°C, in that case overstabilization was occurred due to over sintering effect at 1650°C. During over sintering the grain growth is relatively faster than pore elimination. As a result, pores are entrapped inside the grains and create porosity.

On the other hand, considering the firing temperature effects, bulk density of ceramics decreased gradually with increasing sintering temperature for the lower content of CaO (0-2 wt.%) as shown in **Figure 4.16**. The decline in bulk density is associated with increasing the spinel ($MgAl_2O_4$) phase formation which has the lower density (3.58-3.61 g/cm^3) that is

accompanied by (5-7%) volume expansion, and also increased the phase percentage of baddeleyite (m-ZrO_2) as well as decreased the phase content of tetragonal zirconia [146]. As baddeleyite phase formation is associated with volume expansion (~ 5%), so it has the contribution to reduce the bulk density of the ceramics as well. Additionally, the crystallite size of α-Al_2O_3 also increased with sintering temperature shown in **Table 4.4**.

Oppositely, for the higher content of CaO (3-5 wt.%) in ZTA-TiO_2-MgO ceramics, the bulk density gradually increased with increasing sintering temperature. The increase in bulk density is accompanied by the sintering effect and enhanced compaction through fast removal of pores from the ceramic composites. Furthermore, spinel ($MgAl_2O_4$) phase is not available for the higher content of CaO (3-5 wt.%) in ZTA-TiO_2-MgO ceramics. Moreover, the phase intensity of hibonite is decreased with increasing sintering temperature as well.

4.2.2 Relative density

Relative density refers to the ratio of bulk density and theoretical density in terms of percentages. Theoretical densities were calculated using rule of mixtures [147]. **Figure 4.17** shows the relative density curves of ZTA-TiO_2-MgO ceramics with respect to addition of CeO_2 (5 wt.%) and CaO variations (1-5 wt.%) at different sintering temperature. The curves pattern as well as their explanation follows almost same as bulk density curves that has been extensively discussed in terms of the availability of phases, their densities and microstructural features they have contained is shown in **Figure 4.16** and the highest relative density was obtained for Z15 (ZTA-TiO_2-MgO) ceramics with the value of 94.50 % and the lowest relative density was obtained for Z15Ce5Ca5 ceramics with the value of 65.30 % at 1450°C.

As the sample Z15Ce5Ca5 contains maximum amount of CaO (5 wt.%) with 5 wt.% CeO_2, the green density of the sample was very low (2.31 g/cm^3) shown in **Figure 4.16** compare to other samples. Furthermore, it has shown an exceptional bumping property (as formed fluffy structure) during drying in the oven. Therefore, porous ceramics are formed as their porosity is more than 20%.

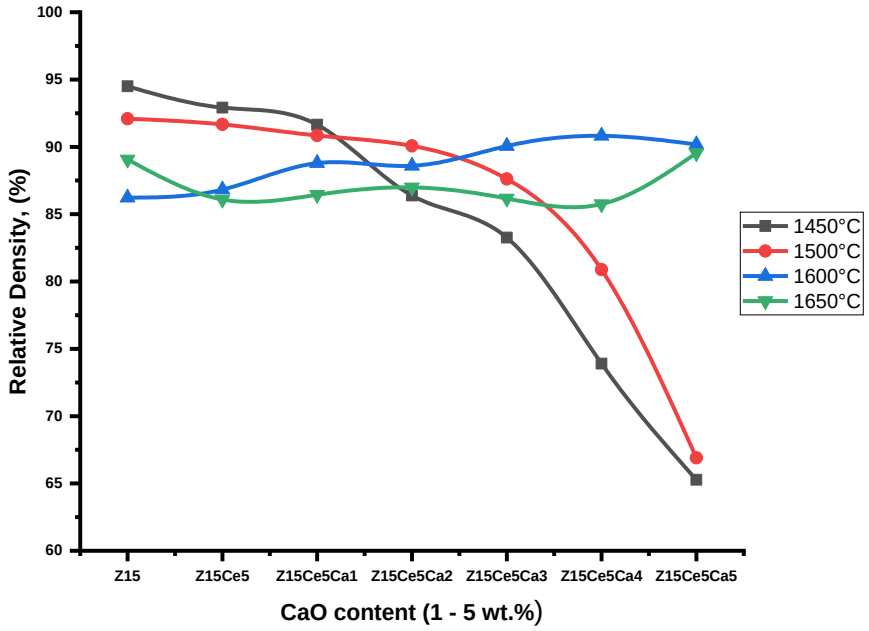

Figure 4.17 Relative density of Z15, Z15Ce5 with various contents of CaO.

4.2.3 Porosity

Figure 4.18 indicates the percentage of porosity of ZTA-TiO_2-MgO ceramic composites with different CaO (1-5 wt.%) contents at different sintering temperatures. The percentages of porosities of the ceramics are almost opposite or reverse of the relative densities as shown in **Figure 4.17**. The lowest porosity was found for the sample ZTA-TiO_2-MgO with the value of 5.5% and the highest porosity was found for the sample Z15Ce5Ca5 with the value of 34.73% at the sintering of 1450°C.

At lower sintering temperature (1450°C & 1500°C), the porosity increases gradually with addition of CaO (1-5 wt.%). As CaO formed new hibonite phase which has the lower density with hexagonal structure and the grain is not spherical in shape. Furthermore, the CaO also less dense material than α-Al_2O_3. On the other side, at higher sintering temperature (1600°C & 1650°C), the porosity slightly decreased with increasing the gradual addition of CaO. As the higher sintering temperature, more pores are eliminated due to sintering effects resulting the enhancement of compaction and thereby increased the density as well. For the maximum sintering temperature at 1650°C, the porosity is slightly increased compared to the porosity curve at 1600°C. In that case, over sintering is happened. During over sintering the grain

growth is relatively faster than pore elimination and some pores are entrapped inside the grains and creates voids. That's why, the porosity slightly increased with compositional variations.

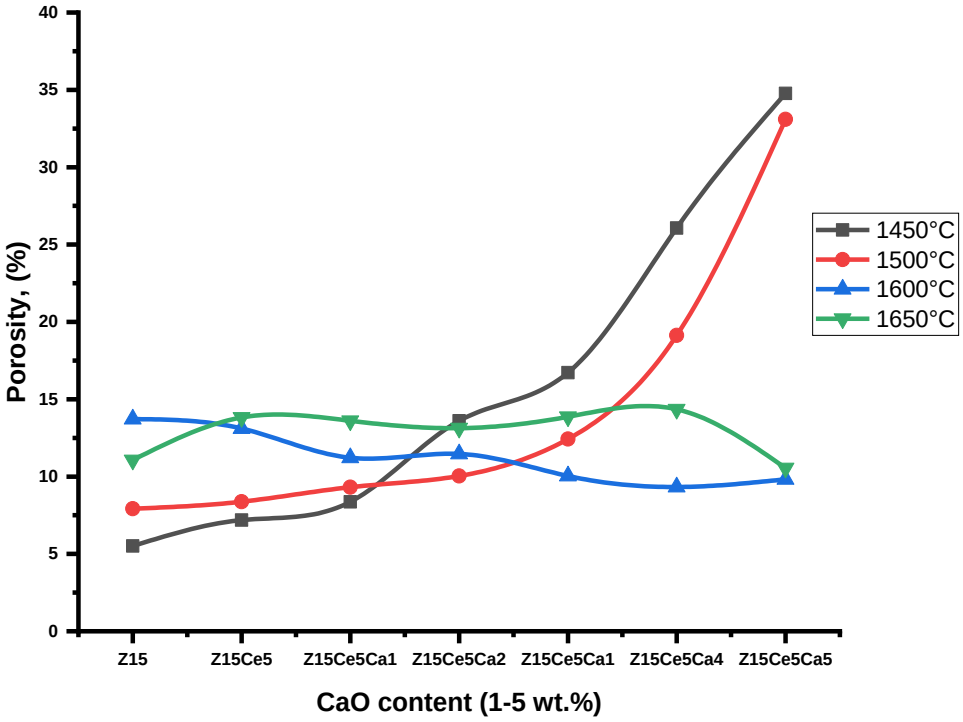

Figure 4.18 Porosity of Z15, Z15Ce5 with various contents of CaO.

On the other hand, considering the sintering temperature effects, the percentages of porosity of the ZTA-TiO_2-MgO ceramic composites increased gradually with increasing sintering temperature for the lower content of CaO (0-2 wt.%) as shown in **Figure 4.18**. The increase in porosity is associated with increasing the spinel ($MgAl_2O_4$) phase formation which has the lower density (3.58-3.61 g/cm^3) that is accompanied by (5-7%) volume expansion [146], and also increased the phase percentage of baddeleyite (m-ZrO_2) as well as decreased tetragonal zirconia phase. As baddeleyite (monoclinic zirconia) phase formation is related to volume growth (3 ~ 5%), so it has the contribution to reduce the bulk density and increase the porosity of the ceramics as well. Additionally, the crystallite size of α-Al_2O_3 also increased with sintering temperature shown in **Table 4.4**. Oppositely, for the higher content of CaO (3-5 wt.%) in ZTA-TiO_2-MgO ceramics, the percentage of porosity gradually decreased with increasing sintering temperature. The decreased in porosity is accompanied by the sintering effect and

enhanced compaction through fast removal of pores from the ceramic composites. Furthermore, spinel ($MgAl_2O_4$) phase is not available for the higher content of CaO (3-5 wt.%) in ZTA-TiO_2-MgO ceramics. Moreover, the phase intensity of hibonite is decreased with increasing sintering temperature as well.

4.2.4 Volume shrinkage

Figure 4.19 displays, volume shrinkage curves of ZTA-TiO_2-MgO ceramics with respect to addition of CeO_2 (5 wt.%) and CaO variations (1-5 wt.%) at different sintering temperature. The curves pattern as well as their approach explanation follows almost same as bulk density curves that has been extensively discussed in terms of the availability of phases, their densities and microstructural features they have contained is shown in **Figure 4.16** and the maximum volume shrinkage was obtained for Z15Ce5Ca5 ceramics with the value of 42.2 % at 1600°C and the minimum value was obtained for the same sample with the value of 19.65 % at 1450°C. As the sample Z15Ce5Ca5 contains maximum amount of CaO (5 wt.%) with 5 wt.% CeO_2, the green density of the sample was very low (2.31 g/cm^3) shown in **Figure 4.16,** compared to other samples. Furthermore, it has shown an exceptional bumping property during drying in the oven.

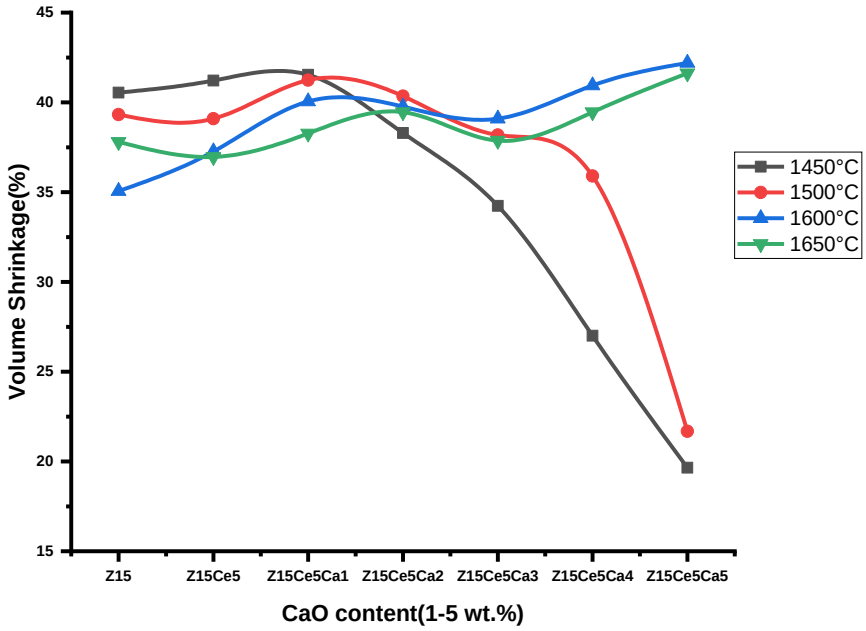

Figure 4.19 Volume shrinkage of Z15, Z15Ce5 with various contents of CaO.

4.2.5 Vickers microhardness

The effect of CeO_2 (5 wt.%) and CaO (1-5 wt.%) addition at different temperature on the Vickers microhardness of the ZTA-TiO_2-MgO ceramic composites is shown in **Figure 4.20**. Initially, at lower sintering temperature (1450°C & 1500°C), the Vickers microhardness value slightly increased with addition of CeO_2 (5 wt. %) due to increase in the density and reduce the porosity by forming cerium aluminate ($CeAl_{11}O_{18}$) phase of the ceramic composites. As the hardness value of $CeAl_{11}O_{18}$ is very near to α-Al_2O_3 (Hardness for α-Al_2O_3 ~ 15 GPa and $CeAl_{11}O_{18}$ ~ 14 GPa), so the addition of denser (CeO_2 ~7.13 g/cm^3) material has the effect to increase density as well as Vickers microhardness. Further, gradually addition of CaO (1-5 wt.%) decreased the microhardness value of the ceramics. As CaO is less dense (CaO ~ 3.30 g/cm^3) material than α-Al_2O_3 and it also formed hibonite phases which have the contribution to increase the porosity and decrease the density of the ceramic composites due to their elongated platelet shaped grains. Moreover, the hardness value (7.5 in Mho's scale) of hibonite phases is lower than α-Al_2O_3. The sudden decrease in microhardness value for the addition of more than 3 wt.% (>3 wt.%) CaO is due to the formation of excess porosity resulting the presence of more hibonite phases.

On the contrary, at higher sintering temperature (1600°C & 1650°C), the Vickers microhardness value abruptly decreased with addition of CeO_2 (5 wt. %) due to significant decrease of YSZ (t-ZrO_2) phase formation and increase in both spinel ($MgAl_2O_4$) and baddeleyite (m-ZrO_2) phases formation simultaneously. As spinel and baddeleyite both phases are associated with volume expansion, so their significant amount of presence in the ceramics would reduce the microhardness value inherently. Then the microhardness value increased gradually with addition of CaO up to 3 wt.% due to increase in density resulting for sintering effects. Moreover, the spinel ($MgAl_2O_4$) and baddeleyite (m-ZrO_2), both phases are also declined by adding CaO to 3 wt.%. After that microhardness value gradually decreased again with the addition of CaO for more than 3 wt.% (>3 wt.%) due to formation of more hibonite ($CaAl_{12}O_{19}$) phases which creates excess porosity in the ceramics. The Vickers microhardness values at 1650°C are slightly lower that 1600°C, as the densities at 1650°C are lower than that at 1600°C due to over sintering occurred at that temperature. That's why it reduces the resistance to indentation for applied loads.

There are two possible explanations for the development of hibonite ($CaAl_{12}O_{19}$) resulting in decrease the Vickers microhardness values, according to earlier studies [134, 148, 149]. First, when the hibonite's ($CaAl_{12}O_{19}$) phase has a significantly lower hardness than its α-Al_2O_3 counterpart. This is the result of the larger softer phase replacing the smaller harder α-Al_2O_3 phase, which lowers the overall ceramics Vickers microhardness. Second, the development of hibonite ($CaAl_{12}O_{19}$) is followed by the porosity increment, that reduces the samples' resistance to applied stresses.

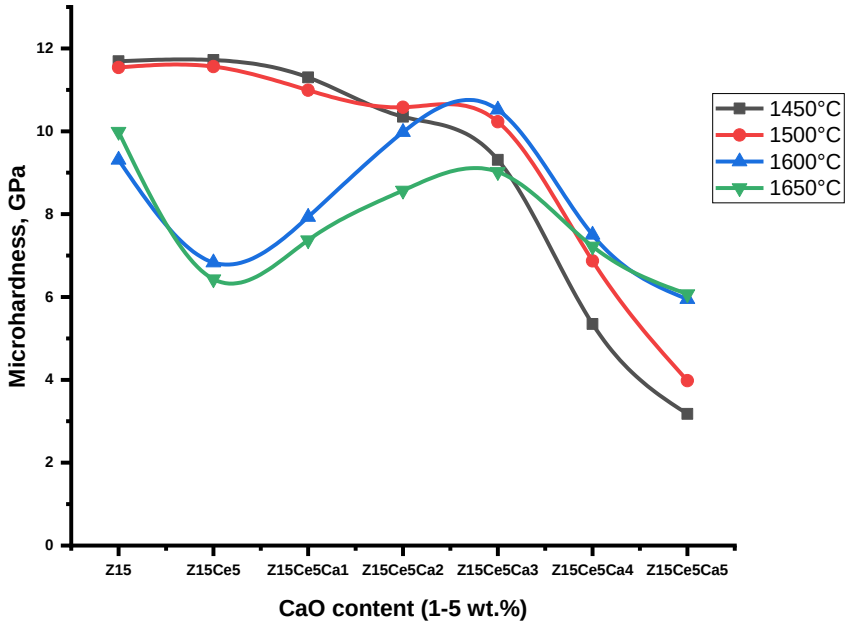

Figure 4.20 Microhardness of Z15, Z15Ce5 with various contents of CaO.

The effects of sintering temperatures on the Vickers microhardness values of ZTA-TiO_2-MgO with addition of CeO_2 and CaO (1-5 wt.%) ceramics are also shown in **Figure 4.20**. Up to the addition of lower content of CaO (0-2 wt.%), From the **Figure 4.20**, it has been shown that as the sintering temperature steadily increased, the microhardness value of ZTA-TiO_2-MgO ceramics gradually decreased. The decrease in microhardness value is associated with the increase in phase formation of baddeleyite (m-ZrO_2) and spinel ($MgAl_2O_4$) as well as significantly decrease in the phase formation of YSZ (t-ZrO_2). Provided that, baddeleyite (m-ZrO_2) and spinel ($MgAl_2O_4$) phases availability increases porosity and decreases density which in turns reduce the Vickers microhardness values. Moreover, significantly reduction of yttria

stabilized zirconia, YSZ (t-ZrO_2) phase also contributed to reduce the Vickers microhardness value through transforming into baddeleyite phase (m-ZrO_2). In contrast to the higher content of CaO (3-5 wt.%), the value of Vickers microhardness gradually increased with increasing firing temperature due to decline porosity as well as increase in density due to sintering effects.

4.2.6 Fracture toughness

In terms of fracture toughness, the effect of CeO_2 (5 wt.%) and CaO (1-5 wt.%) addition at different sintering temperature on the fracture toughness of the ZTA-TiO_2-MgO ceramic composites is shown in **Figure 4.21**. The result of fracture toughness was obtained using Casellas Equation (3.4). The figure displayed the fracture toughness values of ZTA-TiO_2-MgO ceramics as a function of simultaneous CeO_2 and CaO addition. Fracture toughness values were found to increase from 10.62 MPa.$m^{1/2}$ (ZTA-TiO_2-MgO) to 12.92 MPa.$m^{1/2}$ (3 wt.% CaO) at the starting of compositional modifications for the sintering temperature of 1450°C. However, the opposite effect was observed when more than 3 wt.% CaO was added, as the fracture toughness gradually began to decrease as a result of the lowest value of fracture toughness (9.98 MPa.$m^{1/2}$) at 5 wt.% CaO. Because of the presence of hibonite ($CaAl_{12}O_{19}$) phase, the enhanced values for fracture toughness that result from adding more CaO could be attributed to the crack deflection mechanism [134]. According to Sktani et al. [134], the more amount of hibonite ($CaAl_{12}O_{19}$) phase presents, the more crack deflection mechanism could be occurred. Based on that mechanism, the hibonite ($CaAl_{12}O_{19}$) grains distribution deflected the crack's propagation along the grain boundaries. The fracture toughness of the ceramics, however, reduced (12.92 MPa.$m^{1/2}$ to 9.98 MPa.$m^{1/2}$) as the CaO content increased (3 wt.% to 5 wt.%). The cause is that excessive pores were developed when the more hibonite ($CaAl_{12}O_{19}$) phases were formed at higher CaO concentrations. So, the properties of the composites will decrease due to availability of excessive pores. Moreover, from XRD analysis it is observed that, the phase percentage of spinel is decreased with the gradual addition of CaO to the ceramics up to 3 wt.%. As per intrinsic nature, the fracture toughness of spinel ($MgAl_2O_4$) is low [150]. So, the decrease in spinel ($MgAl_2O_4$) phase conversely attributed to increase in fracture toughness value. YSZ (t-ZrO_2) phase remains almost constant for the all compositions.

In case of 1500°C, the fracture toughness curve follows the same trend as 1450°C. But the fracture toughness values are quite higher than former one due to the presence of relatively more hibonite ($CaAl_{12}O_{19}$) and less spinel ($MgAl_2O_4$) phases, according to XRD phase analysis

data. As the grain shape of hibonite is platelet and elongated, it has the ability to increase the fracture toughness value through crack deflection and crack bridging mechanisms. So, fracture toughness increases from 10.68 MPam$^{1/2}$ (ZTA-TiO_2-MgO) to 13.34 MPam$^{1/2}$ (3 wt.% CaO) for the compositional modifications. The highest value of fracture toughness of the ceramics was found 13.34 MPam$^{1/2}$, for the addition of 3 wt.% CaO at the sintering temperature of 1500°C. After that, fracture resistance property declined due to the availability of excess porosity during hibonite phase formation in ceramic composites for the higher content (3-5 wt.%) of CaO.

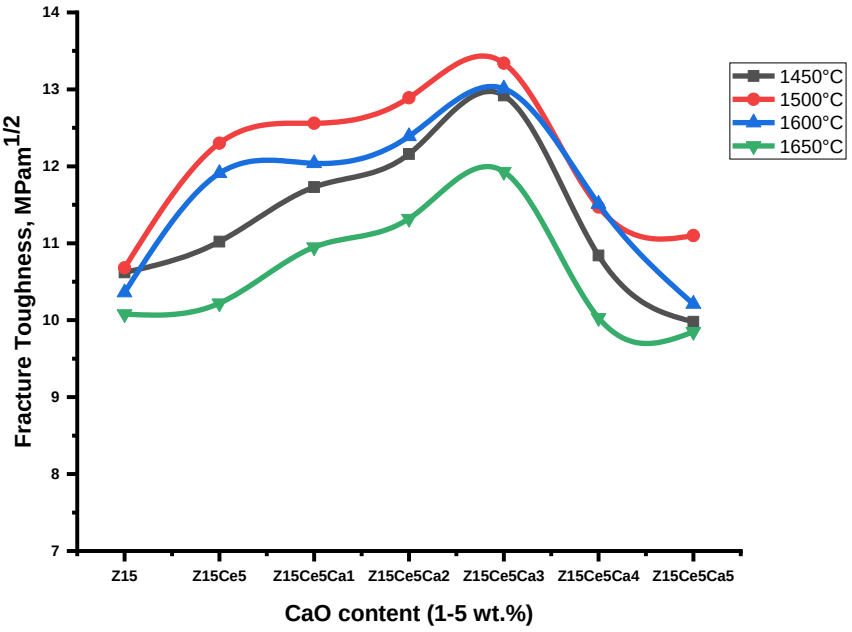

Figure 4.21 Fracture toughness of Z15, Z15Ce5 with various contents of CaO.

Similarly, at higher sintering temperature (1600 & 1650°C), the fracture toughness curves follow the same trend (1450 & 1500°C) for the compositional modification. The value of fracture toughness gradually increased with the addition of CaO up to 3 wt.% then gradually decreased for the addition of CaO up to 5 wt.%. Fracture toughness values were found to increase from 10.36 MPam$^{1/2}$ (ZTA-TiO_2-MgO) to 13.01 MPam$^{1/2}$ (3 wt.% CaO) for the sintering temperature 1600°C and 10.08 MPam$^{1/2}$ (ZTA-TiO_2-MgO) to 11.93 MPam$^{1/2}$ (3 wt.% CaO) for the sintering temperature 1650°C. The lowest fracture toughness value (9.85 MPam$^{1/2}$) was found for the ceramics contain maximum (5 wt.%) CaO and CeO_2 at the

sintering temperature 1650°C. However, the fracture toughness values are quite lower than the values obtained from the sintering temperature at 1500°C. This is because at higher sintering temperature, baddeleyite (m-ZrO_2) phase content is significantly increased and YSZ (t-ZrO_2) phase content is decreased due to long cooling rate pattern of the typical sintering cycle. Moreover, the phase content of hibonite ($CaAl_{12}O_{19}$) decreased and spinel ($MgAl_2O_4$) increased with higher sintering temperature. As, transformation toughening of tetragonal zirconia phases and crack deflection mechanism of hibonite ($CaAl_{12}O_{19}$) phases played the major role for the improvement of fracture toughness of the ceramic composites, therefore, at higher sintering temperature that property became low due to existence of relatively lower content of hibonite ($CaAl_{12}O_{19}$) and tetragonal zirconia (t-ZrO_2) phases as well as higher content of baddeleyite (m-ZrO_2) and spinel ($MgAl_2O_4$) phases.

4.2.7 Diametral tensile strength

The properties of substances like diametral tensile strength, elastic modulus, hardness, compressive strength, and fatigue resistance are closely related [151]. In biomedical applications, a restorative material with high compressive strength, flexural strength, and diametral tensile strength may be used.

The impacts of CeO_2 and CaO inclusions on diametral tensile strength property of ceramic composites is shown in **Figure 4.22**. The result of diametral tensile strength was obtained using Equation 3.6. The graphs for diametral tensile strength showed almost similar trend to that of the relative density results. The highest value of diametral tensile strength for ZTA-TiO_2-MgO ceramics was found 124.93 MPa (no CaO & CeO_2) for the sintering temperature at 1450°C. At the beginning, diametral tensile strength of ZTA-TiO_2-MgO ceramic composites gradually decreased from 124.93 MPa (0 wt.% CaO & CeO_2) to 95.59 MPa (3 wt.% CaO & 5 wt.% CeO_2), before it decreased rapidly from 95.59 MPa (3 wt.% CaO & 5 wt.% CeO_2) to 76.61 MPa (5 wt.% CaO & 5 wt.% CeO_2) after 3 wt.% CaO addition.

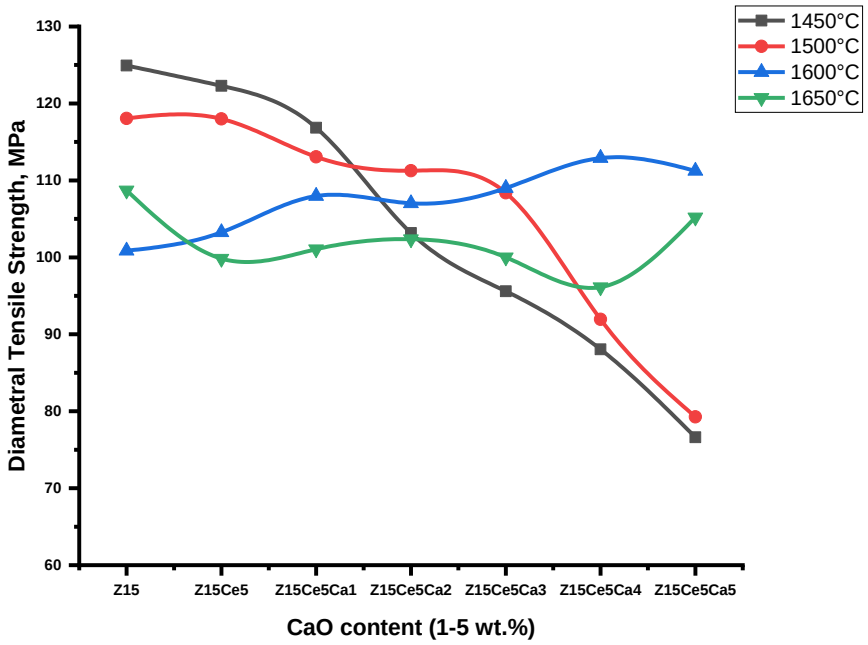

Figure 4.22 Diametral tensile strength of Z15, Z15Ce5 with various contents of CaO.

The decreased in diametral tensile strength value is attributed for the increase in porosity through formation of hibonite phases. As pores (size, shape and amount) are responsible for the reduction of strength because they reduced the cross-sectional area over which a load can be applied. As a result, the stress which support the material is reduced. So, the higher the porosity, the lower the resistance to applied load and easy for cracks to propagate throughout the structure. Similarly, at 1500°C, diametral tensile strength of ZTA-TiO_2-MgO ceramic composites gradually decreased up to 3 wt.% CaO addition then it decreased rapidly up to 5 wt.% CaO addition. However, for higher sintering temperatures (1600 & 1650°C), diametral tensile strength properties gradually increased with the addition of CeO_2 (5 wt.%) and CaO (1-5 wt.%), that is due to the results of decreased in porosity and increased in density as the sintering effects predominant. But for the over sintering reason, the diametral tensile strength of ZTA-TiO_2-MgO ceramics at 1650°C is lower than 1600°C, due to increase in porosity through relatively fast grain growth over pores removal.

On the other hand, it is obvious that the sintering temperature influenced the diametral tensile strength of the ZTA-TiO_2-MgO ceramics. The findings can be explained by the relative

density, porosity, XRD results and microstructure. Studies found that hardness, fracture toughness, and flexural strength of ZTA ceramics varied with the sintering temperature [152]; higher sintering temperatures (1550°C and 1650°C) might result in a larger grain size and potentially have a detrimental effect on the mechanical performance. In the current study, for the lower content of CaO (0-2 wt.%), an increase of crystallite size and spinel as well as enhancement of transformability of YSZ to m-ZrO_2 were observed as the temperature increased and the decline of diametral tensile strength also presented. This can be explained by the matter that spinel and baddeleyite phases increases porosity and decreases density resulting in volume expansion. In contrast, for the higher content of CaO (3-5 wt.%), diametral tensile strength of ZTA-TiO_2-MgO ceramics increased with increasing sintering temperature as the density increased through sintering effects compaction.

4.3 Coefficient of thermal expansion

Coefficient of thermal expansion (CTE) was measured by Thermo-Mechanical Analyzer (TMA) using thermal cycle from room temperature to 500°C which is shown in **Figure 4.23**. From the trend of the curves, it is indicated that, upon addition of CeO_2 (5 wt.%) and CaO (1-5 wt.%) to ZTA-TiO_2-MgO ceramics, at lower sintering temperatures (1450°C & 1500°C), the thermal expansion value declined gradually (from 9.1×10^{-6} °C^{-1} towards 8.31×10^{-6} °C^{-1}) & (8.84×10^{-6} °C^{-1} towards 8.38×10^{-6} °C^{-1}) due to an increase in porosity for the formation of cerium aluminate and hibonite phases. As hibonite and cerium aluminate phases contains elongated platelet grains and these grains are attributed to increase porosity through interlocking among them which is confirmed by FESEM images (**Figures 4.25-4.28**). By contrast, at higher sintering temperatures (1600°C & 1650°C), CTE value slightly increased (8.52×10^{-6} °C^{-1} to 8.62×10^{-6} °C^{-1}) & (8.58×10^{-6} °C^{-1} to 8.61×10^{-6} °C^{-1}) with the addition of CeO_2 (5 wt.%) and CaO (1-5 wt.%) to ZTA-TiO_2-MgO ceramics. This is due to the fact that the density increased at those temperatures for sintering effects resulting enhanced compaction. **Figure 4.23** showed the overall thermal expansion curves of the ZTA-TiO_2-MgO composites, which resulted in an expansion coefficient between 9.1×10^{-6} °C^{-1} and 8.31×10^{-6} °C^{-1} at room temperature to 500°C. This can be compared with a theoretical thermal expansion coefficient for single phase α-Al_2O_3 of 7.9×10^{-6} °C^{-1} and ZTA (zirconia toughened alumina) of (8.0-8.1×10^{-6} °C^{-1}). ZTA-TiO_2-MgO composite with 5 wt.% CeO_2 and 3 wt.% CaO addition had a coefficient of thermal expansion (CTE) of 8.56×10^{-6} °C^{-1}, which is very close to the lower

value of that composites. The CTE values for Al_2O_3-3YSZ composites obtained by other studies [153, 154, 155, 156] are in good agreement with these studies. A composite (ZTA-TiO_2-MgO) with 5 wt.% CeO_2 and 3 wt.% CaO) with a lower CTE value will have stronger thermal shock resistance property and be more suitable for many additional applications where high fracture toughness and thermal shock resistance are needed.

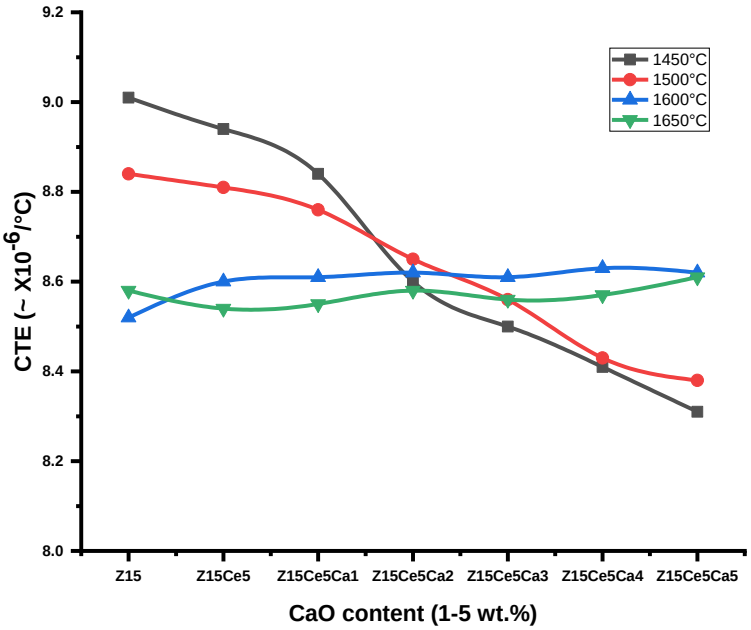

Figure 4.23 Coefficient of thermal expansion of Z15, Z15Ce5 with various contents of CaO.

4.4 Electrical Conductivity

Figure 4.24 shows the flow of current through the ceramic composites (Z15, Z15Ce5Ca5) with respect to pure cotton for a given voltage (in mV) using an electrometer. The curves indicated that the composites behaved like an almost insulating material, as they provide nano ampere (nA) scale current against passing millivoltage (mV) level potential difference. The flow of current is very low (nA) and become constant as like the trend of the curve for pure cotton. So, the composites are treated as electrical insulating materials.

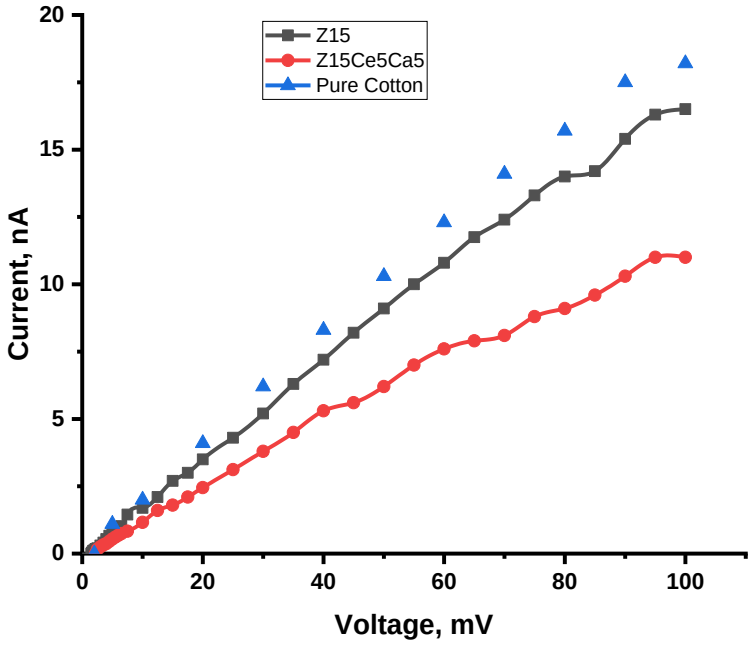

Figure 4.24 Current vs Voltage (I-V) curve for Z15, Z15Ce5Ca5 and pure cotton.

4.5 Microstructural Analysis

4.5.1 FESEM with EDS

The distribution of the secondary phases in terms of grain shape within the microstructure was revealed by FESEM-EDS investigations, allowing for a further understanding of the role of those phases as determined by XRD analysis. The morphological characteristics of the rounded and elongated grains differentiate noticeably as the concentration of CaO increased, as shown in **Figure 4.25**. Corundum (α-Al_2O_3) is represented by the dark grains, and YSZ (t-ZrO_2) by the bright grains. Round grain forms can be seen in both of these primary phases. Only a few elongated grains could be seen in the sample's micrograph at the beginning, after the addition of CaO at 1 wt.%. With the gradual increases in the concentration of CaO, the formation of elongated grains increased gradually and became a dominant phase among all phases. According to quantitative analysis (**Table**

4.3), the addition of CaO results in the $CaAl_{12}O_{19}$ phase at 80.1% for the addition of 3 wt.% CaO at 1500°C. **Figure 4.25** demonstrated the presence of these elongated grains, which were identified as the secondary phase of hibonite ($CaAl_{12}O_{19}$) and observed at 5 wt.% by EDS studies. The back-scattered images demonstrated an excellent distribution of ZrO_2 grains at grain boundaries or embedded within α-Al_2O_3 and $CaAl_{12}O_{19}$ grains. Additionally, it was shown that the addition of CaO increased the number of pores due to the interlocking of elongated hibonite phases each other's [134]. Similar findings about the addition of CaO to Al_2O_3 was also found in another research [157].

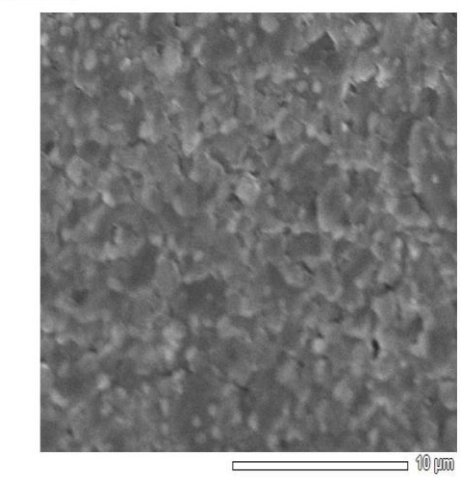

Title : IMG1

Instrument : 7610F
Volt : 15.00 kV
Mag. : x 5,000
Date : 2021/06/30
Pixel : 512 x 384

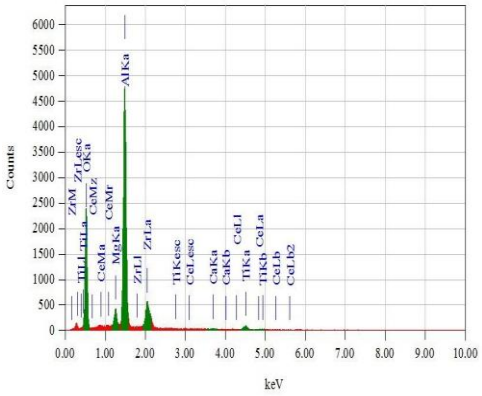

Acquisition Parameter
Instrument : 7610F
Acc. Voltage : 15.0 kV
Probe Current: 1.00000 nA
PHA mode : T3
Real Time : 50.59 sec
Live Time : 50.00 sec
Dead Time : 1 %
Counting Rate: 1905 cps
Energy Range : 0 - 20 ke

ZAF Method Standardless Quantitative Analysis
Fitting Coefficient : 0.0422

Element	(keV)	Mass%	Sigma	Atom%	Compound	Mass%	Cation	K
O K	0.525	47.57	0.38	65.52				47.7046
Mg K	1.253	2.52	0.07	2.29				2.8590
Al K	1.486	34.14	0.24	27.89				36.1515
Ca K*	3.690	0.09	0.04	0.05				0.1157
Ti K	4.508	2.15	0.10	0.99				2.3487
Zr L	2.042	13.52	0.27	3.27				10.8205
Ce L*		ND		ND				
Total		100.00		100.00				

(a) 1450°C (Z15)

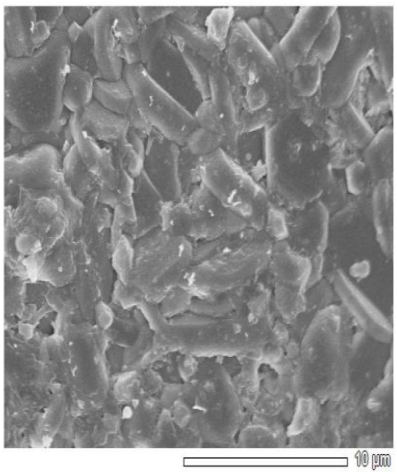

Title : IMG

Instrument : 761
Volt : 10.
Mag. : x 5
Date : 202
Pixel : 512

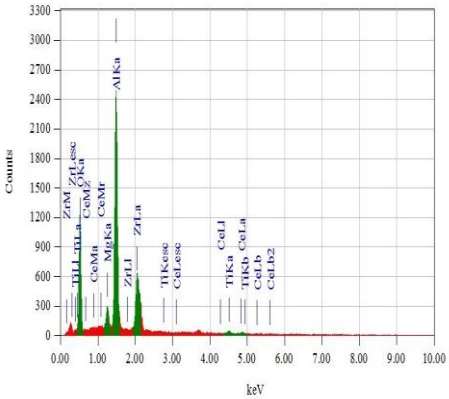

Acquisition Parame
Instrument : 761
Acc. Voltage : 10.
Probe Current: 1.0
PHA mode : T3
Real Time : 50.
Live Time : 50.
Dead Time : 0 %
Counting Rate: 128
Energy Range : 0

ZAF Method Standardless Quantitative Analysis
Fitting Coefficient : 0.0743

Element	(keV)	Mass%	Sigma	Atom%	Compound	Mass%	Cation	K
O K	0.525	29.81	0.34	51.32				26.9049
Mg K	1.253	2.91	0.11	3.30				3.5951
Al K	1.486	34.32	0.34	35.04				40.1755
Ti K	4.508	2.93	0.26	1.69				3.2590
Zr L	2.042	26.07	0.49	7.87				22.2250
Ce L*	4.837	3.95	0.62	0.78				3.8405
Total		100.00		100.00				

(b) 1450°C (Z15Ce5)

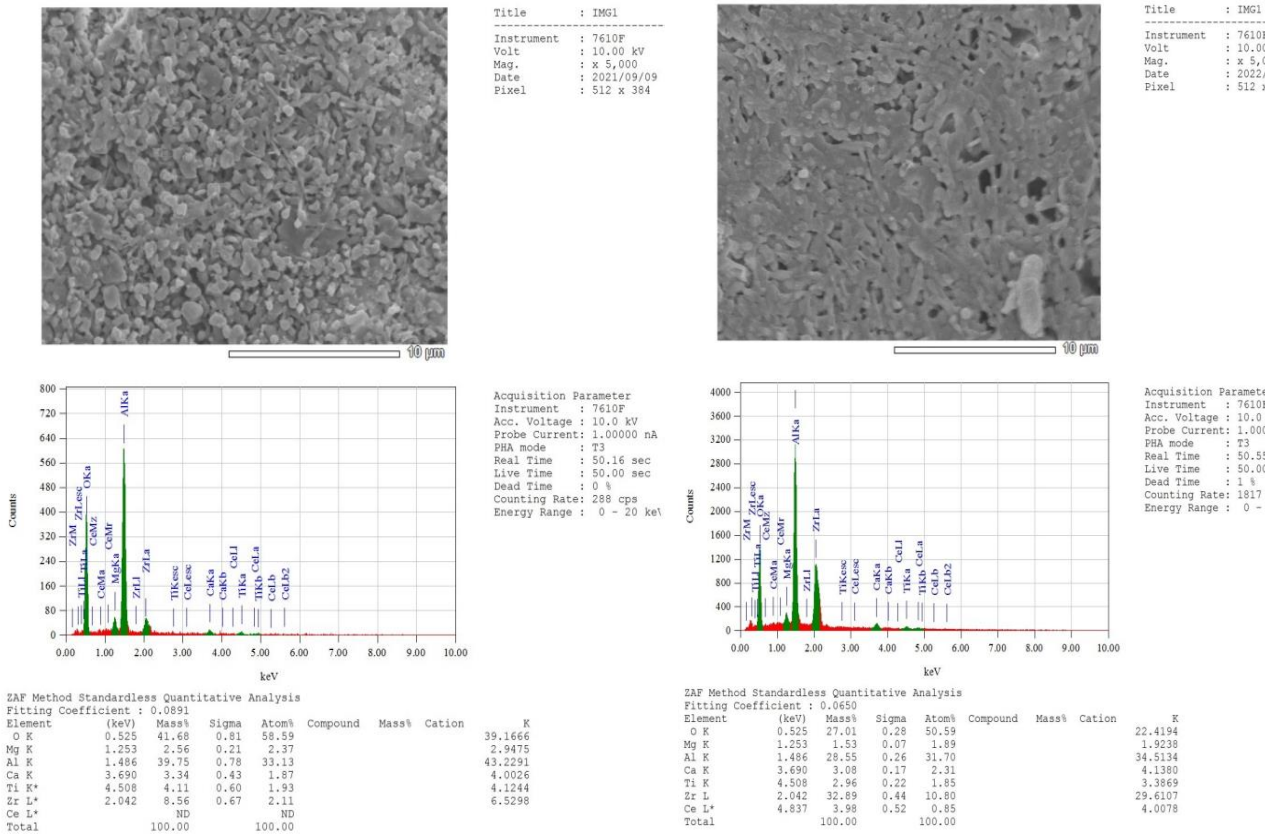

(c) 1450°C (Z15Ce5Ca1) (d) 1450°C (Z15Ce5Ca5)

Figure 4.25(a-d) FESEM with EDS micrographs of different samples at 1450°C.

Figure 4.25(a-d) shows the FESEM micrographs with EDS analysis of ZTA-TiO_2-MgO ceramics containing different wt.% CeO_2 and CaO sintered at 1450°C. As we know that there is an influence of surface morphology on the mechanical properties of ceramic composites. According to **Figure 4.25(a)** of Z15 (ZTA-TiO_2-MgO) ceramics composites, all grains are almost spherical in shape and homogeneously distributed in the composites morphological structure. Upon addition of CeO_2 (5 wt.%) for the composite Z15Ce5 show in **Figure 4.25(b)**, formed elongated platelet shape cerium aluminate ($CeAl_{11}O_{18}$) grains resulting in increasing porosity and decreasing strength. Moreover, further addition of CaO (1 & 5 wt.%) show in **Figure 4.25(c, d)**, formed hibonite phases which is also elongated platelet shape and became predominant gradually resulting in producing excess porosity and decrease strength as well.

In contrast, the effect of firing temperatures (1450, 1500, 1600 & 1650°C) regarding the surface morphology of Z15Ce5Ca5 ceramics are shown in **Figure 4.26(a-d)**. Based on the Figures it is observed that grain size increased with the gradual increased in sintering temperature. However, at higher sintering temperatures (1600°C & 1650°C), intermetallic glassy phases are formed shown in **Figure 4.26(c, d)** which looked like fused grains and probably due to the long cooling rate pattern. But, the mechanical properties (strength, fracture toughness etc.) of higher sintering temperatures are comparatively better than those of lower sintering temperatures (1450°C & 1500°C), as the porosity decreased and density increased resulting for the sintering effects. Additionally, at higher sintering temperatures, composites contained more close pores rather than open pores considering out of total pores exist in the microstructure.

Figure 4.27(a-d) and **Figure 4.28(a-d)** shows the surface morphology or microstructure of the fractured surface of the different ceramic composites (Z15, Z15Ce5, Z15Ce5Ca1, and Z15Ce5Ca5) for firing temperatures such as 1500°C as well as 1600°C, respectively. During the solid-state sintering of polycrystalline ceramics, densification and grain growth occurred simultaneously. The diffusion of the materials from the grain boundaries (the source) to the pores (the sink) causes densification. The diffusion distance, or the size of the grain, between the source of materials and the sink must be kept as small as possible for rapid densification. Since long sintering durations are necessary to reach the desired density, rapid grain growth drastically reduces the densification rate, which raises the chances of abnormal grain growth.

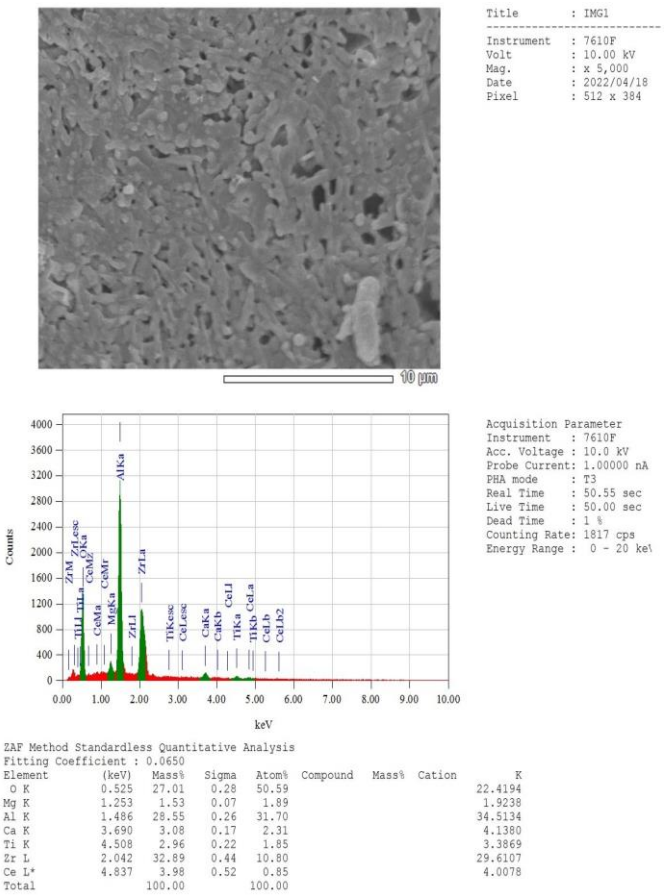

ZAF Method Standardless Quantitative Analysis
Fitting Coefficient : 0.0650

Element	(keV)	Mass%	Sigma	Atom%	Compound	Mass%	Cation	K
O K	0.525	27.01	0.28	50.59				22.4194
Mg K	1.253	1.53	0.07	1.89				1.9238
Al K	1.486	28.55	0.26	31.70				34.5134
Ca K	3.690	3.08	0.17	2.31				4.1380
Ti K	4.508	2.96	0.22	1.85				3.3869
Zr L	2.042	32.89	0.44	10.80				29.6107
Ce L*	4.837	3.98	0.52	0.85				4.0078
Total		100.00		100.00				

(a)1450°C (5 CeO_2 & 5CaO)

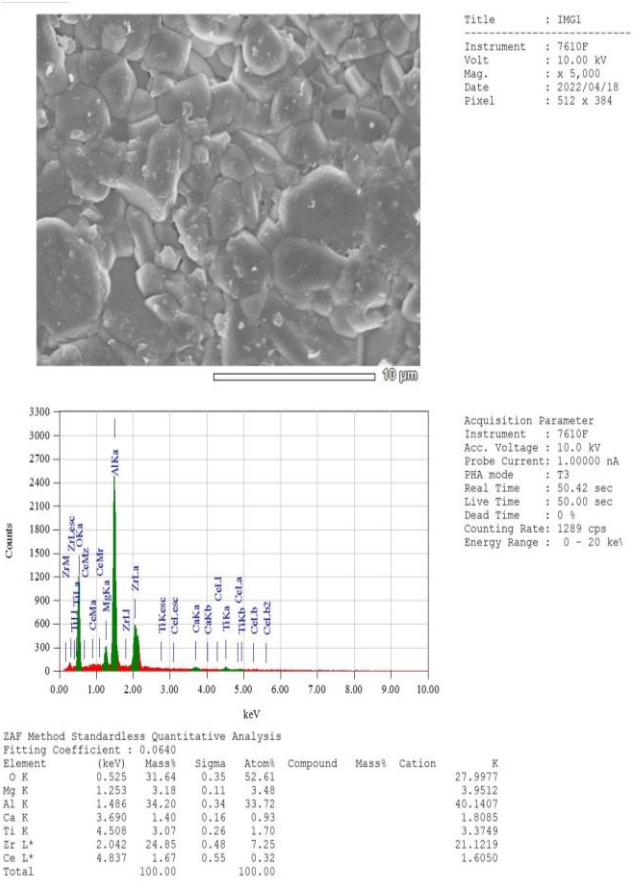

ZAF Method Standardless Quantitative Analysis
Fitting Coefficient : 0.0640

Element	(keV)	Mass%	Sigma	Atom%	Compound	Mass%	Cation	K
O K	0.525	31.64	0.35	52.61				27.9977
Mg K	1.253	3.18	0.11	3.48				3.9512
Al K	1.486	34.20	0.34	33.72				40.1407
Ca K	3.690	1.40	0.16	0.93				1.8085
Ti K	4.508	3.07	0.26	1.70				3.3749
Zr L*	2.042	24.85	0.48	7.25				21.1219
Ce L*	4.837	1.67	0.55	0.32				1.6050
Total		100.00		100.00				

(b) 1500°C (5 CeO_2 & 5CaO)

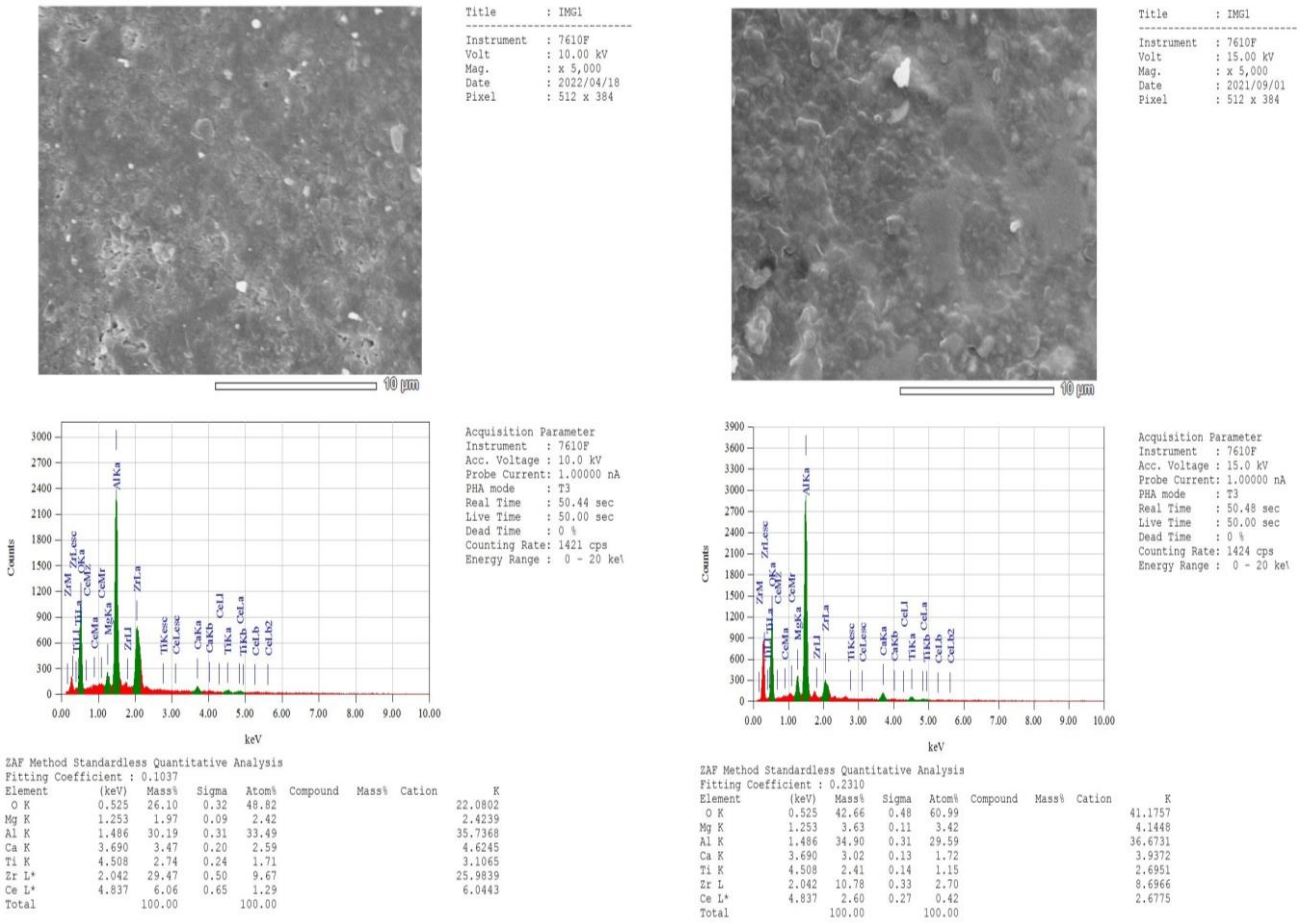

(c) 1600°C (5 CeO_2 & 5CaO)

(d) 1650°C (5 CeO_2 & 5CaO)

Figure 4.26(a-d) FESEM with EDS micrographs of sample Z15Ce5Ca5 at various firing temperatures.

For **Figures 4.27(a)** and **4.28(a)**, the microstructures of ZTA-TiO_2-MgO ceramics are depicted without CeO_2 and CaO. The grain size increased with increasing temperature and some intragranular grains are formed inside the large grains at higher sintering temperature like 1600°C for the faster grain growth of the ceramics.

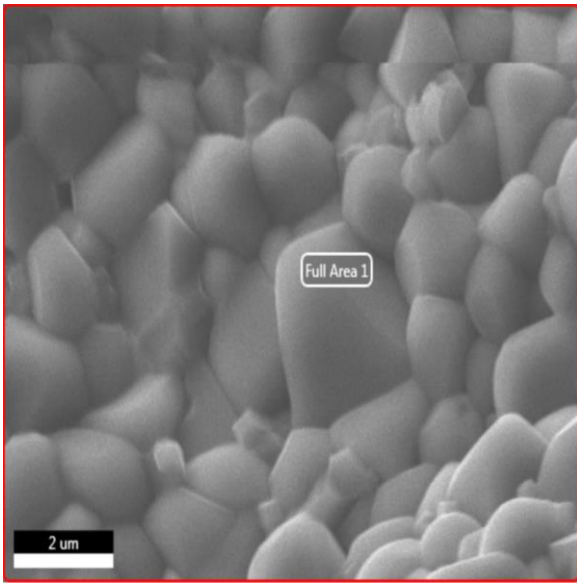

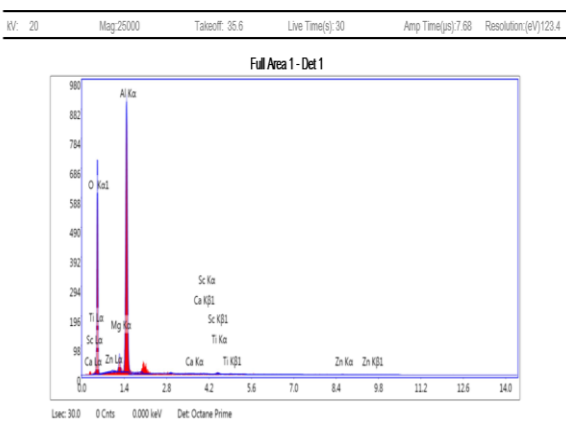

eZAF Smart Quant Results

Element	Weight %	Atomic %
O K	53.58	66.13
MgK	3.30	2.68
AlK	42.05	30.78
CaK	0.07	0.03
CeK	0.09	0.04
TiK	0.56	0.23
ZrK	0.35	0.10

(a) Z15 (1500°C)

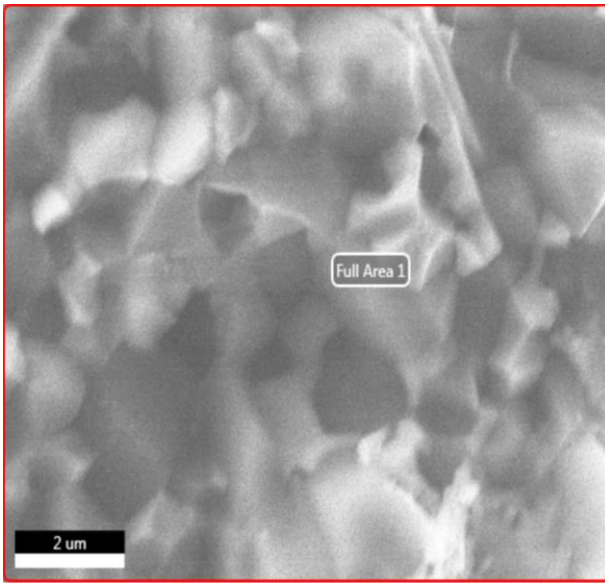

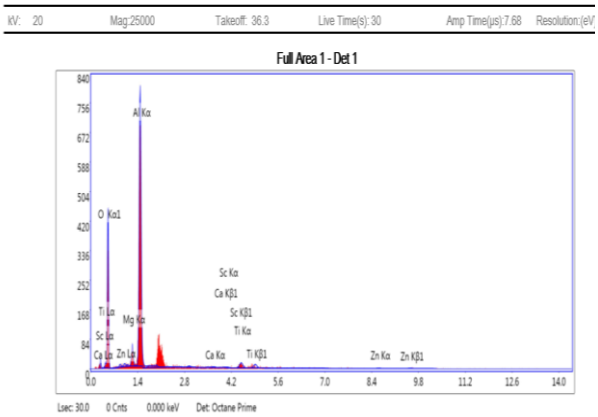

eZAF Smart Quant Results

Element	Weight %	Atomic %
O K	48.47	61.86
MgK	3.71	3.12
AlK	44.43	33.63
CaK	0.25	0.13
ScK	0.18	0.08
TiK	2.30	0.98
ZnK	0.64	0.20

(b) Z15Ce5 (1500°C)

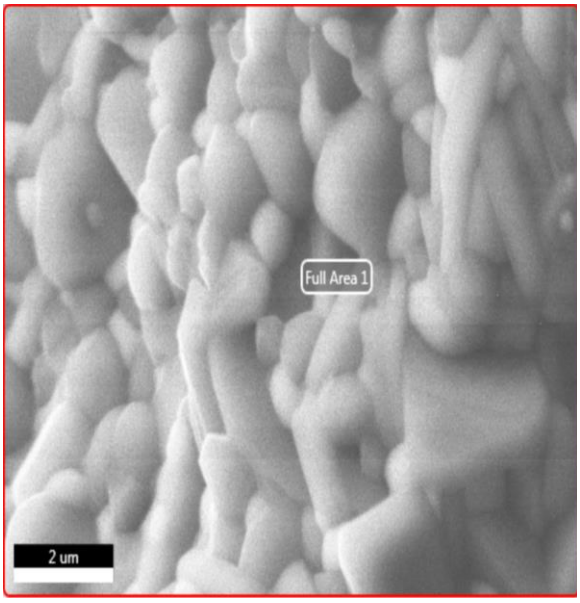

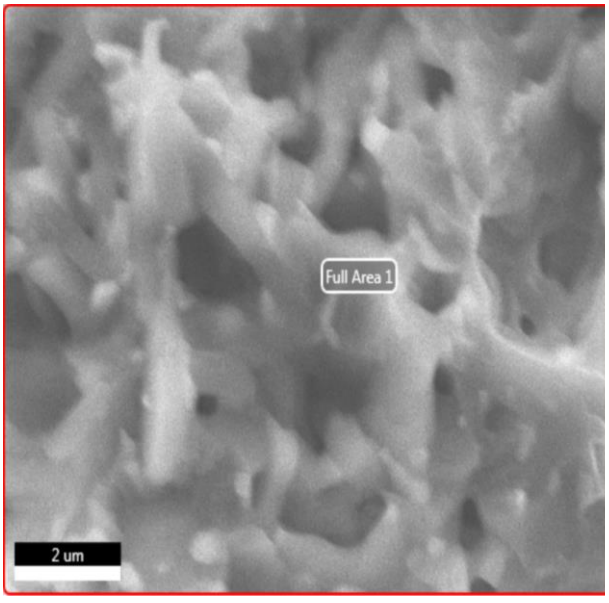

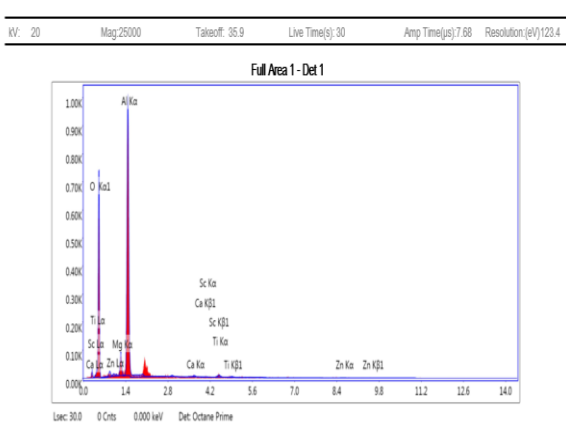

eZAF Smart Quant Results

Element	Weight %	Atomic %
O K	52.77	65.52
MgK	3.75	3.06
AlK	41.68	30.68
CaK	0.39	0.19
ScK	0.08	0.03
TiK	0.92	0.38
ZnK	0.40	0.12

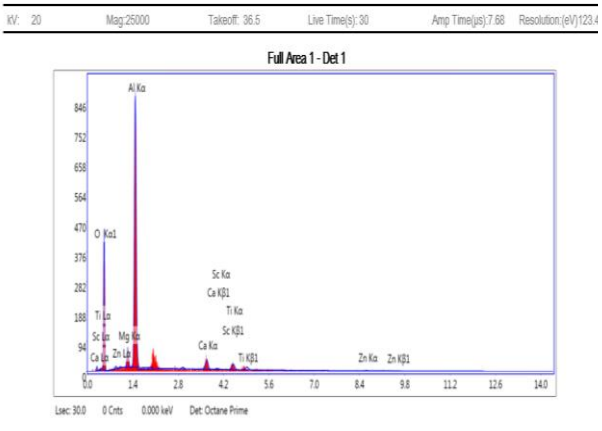

eZAF Smart Quant Results

Element	Weight %	Atomic %
O K	47.35	61.31
MgK	3.30	2.81
AlK	42.66	32.75
CaK	3.47	1.79
ScK	0.08	0.04
TiK	2.61	1.13
ZnK	0.52	0.17

(c) Z15Ce5Ca1 (1500°C)

(d) Z15Ce5Ca5 (1500°C)

Figure 4.27(a-d) FESEM with EDS micrographs at 1500°C for fractured surfaces.

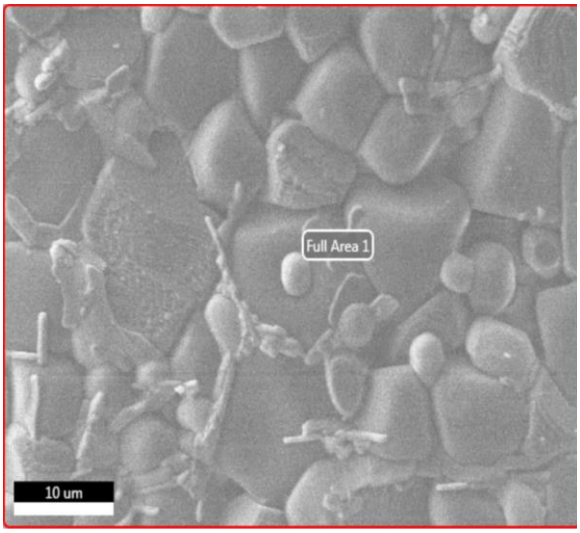

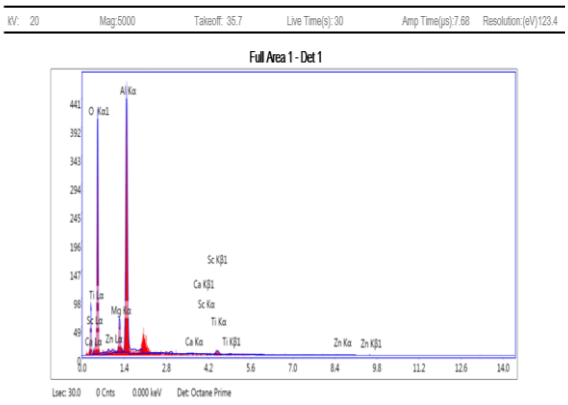

eZAF Smart Quant Results

Element	Weight %	Atomic %
O K	55.21	67.61
MgK	5.16	4.15
AlK	37.96	27.57
CaK	0.13	0.06
ScK	0.12	0.05
TiK	1.20	0.49
ZnK	0.24	0.07

(a) Z15 (1600°C)

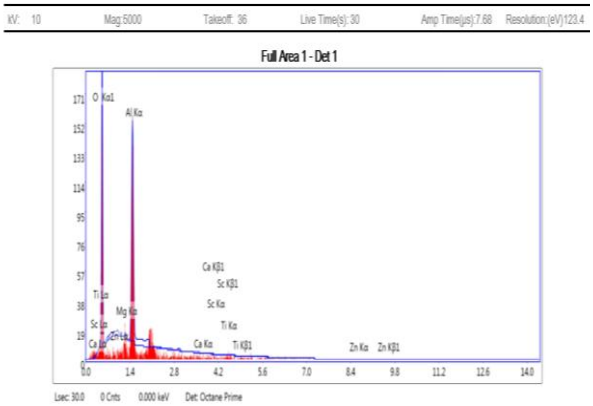

eZAF Smart Quant Results

Element	Weight %	Atomic %
O K	50.04	62.90
ZnL	0.00	0.00
MgK	1.24	1.03
AlK	47.93	35.73
CaK	0.00	0.00
ScK	0.15	0.07
TiK	0.64	0.27

(b) Z15Ce5 (1600°C)

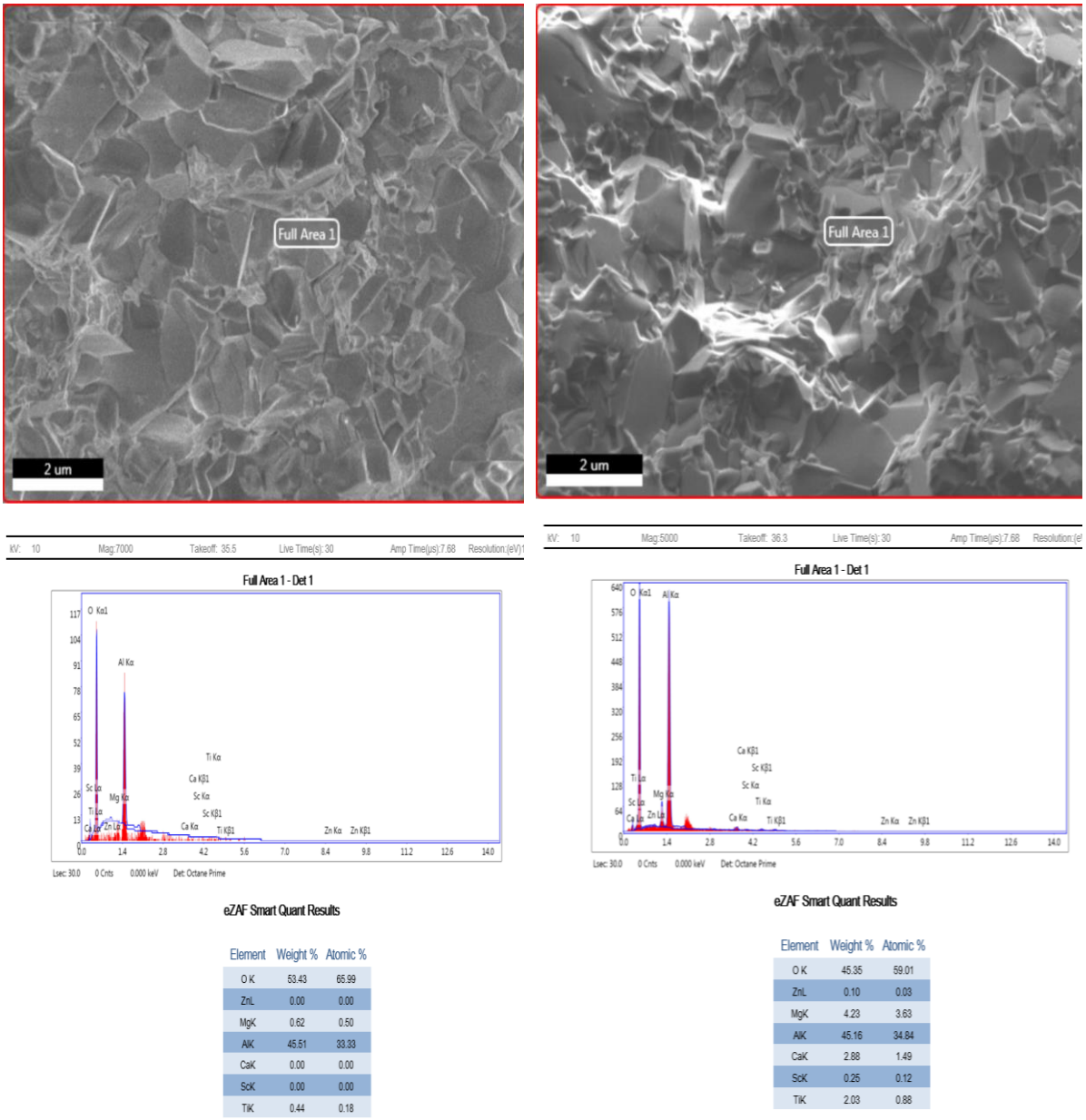

(c) Z15Ce5Ca1 (1600°C)

(d) Z15Ce5Ca5 (1600°C)

Figure 4.28(a-d) FESEM with EDS micrographs of fractured surfaces of different samples at 1600°C.

The microstructures of ZTA-TiO_2-MgO with CeO_2 (5 wt.%) and CaO (1 & 5 wt.%) are depicted in the remaining three **Figures 4.27(b, c & d)** and **4.28(b, c & d)**. Comparing those

micrographs reveals that porosity of ZTA-TiO_2-MgO ceramics enhanced for the inclusion of CeO_2 and CaO through forming cerium aluminate and hibonite phases.

4.5.2 Atomic Force Microscopy

Atomic Force Microscopy (AFM) images of ZTA-5TiO_2-5MgO ceramic composites in two dimension (2D) and three dimensions (3D) are demonstrated through **Figure 4.29**. Additionally, **Figure 4.30** illustrates the outcome of the AFM images. Generally, AFM technique is used for investigating the surfaces and characteristics of different materials in nanometer scale. Accurate surface roughness measurement is important for understanding the material structures and failure mechanisms. How an object interacts with its surrounding environment depends on the surface roughness average (Ra). In addition to having better adhesion property, rough surfaces also tend to wear out more quickly. Ra (average surface roughness) gives a summary of the surface height changes, whereas RMS (root mean square) average counts the standard deviations of the average height from the mean.

Following **Figure 4.29** shows that, ceramic composites surfaces are well-shaped and homogeneous. Moreover, **Figure 4.30** displays grain size distribution on surfaces of the ceramic composites increases from 0.62 μm to 2.12 μm as the concentration of CaO gradually increased from 1-5 wt.%. For ZTA-5TiO_2-5MgO sample and ZTA-5TiO_2-5MgO with CeO_2 and CaO samples, however, Ra (roughness average) and RMS (root mean square) values of the surface increased from (23.85, 28.84) nm to (67.09, 84.21) nm. This is due to the effect of CeO_2 and CaO additives as they are formed relatively larger size grains than the grains in the α-Al_2O_3. However, these Ra and RMS values are within nanometer scale (<100 nm), which are in allowable range for biomedical applications like orthopedics and dental implants. As smooth surfaces have better clinical performance, according to orthopedic surgeons, surface roughness with 0.7 μm clinically most relevant for THA (total hip arthroplasty).

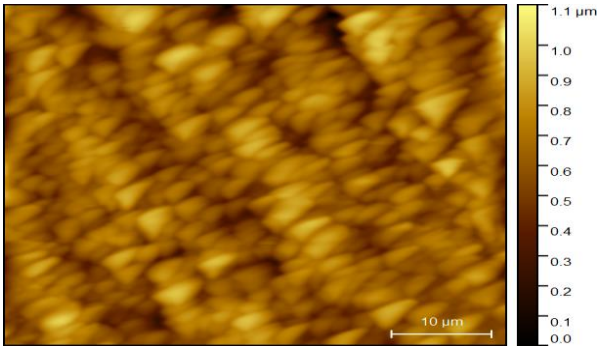

(a) 2D roughness of Z15

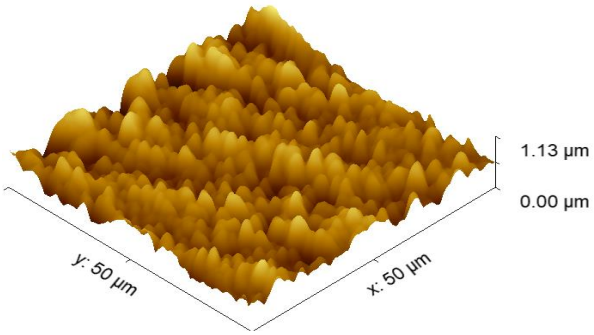

(b) 3D roughness of Z15

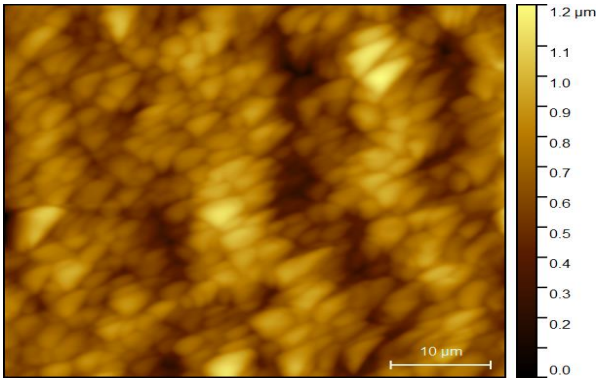

(c) 2D roughness of Z15Ce5

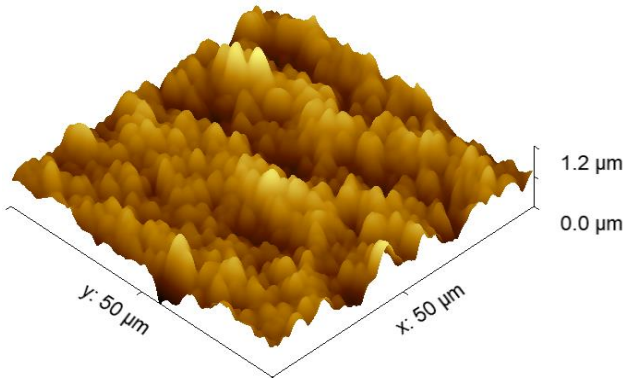

(d) 3D roughness of Z15Ce5

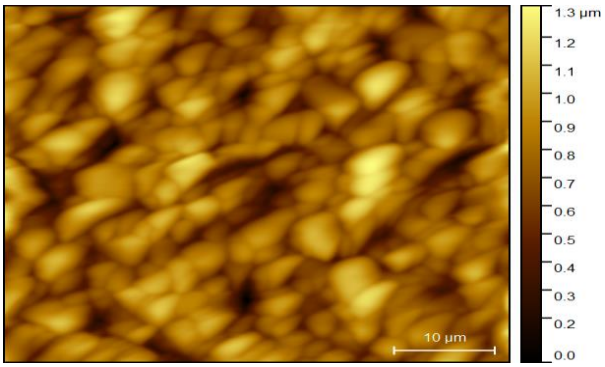

(e) 2D roughness of Z15Ce5Ca1

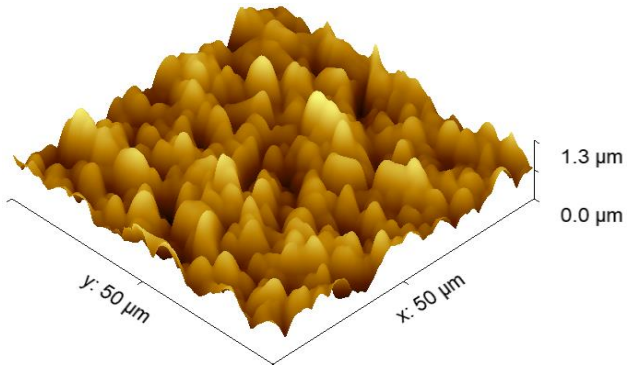

(f) 3D roughness of Z15Ce5Ca1

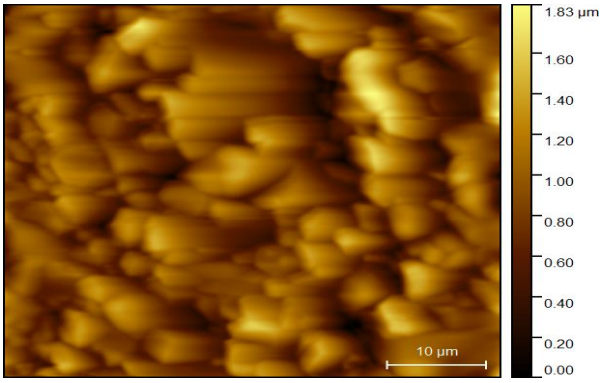

(g) 2D roughness of Z15Ce5Ca2

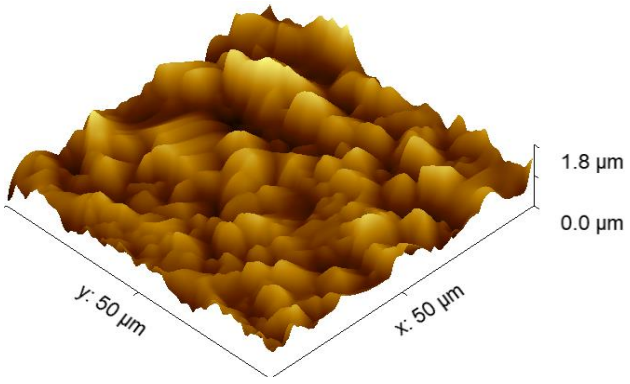

(h) 3D roughness of Z15Ce5Ca2

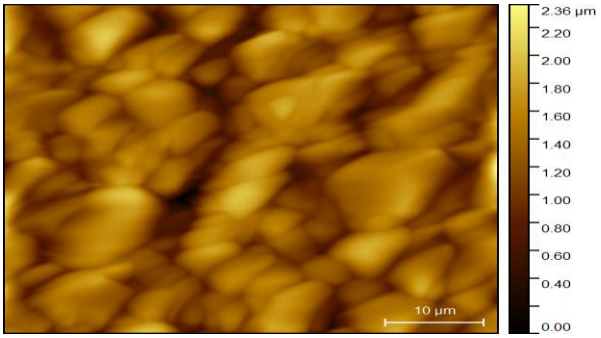

(i) 2D roughness of Z15Ce3

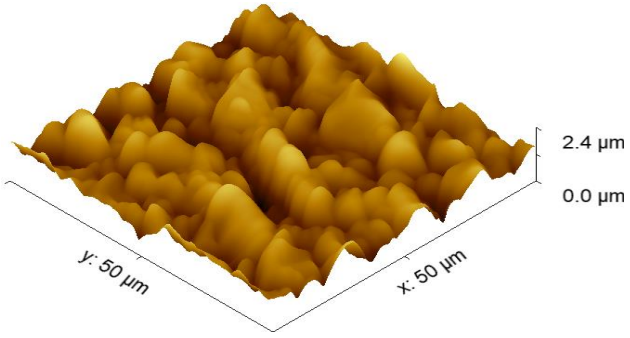

(j) 3D roughness of Z15Ce3

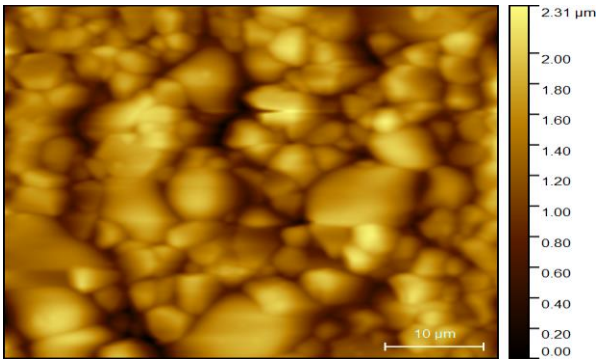

(k) 2D roughness of Z15Ce5Ca4

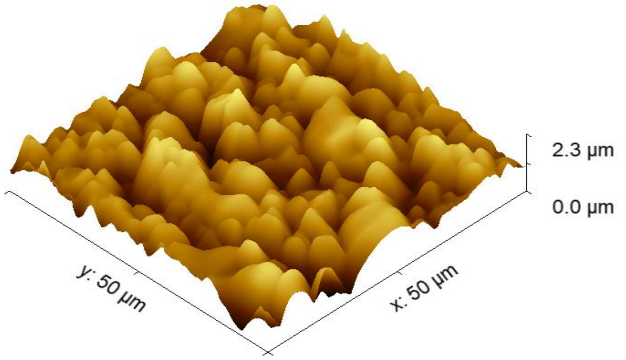

(l) 3D roughness of Z15Ce5Ca4

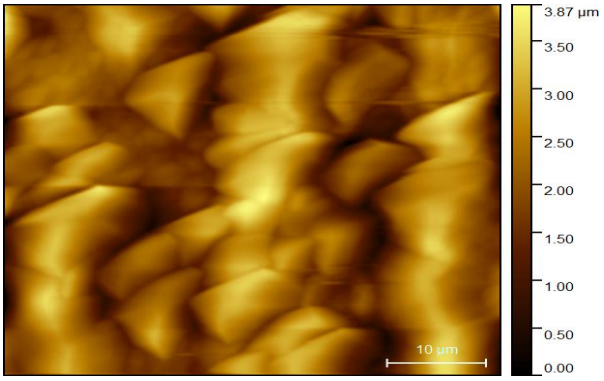

(m) 2D roughness of Z15Ce5Ca5

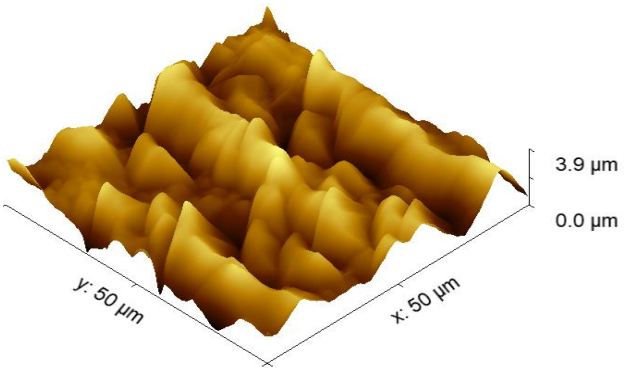

(n) 3D roughness of Z15Ce5Ca5

Figure 4.29(a-n) The AFM 2D & 3D images of various samples at 1500°C.

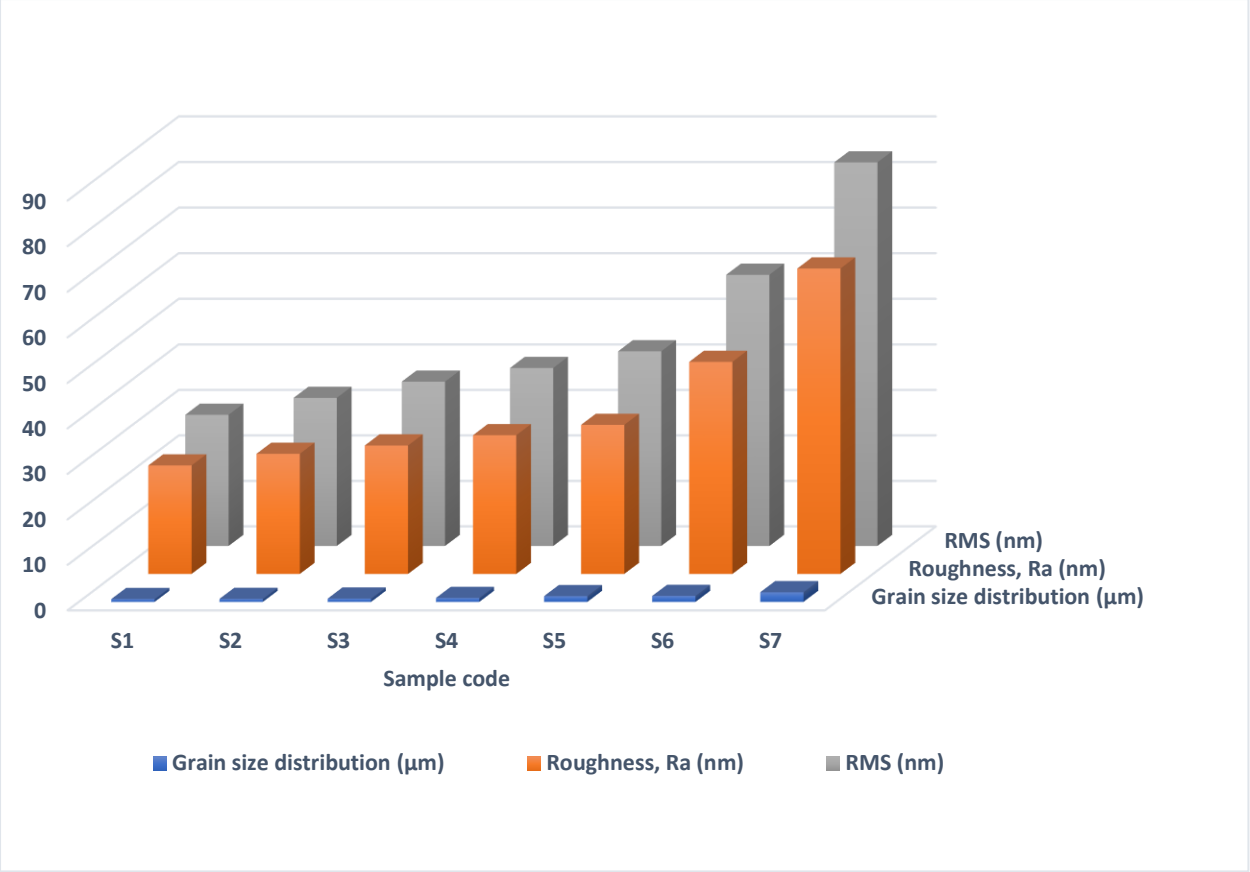

Figure 4.30 Results of AFM data analysis graph where sample code (S1-S7) represents the composites (Z15-Z15Ce5Ca5) respectively.

Table 4.6 AFM data calculated from images using gwyddion software.

Sample Code	Surface Roughness, Ra (nm)	RMS roughness (nm)	Av. Grain Size (µm)
S1 (Z15)	23.85	28.84	0.62
S2 (Z15Ce5)	26.41	32.55	0.66
S3 (Z15Ce5Ca1)	28.24	36.12	0.74
S4 (Z15Ce5Ca2)	30.50	39.12	0.86
S5 (Z15Ce5Ca3)	32.77	42.78	1.27
S6 (Z15Ce5Ca4)	46.61	59.56	1.31
S7 (Z15Ce5Ca5)	67.09	84.21	2.12

4.6 Biomedical Properties Analysis

4.6.1 Antimicrobial Susceptibility Test

Zirconia toughened alumina being an inert bio-ceramic has been used in many orthopedic applications. Nevertheless, extensive researches are being carried out recently to incorporate antimicrobial characteristics into ZTA. In this work, antimicrobial test has been performed on some samples to see if presence of CeO_2 or CaO could enhance the antimicrobial activity of TiO_2 and MgO doped ZTA. The result of antimicrobial sensitivity test against E. Coli (E) and Staphylococcus aureus bacteria is shown in **Figure 4.31**.

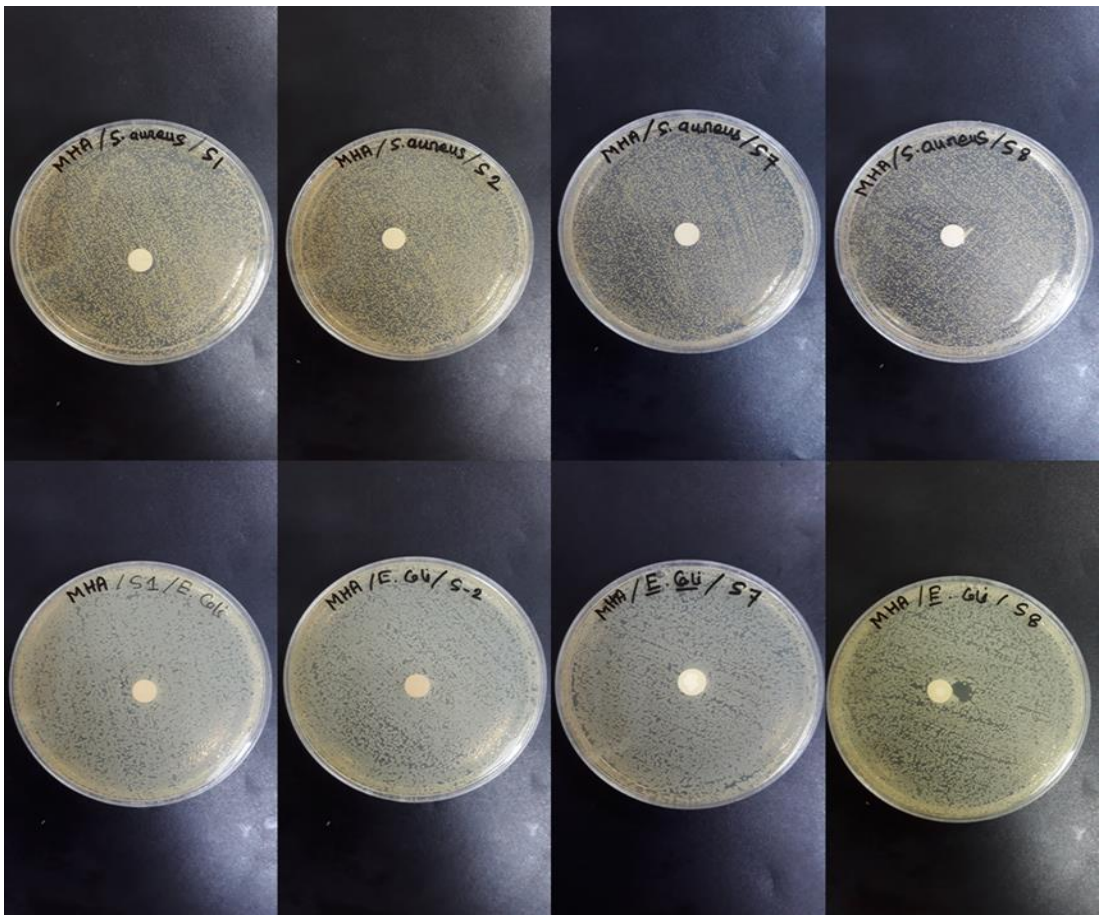

Figure 4.31 Antimicrobial activity of zirconia toughened alumina samples against bacteria Staphylococcus aureus (a-d) and E. coli (e-h) using disk agar diffusion method. Disk in (a, e) is for Z15, (b, f) for Z15Ce5, (c, g) for Z15Ce5Ca5 and (d, h) for Z15Ca5 samples.

According to Kirby-Bauer disk diffusion method, a zone of inclusion where bacteria cannot grow, forms around the sample if it has antibacterial properties. The larger the radius of the

zone of inclusion, the stronger the antibacterial activity. Whereas absence of zone of inhibition (ZOI) means the tested bacteria species are resistant to the specimen, indicating no antibacterial activity. From the **Figure 4.31**, it is evident that most of the samples could not form zone of inclusion in the bacteria infested disk. Hence sample Z15Ce5 and Z15Ce5Ca5 have no antibacterial property. However, Z15 shows very small ZOI against Staphylococcus aureus and Z15Ca5 shows an irregular ZOI against E. Coli. So, it can be inferred that the presence of Cerium in sample Z15Ce5 and Z15Ce5Ca5 disables the antibacterial properties otherwise active in sample Z15 and Z15Ca5 where Cerium is absent.

4.6.2 Cytotoxicity/Cell Viability Test

Cytotoxicity is the ability of a material or drug or other cells to destroy living cells. Cytotoxicity tests are conducted on chemicals or materials to ensure they have no cytotoxicity prior to their use in living things. Hence cytotoxicity test is very important for biomaterials like ZTA as they are used as prosthetics such as bone replacement. **Figure 4.32** shows the result of in vitro cytotoxicity test on the fibroblast cell line of kidney of a baby hamster.

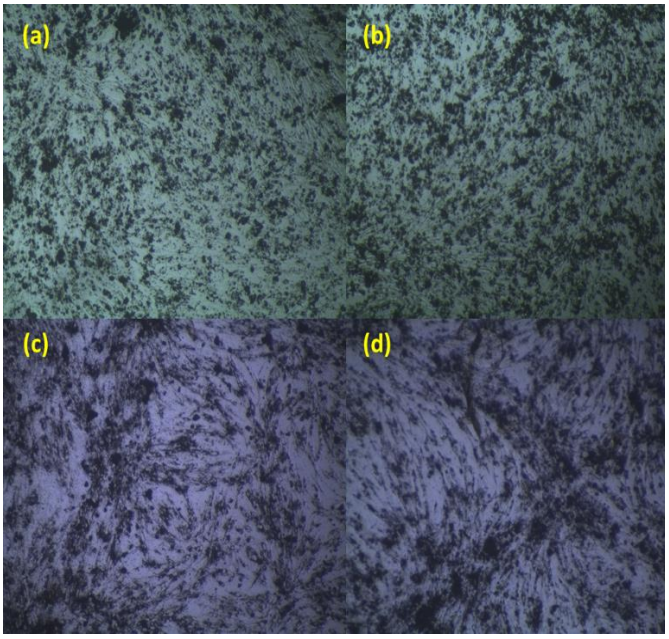

Samples	Survival of Cells
Negative control	100 %
Positive control	> 95 %
Z15	80-90 %
Z15Ce5	80-90 %
Z15Ce5Ca5	70-80 %
Z15Ca5	70-80 %

Figure 4.32 Cytotoxicity test of (a) Z15, (b) Z15Ce5, (c) Z15Ce5Ca5 and (d) Z15Ca5 samples.

As evident from the **Figure 4.32**, the cell viability is above 70% for all samples and can be considered as good as per standards. Sample Z15 and Z15Ce5 have 80-90% cell viability whereas a decrease is seen in sample Z15Ce5Ca5 and Z15Ca5. Presence of Calcium could be the reason behind this decrease as these samples contain hibonite phases. Slight change in cell size and morphology is also observed. Fibroblast cell lines are long thin cells which became fatter and less distinct in presence of Ca containing ZTA samples. This change in morphology is mainly due to break down of cell membranes and lysis. Our result is consistent with the literature where CoCr-ZTA composite also decreases growth of osteoblast cells of *Mus musculus* [158]. However, ZTA had increases the cell viability and growth in myoblast cell line C2C12 of mouse [159].

This analysis showed promising results, because the cell viability of the composite material is clearly above the 70% of viability limit, which indicates an excellent biocompatibility of the material. Therefore, it can be affirmed that the composite materials obtained in this work can be classified as non-cytotoxic. Therefore, they have great potential for possible application as implants. The findings of this experiments are summarized in the table as follows:

Table 4.7 Results of cytotoxicity test.

Samples	Survival of cells
Negative control	100%
Positive control	>95%
Z15	80-90%
Z15Ce5	80-90%
Z15Ce5Ca5	70-80%
Z15Ca5	70-80%

SUMMARY AND CONCLUSIONS

CHAPTER 5
SUMMARY AND CONCLUSIONS

5.1 Summary

This study used the traditional solid state reaction method to synthesis ZTA-TiO_2-MgO ceramic composites with simultaneous additions of CeO_2 and CaO.

Followings are the summary of the findings of this investigation:

- Density of ZTA-TiO_2-MgO composite initially increased with CeO_2 content then decreased with the addition of CaO up to 5 wt.% at lower sintering temperatures (1450°C, 1500°C). However, at higher sintering temperatures (1600°C, 1650°C) density slightly increased with CeO_2 and CaO content, though densities observed at 1600°C were comparatively higher than 1650°C.

- Porosity of ZTA-TiO_2-MgO composite initially decreased with CeO_2 content then increased for CaO inclusions (gradually 1-5 wt.%) at lower sintering temperatures (1450°C, 1500°C). However, at higher sintering temperatures (1600°C, 1650°C) porosity slightly increased with CeO_2 and CaO content, though porosities observed at 1600°C were comparatively lower than 1650°C.

- Microhardness decreased with the effects of CeO_2 and CaO, as they formed secondary phases cerium aluminate ($CeAl_{11}O_{18}$) and hibonite ($CaAl_{12}O_{19}$), whose have significantly lower hardness value than the base element alumina. Additionally, they also increased porosity that decreased the hardness as well.

- With increasing CaO content, fracture toughness increased due to formation of hibonite phases whose are responsible for crack deflection and crack bridging mechanisms. The fracture resistance has been enhanced by inclusion of 3 wt.% CaO to a maximum of 13.34 $MPam^{1/2}$ at 1500°C.

- Significant diametral tensile strength was found for the optimal composition (Z15Ce5Ca3) at relatively lower sintering temperature (1500°C), where the fracture toughness property was also maximum.

- For ZTA-TiO_2-MgO composite at 1450°C and 1500°C, the coefficient of thermal expansion (CTE) was measured and found to be $9.1X10^{-6}$ $°C^{-1}$ and $8.84X10^{-6}$ $°C^{-1}$, respectively. The ZTA-TiO_2-MgO with 5 wt. % CeO_2 and 5 wt.% CaO reduced the CTE to $8.31X10^{-6}$ $°C^{-1}$ and $8.38X10^{-6}$ $°C^{-1}$. A composite (ZTA-TiO_2-MgO) with a lower CTE value will have higher thermal shock resistance characteristics and will be more suitable for many more applications where high fracture toughness and thermal shock resistance are required.

- Almost insulating in nature considering electrical conductivity.

- For the optimal composition (Z15Ce5Ca3), the elongated platelet-shaped hibonite grains with homogenous microstructure (average grain size 1.27 μm, and minimum porosity ~ 5% of theoretical density, D_{th}) were found. The improved fracture toughness of this composite is a result of the interaction of more efficient energy-consuming mechanisms, including a mixed inter and trans granular fracture mode, crack deflection and crack bridging, as well as a transformation toughening mechanism for phase change.

- Surface roughness of the composites was in the nanometer scale and increased roughness provided more osteo-integration probability within the nano scale range.

- According to antibacterial susceptibility activity, the composites have no effect against microorganisms like gram (-) as well as gram (+) bacteria.

- Considering cell viability properties, primarily they are not harmful to living cells which has been observed by in vitro cytotoxicity analysis.

5.2 Conclusions

On the physical, mechanical, and microstructural characteristics of ZTA-TiO_2-MgO ceramic composites, the effects of CaO and CeO_2 addition were studied. CaO was content in varying amounts (1-5 wt.%), while CeO_2 content was 5 wt.%. The samples were pressurelessly sintered for three hours (3 hrs.) at 1450°C, 1500°C, 1600°C as well as 1650°C.

The characteristics of ZTA-TiO_2-MgO ceramics are influenced by the addition of CeO_2 (5 wt.%) and CaO (1-5 wt.%). The density slightly increased when CeO_2 was added, then gradually decreased when CaO was added up to 5 wt.%, reaching its lowest value (2.72 g/cm^3) at 1450°C. The maximum density was about 95% of the composites theoretical density and represented by 3.92 g/cm^3. At this condition, the material porosity was the lowest (~ 5%), while its Vickers microhardness value was the highest (11.72 GPa).

In ZTA-TiO_2-MgO composites, MgO initially interacted with Al^{3+} to create the secondary phase, $MgAl_2O_4$, while TiO_2 promoted density as well. Later, CeO_2 and CaO combine with Al^{3+} ions to generate $CeAl_{11}O_{18}$ and hibonite phases. The mechanical characteristics of ceramic composites are significantly affected by these secondary phases. When the hibonite phase was present in the highest percentage (3 wt.% CaO, sintering temperature 1500°C), the ceramic composites were shown to have the highest fracture toughness (13.34 $MPam^{1/2}$). At this point, the Vickers microhardness and the diametral tensile strength were both moderately significant with 10.23 GPa and 108.39 MPa respectively. The distribution and quantity of the hibonite elongated grains in this ceramic's microstructure control its key mechanical characteristics. Therefore, by simply adjusting the proportion of hibonites (i.e., addition of CaO), different combinations of this ceramic's properties (fracture toughness, strength, hardness) can be tailored as per desired ultimate applications.

5.3 Scopes for future works

ZrO_2 toughened Al_2O_3 (ZTA composite), which has an outstanding biocompatibility and can be formed into specific sizes, has a wide range of applications in engineering and medical sciences. Therefore, numerous in vitro and in vivo research are required in order to understand the biological activity of ZTA compound. Additionally, understanding mechanical characteristics would be much more important for selecting the proper ZTA composite depending on the site of implantation. To get better accurate outcome of its effectiveness in a biomedical practice, mechanical properties including flexural strength, wear resistance, and thermal conductivity of ZTA composite with proper ZrO_2, MgO, TiO_2, CaO, CeO_2 or along with presence of other additives, controlled sintering temperature and sintering duration should be optimized. For further enhance mechanical properties, various compositions, sample preparation methods, and sintering conditions, sintering rates and stages should be investigated.

REFERENCES

References

[1] D. W. Richerson, “The Magic of Ceramics”, Wiley-American Ceramic Society, USA, 2000

[2] O. L. Ighodaro and O. I. Okoli, “Fracture toughness enhancement for alumina systems: A review,” *Int. J. Appl. Ceram. Technol.*, vol. 5, no. 3, pp. 313-323, 2008.

[3] H. Hori, S., Somiya, H.Y. and Kaji, “Change of Tetragonal Zirconia Content in Zirconia-Toughened Alumina by Hot Iso-stating Pressing,” *J. Mater. Sci. Lett.*, vol. 3, pp. 242-244, 1988.

[4] S. W. Kim and K. A. R. Khalil, “High-frequency induction heat sintering of mechanically alloyed alumina-yttria-stabilized zirconia nano-bioceramics,” *J. Am. Ceram. Soc.*, vol. 89, no. 4, pp. 1280-1285, 2006.

[5] A.H. De Aza, J. Chevalier, G. Fantozzi, M.S.R. Torrecillas, A.H. De Aza, J. Chevalier, G. Fantozzi, M. Schehl, R. Torrecillas, Crack growth resistance of alumina, zirconia and zirconia toughened alumina ceramics for joint prostheses, J. Biomater. 23 (2002) 937-945. https://doi.org/10.1016/S0142-9612(01)00206-X.

[6] H. Fischer, W. Rentzsch, R. Marx, Elimination of low-quality ceramic posts by proof testing, Dent. Mater. 18 (2002) 570-575. https://doi.org/10.1016/S0109-5641(01)00091-4.

[7] S. Nazarpour, C. Zamani, J. M. Fernández-Sanjuán and A. Cirera, "Phase transformation studies on YSZ doped with alumina. Part 1: Yttria segregation", J. Al and Comp, vol. 505. no. 2, pp 527-533, 2010.

[8] S. Nazarpoura, C. L. Gándaraa, C. Zamania and A. Cirera "Phase transformation studies on YSZ doped with alumina. Part 2: Yttria segregation" *J. All. and Comp.* 505, pp 534-541, 2010.

[9] M. Hasanuzzaman, A. Rafferty, A. G. Olabi, and T. Prescott, “Sintering and characterization of nano-sized yttria-stabilized zirconia,” Int. J. Nanoparticles, vol. 1, no. 1, pp. 50-65, 2008.

[10] D. Chakravarty, S. Bysakh, K. Muraleedharan, T. N. Rao, and R. Sundaresan, “Spark plasma sintering of magnesia-doped alumina with high hardness and fracture toughness,” *J. Am. Ceram. Soc.*, vol. 91, no. 1, pp. 203-208, 2008.

[11] Z. D. I. Sktani, A. Z. A. Azhar, M. M. Ratnam, and Z. A. Ahmad, “The influence of in-situ formation of hibonite on the properties of zirconia toughened alumina (ZTA) composites,” *Ceram. Int.*, vol. 40, no. 4, pp. 6211-6217, 2014.

[12] A. Senthil Kumar, A. Raja Durai, and T. Sornakumar, “Development of alumina-ceria ceramic composite cutting tool,” *Int. J. Refract. Met. Hard Mater.*, vol. 22, no. 1, pp. 17-20, 2004.

[13] A. H. Heuer, N. Claussen, W. M. Kriven, and M. Ruhle, “Stability of Tetragonal ZrO_2 Particles in Ceramic Matrices,” *J. Am. Ceram. Soc.*, vol. 65, no. 12, pp. 642-650, Dec. 1982.

[14] D.X. Tang, H.B. Lim, K.J. Lee, C.H. Lee and W.S. Cho. Evaluation of mechanical reliability of zirconia-toughened alumina composites for dental implants. Ceram Int; 38(3): 2429-36, 2012.”

[15] L. K. Bhalla, “*Influence of Strontium Oxide on Mechanical Response of Zirconia Toughened Alumina*". M.Sc. Thesis. Department of Ceramic Engineering, National Institute of Technology Rourkela, 2014.

[16] M.T. Hernandez, M. Gonzá lez, A. De Pablos, C-diffusion during hot press in the Al_2O_3-Cr_2O_3 system, Acta Mater. 51 (2003) 12.

[17] A. Al Mahmood, M. A. Gafur, and M. E. Hoque, “Effect of MgO on the physical, mechanical and microstructural properties of ZTA-TiO_2 composites,” *Mater. Sci. Eng. A*, vol. 707, pp. 118-124, 2017.

[18] W. E. Lee and W. M. Rainforth, *Ceramic microstructures: property control by processing*.London: Springer Science & Business Media., 1994.

[19] A. R. Olszyna, P. Marchlewski and K. J. Kurzydłowski, “Sintering of high-density, high-purity alumina ceramics,” *Ceram. Int.*, vol. 23, no. 4, pp. 323-328, 1997.

[20] G. Maccauro, P. R. Iommetti, L. Raffaelli, P. F. Manicone, and R. Pignatello, *Alumina andZirconia Ceramic for Orthopaedic and Dental Devices, Biomaterials Applications for Nanomedicine*. 2011.

[21] S. Pramanik, A. K. Agarwal, and K. N. Rai, “Chronology of total hip joint replacement andmaterials development,” *Trends Biomater. Artif. Organs*, vol. 19, no. 1, pp. 15-26, 2005.

[22] P. Palmero, L. Montanaro, H. Reveron, and J. Chevalier, “Surface Coating of Oxide Powders: A New Synthesis Method to Process Biomedical Grade Nano-Composites,” *Materials (Basel).*, vol. 7, no. 7, pp. 5012-5037, 2014.

[23] C. Piconi, S. C. Condo, T. Kosmač, and J. Shen, “Alumina and zirconia-based ceramics forload-bearing applications. In Advanced Ceramic for Dentistry,” in *Advanced Ceramics forDentistry*, Elsevier Inc, 2014, pp. 219-253.

[24] R. H. J. Hannink, P. M. Kelly, and B. C. Muddle, “Transformation toughening in zirconia-containing ceramics,” *J. Am. Ceram. Soc.*, vol. 77, 2000.

[25] P. Duwez, F. H. Brown, and F. Odell, “The Zirconia- Yttria System,” *J. Electrochem. Soc.*, vol. 98, no. 9, pp. 356-362, Sep. 1951.

[26] H.G. Scott, “Phase relationships in the zirconia-yttria system,” J. Mate. Sci., vol. 10, pp. 1527-1535, 1975.

[27] M. Asadikiya, H. Sabarou, M. Chen, and Y. Zhong, “Phase diagram for a nano-yttria-stabilized zirconia system,” *RSC Adv.*, vol. 6, no. 21, pp. 17438-17445, 2016.

[28] S.R. Choi and N.P. Bansal, ìStrength, "Fracture Toughness, and Slow Crack Growth of Zirconia / Alumina Composites at Elevated Temperaturem". î *NASA/TMó* -212108, 2003.

[29] S. Nazarpoura, C. L. Gándaraa, C. Zamania and A. Cirera "Phase transformation studies on YSZ doped with alumina. Part 2: Yttria segregation" *J. All. and Comp.* 505, pp 534-541, 2010.

[30] H.G. Scott, “Phase relationships in the zirconia-yttria system,” J. Mate. Sci., vol. 10, pp. 1527-1535, 1975.

[31] P. Doerner, L. J. Gauckler, H. Krieg, H. L. Lukas, G. Petzow, and J. Weiss, 'Comput. Coupling Phase Diagrams", *Thermochem.*, 3 [4] 241-257, 1979.

[32] M. Hasanuzzaman, A. Rafferty, A. G. Olabi, and T. Prescott, “Sintering and characterization of nano-sized yttria-stabilized zirconia,” Int. J. Nanoparticles, vol. 1, no. 1, pp. 50-65, 2008.

[33] S.R. Choi and N.P. Bansal, "Strength and Fracture Toughness of YSZ/Alumina Composites for Solid Oxide Fuel Cells", Ceram. Eng. Sci. Proc., 23 [3] 741-750, 2002.”

[34] F. Tarasi, M. Medraj, A. Dolatabadi and C. Moreau, Amorphous and Crystalline Phase Formation During Suspension Plasma Spraying of Alumina-YSZ Composite Coatings, J. Eur. Ceram. Soc vol. 31. 2903-2913, 2011.

[35] S. Lakiza and L. Lopato, Phase Diagram of the Alumina–Zirconia–Samaria System, J. Am. Ceram. Soc. vol. 89, 3516-3521, 2006.

[36] P. Ctibor, P. Rohan, T. Chraska, and K. Neufuss, "Fabrication of bulk nanocrystalline alumina – zirconia materials," Ceram. Int., vol. 34, pp. 1229-1236, 2008.

[37] N. Claussen, and J. Jahn, "Transformation of Tetragonal ZrO_2 Particles in a Ceramic Matrix," Berichte der Dtsch. Keramischen Gesellschaft, vol. 55, pp. 487-491, 1978.

[38] K. H. Brosnan, G. L. Messing, and D. K. Agrawal, "Microwave Sintering of Alumina at 2.45 GHz," J. Am. Ceram. Soc., vol. 86, no. 8, pp. 1307-1312, Aug. 2003.

[39] M. C. C. S. Moraes, C. N. Elias, J. Duailibi Filho, and L. G. de Oliveira, "Mechanical properties of alumina-zirconia composites for ceramic abutments," Mater. Res., vol. 7, no. 4, pp. 643-649, 2004.

[40] S. W. Kim and K. A. R. Khalil, "High-frequency induction heat sintering of mechanically alloyed alumina-yttria-stabilized zirconia nano-bioceramics," J. Am. Ceram. Soc., vol. 89, no. 4, pp. 1280-1285, 2006.

[41] A. Z. A. Azhar, M. M. Ratnam, and Z. A. Ahmad, "Effect of Al_2O_3/YSZ microstructures on wear and mechanical properties of cutting inserts," J. Alloys Compd., vol. 478, no. 1-2, pp. 608-614, 2009.

[42] N. A. Rejab, A. Z. A. Azhar, M. M. Ratnam, and Z. A. Ahmad, "The relationship between microstructure and fracture toughness of zirconia toughened alumina (ZTA) added with MgO and CeO_2," Int. J. Refract. Met. Hard Mater., vol. 41, pp. 522-530, 2013.

[43] A. Rittidech, R. Somrit, and T. Tunkasiri, "Effect of adding Y_2O_3 on structural and mechanical properties of Al_2O_3-ZrO_2 ceramics," Ceram. Int., vol. 39, no. SUPPL.1, pp. S433-S436, 2013.

[44] S. M. Naga, A. M. Hassan, H. F. El-Maghraby, M. Awaad, and H. Elsayed, "Insitu sintering reaction of Al_2O_3-$LaAl_{11}O_{18}$-ZrO_2 Composite," Int. J. Refract. Met. Hard Mater., vol. 54, pp. 230-236, 2016.

[45] M. A. Gafur, M. S. R. Sarker, M. Z. Alam, and M. R. Qadir, “Effect of 3 mol% Yttria Stabilized Zirconia Addition on Structural and Mechanical Properties of Alumina-Zirconia Composites,” Mater. Sci. Appl., vol. 08, no. 07, pp. 584-602, 2017.

[46] P. G. Rao, M. Iwasa, T. Tanaka, I. Kondoh and T. Inoue, “Preparation and mechanical properties of Al_2O_3-15wt % ZrO_2 composites”, Scripta Materialia, 48, 437- 441, 2003.

[47] D. Jayaseelan, T. Nishikawa, H. Awaji and F. D. Gnanam, “Pressure less sintering of sol-gel derived alumina-ZrO_2 composites”, Mat. Sci. Engr., 256, 265-270, 1998.

[48] F. M. J. K. Daguano, C. Santos, R. C. Souza, R. M. Balestra, K. Strecker and C. N. Elias, “Properties of ZrO_2-Al_2O_3 composite as a function of isothermal holding time”, Int. J. Refrac. Met. Hard Mat., 25, 374-379, 2007.

[49] A. Fortulan, P.F. Dulcina and de Souza, “Microstructural Evolution of the Al_2O_3-ZrO_2 composite and its correlation with electrical conductivity”, Mat. Res., 2, 205-210, 1999.

[50] M. Cecilia, C. N. Elias, J. D. Filho and L. G. de Oliveira, “Mechanical properties of Al_2O_3- ZrO_2 composites for ceramic abutments”, Mat. Res., 7, 643-649, 2004.

[51] D. Sarkar, S. Adak and N. K. Mitra, “Preparation and characterization of an Al_2O_3-ZrO_2 nanocomposite, Part I: Powder synthesis and transformation behavior during fracture”, Composites A, 2006.

[52] C. J. Wang and C. Y. Huang, “Effect of TiO_2 addition on the sintering behavior, hardness and fracture toughness of an ultrafine alumina,” Mater. Sci. Eng. A, vol. 492, no. 1-2, pp. 306-310, 2008.

[53] Y. Zu et al., “Effects of liquid phases on densification of TiO_2-doped Al_2O_3-ZrO_2 composite ceramics,” Ceram. Int., vol. 40, no. 3, pp. 3989-3993, 2014.

[54] Y. Ai, K. Wu and B. Liang, “Mechanical properties of La_2O_3 and Nb_2O_5 doped Al_2O_3 ceramics prepared by microwave sintering,” J. Ceram. Soc. Japan, vol. 122, no. 1422, pp. 166-170, 2014.

[55] X. S. Yang, Y. Wang, and Y. Zhao, “Effect of Nb_2O_3 and La_2O_3 on the microstructure and electrical properties of Al_2O_3 ceramics,” Mater. Chem. Phys., vol. 98, no. 2-3, pp. 225-230, 2006.

[56] A. M. Hassan, S. M. Naga, and M. Awaad, “Toughening and strengthening of Nb_2O_5 doped Zirconia/Alumina (ZTA) composites,” Int. J. Refract. Met. Hard Mater., vol. 48, pp. 338-345, 2015.

[57] D.-H. Kim and C. H. Kim, “Effect of Heating Rate on Pore Shrinkage in Yttriadoped Zirconia,” J. Am. Ceram. Soc., vol. 76, no. 7, pp. 1877-1878, 1993.

[58] Y. Wu, Y. Zhang, and X. Huang, “Preparation, sintering and fracture behavior of $Al_2O_3/LaAl_{11}O_{18}$ ceramic composites,” J. Mater. Sci., vol. 6, pp. 4195-4199, 2000.

[59] F. Kern, "A comparison of microstructure and mechanical properties of 12Ce-TZP reinforced with alumina and in situ formed strontium- or lanthanum hexa-aluminate precipitates", J. Eur. Ceram. Soc., vol. 34. pp 413-423, 2014.

[60] Z. Negahdari and M. Willert-Porada, “Tailoring the microstructure of reaction sintered alumina/lanthanum hexa-aluminate particulate composites,” J. Eur. Ceram. Soc., vol. 30, no. 6, pp. 1381-1389, 2010.

[61] A. Ceylan and P. A. Fuierer, “Fracture toughness of alumina/lanthanum titanate laminate composites with a weak interface,” Mater. Lett., vol. 61, no. 2, pp. 551-555, 2007.

[62] Sajib Aninda Dhar, Shoumya Nandy Shuvo, A.K.M.B. Rashid, Mechanical and Microstructural Properties of TiO_2 doped Zirconia Toughened Alumina (ZTA) Ceramic Composites at different TiO_2 contents, American Journal of Engineering Research (AJER) Volume-4, Issue-11, pp.08-12.

[63] N.A. Rejab, A.Z.A. Azhar, K.S. Kian, M.M. Ratnam, Z.A. Ahmad, Effects of MgO addition on the phase, mechanical properties, and microstructure of zirconia-toughened alumina added with CeO_2 (ZTA-CeO_2) ceramic composite, Materials Science and Engineering A 595(2014) 18-24.

[64] J. Wang, S. Y. Lim, S. C. Ng, C. H. Chew, and L. M. Gan, “Dramatic effect of a small amount of MgO addition on the sintering of Al_2O_3-5 vol% SiC nanocomposite,” *Mater. Lett.*, vol. 33, no. 5-6, pp. 273-277, 1998.

[65] D. Chakravarty, S. Bysakh, K. Muraleedharan, T. N. Rao, and R. Sundaresan, “Spark plasma sintering of magnesia-doped alumina with high hardness and fracture toughness,” *J. Am. Ceram. Soc.*, vol. 91, no. 1, pp. 203-208, 2008.

[66] A. Z. A. Azhar, L. C. Choong, H. Mohamed, M. M. Ratnam, and Z. A. Ahmad, “Effects of Cr_2O_3 addition on the mechanical properties, microstructure and wear

performance of zirconia-toughened-alumina (ZTA) cutting inserts," *J. Alloys Compd.*, vol. 513, pp. 91-96, 2012.

[67] D. Casellas, M. M. Nagl, L. Llanes, and M. Anglada, "Fracture toughness of alumina and ZTA ceramics: Microstructural coarsening effects," *J. Mater. Process. Technol.*, vol. 143-144, no. 1, pp. 148-152, 2003.

[68] A. Rittidech, R. Somrit, and T. Tunkasiri, "Effect of adding Y_2O_3 on structural and mechanical properties of Al_2O_3-ZrO_2 ceramics," *Ceram. Int.*, vol. 39, no. SUPPL.1, pp. S433-S436, 2013.

[69] R. Sarker, G. Banerjee, Effect of Compositional Variation and Fineness in the Densification of MgO-Al_2O_3 Compacts, J. Eur. Ceram. Soc. 19 (1999) 7.

[70] A. Senthil Kumar, A. Raja Durai, and T. Sornakumar, "Development of alumina-ceria ceramic composite cutting tool," *Int. J. Refract. Met. Hard Mater.*, vol. 22, no. 1, pp. 17-20, 2004.

[71] A. Miyaoka, Y. Mizutani, M. Tsuchiya, K. Kawahara, and T. Okajima, "Rheological properties of growth-arrested fibroblast cells under serum starvation measured by atomic force microscopy," *Jpn. J. Appl. Phys.*, vol. 50, no. 8 PART 4,

[72] N. Claussen, and J. Jahn, "Transformation of Tetragonal ZrO_2 Particles in a Ceramic Matrix," *Berichte der Dtsch. Keramischen Gesellschaft*, vol. 55, pp. 487-491, 1978.

[73] J. B. Wachtman, *Mechanical Properties of Ceramics*, ISBN-13. Wiley-Interscience, May, 1996.

[74] I. Akin, E. Yilmaz, F. Sahin, O. Yucel, and G. Goller, "Effect of CeO_2 addition on densification and microstructure of Al_2O_3-YSZ composites," *Ceram. Int.*, vol. 37, no. 8, pp. 3273-3280, 2011.

[75] A. Z. A. Azhar, L. C. Choong, H. Mohamed, M. M. Ratnam, and Z. A. Ahmad, "Effects of Cr_2O_3 addition on the mechanical properties, microstructure and wear performance of zirconia-toughened-alumina (ZTA) cutting inserts," *J. Alloys Compd.*, vol. 513, pp. 91-96, 2012.

[76] N. A. Rejab, A. Z. A. Azhar, M. M. Ratnam, and Z. A. Ahmad, "The effects of CeO_2 addition on the physical, microstructural and mechanical properties of yttria stabilized zirconia toughened alumina (ZTA)," *Int. J. Refract. Met. Hard Mater.*, vol. 36, pp. 162-166, 2013.

[77] M. S. Koji Tsukuma, ‘Strength, fracture toughness and Vickers hardness of CeO_2 - stabilized tetragonal ZrO_2 polycrystals (Ce-TZP),’ Journal of Materials Science, vol. 20, no. 4, pp. 1178-1184, 1985.

[78] Z. D. I. Sktani, A. Z. A. Azhar, M. M. Ratnam, and Z. A. Ahmad, “The influence of in-situ formation of hibonite on the properties of zirconia toughened alumina (ZTA) composites,” Ceram. Int., vol. 40, no. 4, pp. 6211-6217, 2014.

[79] C. Zeng, Z. Huang, J. Huang, Y. Li, Y. Xu, S. Yi, M. Fang, Y.G. Liu, Preparation of Calcium Hexa-aluminate using Al_2O_3 and White Beach Sand from Western Australia, Key Eng. Mater. 512-515 (2012) 940-944, https://doi.org/10.4028/ www.scientific.net/KEM.512-515.940.

[80] T. Hainschwang, F. Notari, L. Massi, T. Armbruster, B. Rondeau, E. Fritsch, M. Nagashima, Hibonite: A New Gem Mineral, Rapid Commun. 46 (2) (2010) 135-138.

[81] A.J. Sánchez-Herencia, R. Moreno, C. Baudı´ n, Fracture behaviour of alumina calcium hexa-aluminate composites obtained by colloidal processing, J. Eur. Ceram. Soc. 20 (14-15) (2000) 2575-2583, https://doi.org/10.1016/S0955-2219(00)00123-0.

[82] L. K. Bhalla, “Influence of Strontium Oxide on Mechanical Response of Zirconia Toughened Alumina". M.Sc. Thesis. Department of Ceramic Engineering, National Institute of Technology Rourkela, 2014.

[83] Y. K. Jeong and K. Niihara, “Microstructure and properties of alumina-silicon carbide nanocomposites fabricated by pressureless sintering and post hot-isostatic pressing,” Trans. Nonferrous Met. Soc. China (English Ed., vol. 21, no. SUPPL. 1, pp. s1-s6, 2011.

[84] M. Parchovianský, D. Galusek and J. Sedláček. “Microstructure and mechanical properties of hot pressed Al_2O_3/SiC nanocomposites,” J. Eur. Ceram. Soc., vol. 33, no. 12, pp. 2291-2298, 2013.

[85] R. Klement, P. Švančárek, M. Parchovianský, J. Sedláček, and D. Galusek, "Al_2O_3-SiC nanocomposites: Preparation, microstructure, and properties". 50 Adv. Ceram. Mat. Comp., pp 49-92, 2018.

[86] J. Liu, H. Yan, M. J. Reece, and K. Jiang, “Toughening of zirconia/alumina composites by the addition of graphene platelets,” J. Eur. Ceram. Soc., vol. 32, no. 16, pp. 4185-4193, 2012.

[87] H. Porwal, P. Tatarko, S. Grasso, J. Khaliq, I. Dlouhý, and M. J. Reece, “Graphene reinforced alumina nano-composites,” Carbon N. Y., vol. 64, no. July, pp. 359-369, 2013.

[88] M. H. Bocanegra-Bernal, C. Dominguez-Rios, J. Echeberria, A. Reyes-Rojas, A. Garcia-Reyes, and A. Aguilar-Elguezabal, “Effect of low-content of carbon nanotubes on the fracture toughness and hardness of carbon nanotube reinforced alumina prepared by sinter, HIP and sinter + HIP routes,” Mater. Res. Express, vol. 4, no. 8, 2017.

[89] W. Acchar, A. E. Martinelli, and C. A. A. Cairo, “Reinforcing Al_2O_3 with W-Ti mixed carbide,” Mater. Lett., vol. 46, no. 4, pp. 209-211, 2000.

[90] W. Acchar and A. M. Segadães, “Properties of sintered alumina reinforced with niobium carbide,” Int. J. Refract. Met. Hard Mater., vol. 27, no. 2, pp. 427-430, 2009.

[91] Y. Cheng, S. Sun, and H. Hu, “Preparation of Al_2O_3/TiC micro-composite ceramic tool materials by microwave sintering and their microstructure and properties,” Ceram. Int., vol. 40, no. PB, pp. 16761-16766, 2014.

[92] Y. Cheng, Y. Zhang, T. Wan, Z. Yin, and J. Wang, “Mechanical properties and toughening mechanisms of graphene platelets reinforced Al_2O_3/TiC composite ceramic tool materials by microwave sintering,” Mater. Sci. Eng. A, vol. 680, pp. 190-196, 2017.

[93] Z. Yin, J. Yuan, Z. Wang, H. Hu, Y. Cheng, and X. Hu, “Preparation and properties of an Al_2O_3/Ti(C, N) micro-nano-composite ceramic tool material by microwave sintering,” Ceram. Int., vol. 42, no. 3, pp. 4099-4106, 2016.

[94] X. Bai, C. Huang, J. Wang, B. Zou, and H. Liu, “Fabrication and characterization of Si_3N_4 reinforced Al_2O_3-based ceramic tool materials,” *Ceram. Int.*, vol. 41, no. 10, Part A, pp. 12798-12804, 2015.

[95] Z. Yin, J. Yuan, Z. Wang, H. Hu, Y. Cheng, and X. Hu, “Preparation and properties of an Al_2O_3/Ti(C, N) micro-nano-composite ceramic tool material by microwave sintering,” *Ceram. Int.*, vol. 42, no. 3, pp. 4099-4106, 2016.

[96] M. Cheng, H. Liu, B. Zhao, C. Huang, P. Yao, and B. Wang, “Mechanical properties of two types of Al_2O_3/TiC ceramic cutting tool material at room and elevated temperatures,” *Ceram. Int.*, vol. 43, no. 16, pp. 13869-13874, 2017.

[97] A. H. Heuer, N. Claussen, W. M. Kriven, and M. Ruhle, “Stability of Tetragonal ZrO_2 Particles in Ceramic Matrices,” J. Am. Ceram. Soc., vol. 65, no. 12, pp. 642-650, Dec. 1982.

[98] D.X. Tang, H.B. Lim, K.J. Lee, C.H. Lee and W.S. Cho. Evaluation of mechanical reliability of zirconia-toughened alumina composites for dental implants. Ceram Int; 38(3): 2429-36, 2012.”

[99] P. Palmero, L. Montanaro, H. Reveron, and J. Chevalier, Surface Coating of Oxide Powders: A New Synthesis Method to Process Biomedical Grade Nano Composites, Mat. vol. 7. pp 512-537, 2014

[100] I. Jabber, T. Mohammed, M. Alkhafagy, O. Abed, and A.H. Al-Badry, "Effect of Adding Nano Alumina on the Grain Size and the Mechanical Properties of Yttria Stabilized Tetragonal Zirconia Polycrystals (Y-TZP)", IJMME-IJENS vol. 17. pp 86-99, 2017.

[101] Stevens R, Zirconia and Zirconia Ceramics, Magnesium Elektron Ltd, 1986, p18-19.

[102] Claussen N, J.Am. Ceram. Soc., 59, 49, (1976).

[103] A. H. De Aza, J. Chevalier, G. Fantozzi, M. Schehl, and R. Torrecillas, “Crack growth resistance of alumina, zirconia and zirconia toughened alumina ceramics for joint prostheses,” Biomaterials, vol. 23, no. 3, pp. 937-945, 2002.

[104] N. Claussen, J. Steeb, and R. F. Pabst, “Effect on induced microcracking on the fracture toughness of ceramics,” *Am. Ceram. Soc. Bull.*, vol. 56, no. 6, pp. 559-562, 1977.

[105] T. Kosmač, M. V Swain, and N. Claussen, “The role of tetragonal and monoclinic ZrO_2 particles in the fracture toughness of Al_2O_3-ZrO_2 composites,” *Mater. Sci. Eng.*, vol. 71, pp. 57-64, 1985.

[106] G. H. Campbell, M. Rühle, B. J. Dalgleish, and A. G. Evans, “Whisker toughening: a comparison between aluminum oxide and silicon nitride toughened with silicon carbide,” *J. Am. Ceram. Soc.*, vol. 73, no. 3, pp. 521-530, 1990.

[107] C. O. McHugh, T. J. Whalen, and M. Humenik, “Dispersion-Strengthened Aluminum Oxide,” *J. Am. Ceram. Soc.*, vol. 49, no. 9, pp. 486-491, 1966.

[108] R. P. Wahi and B. Ilschner, “Fracture behaviour of composites based on Al_2O_3-TiC,” *J. Mater. Sci.*, vol. 15, no. 4, pp. 875-885, 1980.

[109] M. Yoshimura, “Phase stability of zirconia,” *Am. Ceram. Soc. Bull. ;(United States)*, vol. 67, no. 12, 1988.

[110] N. Claussen, M. Ruhle, and A. H. Heuer, “Advances in Ceramics, vol. 12,” *Sci. Technol. zirconia II*, 1984.

[111] S. M. Kurtz, S. Kocagöz, C. Arnholt, R. Huet, M. Ueno, and W. L. Walter, “Advances in zirconia toughened alumina biomaterials for total joint replacement,” J. Mech. Behav. Biomed. Mater., vol. 31, pp. 107-116, 2014.

[112] R. A. Cutler, R. J. Mayhew, K. M. Prettyman, and A. V Virkar, “High-Toughness Ce- TZP/Al_2O_3 Ceramics with Improved Hardness and Strength,” *J. Am. Ceram. Soc.*, vol. 74,no. 1, pp. 179-186, 1991.

[113] C. Schmid, E. Lucchini, O. Sbaizero, and S. Maschio, “The synthesis of calcium or strontium hexa-aluminate added ZTA composite ceramics,” *J. Eur. Ceram. Soc.*, vol. 19, no.9, pp. 1741-1746, 1999.

[114] M. Belmonte, A. J. Sanchez-Herencia, R. Moreno, P. Miranzo, J. S. Moya, and A. P. Tomsia, “In situ formation of CA_6 platelets in Al_2O_3 and Al_2O_3/ZrO_2 matrices,” *Le J. Phys. IV*, vol. 3, no. C7, pp. C7-1443-C7-1447, 1993.

[115] S. Maity, S. Catterjee, and M. K. Basu, “Improvement of mechanical properties of zirconia-toughened alumina in presence of $SrAl_{12}O_{19}$,” *Third Euro-Ceram.*, vol.3, pp. 731-736, 1993.

[116] M. Alsebaie, “Characterisation of Alumina-Zirconia Composites Produced By 84 Micron-Sized Powders,” M.Engg. Thesis, School of Mechanical and Manufacturing Engineering, Dublin City Univ., 2005.

[117] Biswas and S. P. Chaudhuri, “Sintering and fracture toughness of alumina-zirconia composites,” Indian J. Eng. Mater. Sci., vol. 5, no. 5, pp. 307-311, 1998.

[118] J. Fan, T. Lin and F. Hu, “Effect of sintering temperature on microstructure and mechanical properties of zirconia-toughened alumina machinable dental ceramics,” Ceram. Int., vol. 43, no. 4, pp. 3647-3653, 2017.

[119] K. He, J. Chen, W. Weng, C. Li, and Q. Li, “Microstructure and mechanical properties of plasma sprayed Al_2O_3-YSZ composite coatings,” Vacuum, vol. 151, 83 pp. 209-220, May 2018.

[120] K.J. Hwang, M. Shin, M.H. Lee, H. Lee, M. Y. Oh, and T. H. Shin, “Investigation on the phase stability of yttria-stabilized zirconia electrolytes for high-temperature electrochemical application,” Ceram. Int., Sep. 2018.

[121] Muhammad Moazzam Hossen, “Preparation and Characterization of Alumina-Zirconia Composites (ZTA)”. Department of Physics, Chittagong University of Engineering and Technology (2014).

[122] W. Pabst, E. Gregorova, G. Ticha and E. Tynova, “Effective Elastic Properties of Al_2O_3-ZrO_2 Composite Ceramics Part 4. Tensile modulus of porous Al_2O_3 and ZrO_2”, Ceramics-Silikáty, 48, 165-174, 2004.

[123] M. Cecilia, C. N. Elias, J. D. Filho and L. G. de Oliveira, “Mechanical properties of Al_2O_3-ZrO_2 composites for ceramic abutments”, Mat. Res., 7, 643-649, 2004.

[124] C. Santos, R.C. Souza, J.K.M.F. Daguano, C. N. Elias and S. O. Rogero, “Development of ZrO_2-Al_2O_3 composite”, The 51st Brazilian Congress on Ceramics, 2007.

[125] Lidija Ćurković, Vera Rede, Krešimir Grilec, Alen Mulabdić, “Hardness and Fracture Toughness of Alumina Ceramics”. Conference on Materials, Processes, Friction and Wear, MATRIB’07 vela luka (2007).

[126] G. R. ANSTIS, P. CHANTIKUL, B. R. LAWN, and D. B. MARSHALL, “A Critical Evaluation of Indentation Techniques for Measuring Fracture Toughness: I, Direct Crack Measurements,” *J. Am. Ceram. Soc.*, vol. 64, no. 9, pp. 533-538, 1981, doi: 10.1111/j.1151-2916.1981.tb10320.x.

[127] B.R Lawn, A.G. Evans and D.B. Marshall, J. Am. Ceram. Soe., 63, 574-581 (1980).

[128] M. M. Hossen, M. A. Gafur, and A. K. M. A. Hakim, “Structural and Mechanical Properties of Zirconia Toughened Alumina (ZTA) Composites,” vol. 3, no. 2, pp. 2128-2134, 2014.

[129] E. Bresciani, T.J.E.E. Barata, T.C. Fagundes, A. Adachi, M.M. Terrin, M. F. L. Navarro, “Compressive and diametral tensile strength of glass ionomer cements”, J. Appl. Oral Sci. vol.12 no.4 Bauru Oct./Dec. 2004. http://dx.doi.org/10.1590/S1678-77572004000400017

[130] Della Bona A, Benetti P, Borba M, Cecchetti D, “Flexural and diametral tensile strength of composite resins”. Braz Oral Res 2008; 22(1):84-9

[131] P. G. Rao, M. Iwasa, T. Tanaka, I. Kondoh, and T. Inoue, “Preparation and mechanical properties of Al_2O_3-15wt.% ZrO_2 composites,” *Scr. Mater.*, vol. 48, no. 4, pp. 437- 441, 2003, doi: 10.1016/S1359-6462(02)00440-2.

[132] Brundle, C. R., Evans, C. A., and Wilson, S. (1992) Encyclopedia of Materials Characterization: surfaces, interfaces, thin films. Gulf Professional Publishing, London.

[133] E. Casero, L. Vázquez, A. Parra-Alfambra, and E. Lorenzo, "AFM, SECM and QCM as useful analytical tools in the characterization of enzyme-based bioanalytical platforms.," Analyst, vol. 135, no. 8, pp. 1878-1903, 2010

[134] Z.D.I. Sktani, A.Z.A. Azhar, M.M. Ratnam, Z.A. Ahmad, The influence of in-situ formation of hibonite on the properties of zirconia toughened alumina (ZTA) composites, Ceram. Int. 40 (2014) 6211-6217.

[135] S.G. Huang, K. Vanmeensel, O. Van Der Biest, J. Vleugels, Influence of CeO_2 Reduction on the Microstructure and Mechanical Properties of Pulsed Electric Current Sintered Y_2O_3-CeO_2 Co-Stabilized ZrO_2 Ceramics, J. Am. Ceram. Soc. 90 (2007) 1420-1426.

[136] R.D. Shannon, Revised effective ionic radii and systematic studies of interatomic distances in halides and chalcogenides, Acta Crystallogr. Sect. A. 32 (1976) 751-767.

[137] L.J. Yin, G.Z. Chen, C. Wang, X. Xu, L.Y. Hao, H.T. (Bert) Hintzen, Tunable Luminescence of $CeAl_{11}O_{18}$ Based Phosphors by Replacement of $(AlO)^+$ by $(SiN)^+$ and Co-Doping with Eu, ECS J. Solid State Sci. Technol. 3 (2014) R131-R138.

[138] L. Truffault, M.-T. Ta, T. Devers, K. Konstantinov, V. Harel, C. Simmonard, et al., Application of nanostructured Ca doped CeO_2 for ultraviolet filtration, Mater. Res. Bull. 45 (2010) 527-535.

[139] G. Magnani, A. Brillante, Effect of the composition and sintering process on mechanical properties and residual stresses in zirconia-alumina composites, J. Eur.Ceram.Soc.25(2005)3383-3392. doi: 10.1016/j.jeurceramsoc.2004.09.025.

[140] B. Basu, J. Vleugels, O. Vander Biest, Toughness tailoring of yttria-doped zirconia ceramics, Mater. Sci. Eng. A380 (2004) 215-221, http://dx.doi.org/ 10.1016/j.msea.2004.03.065.

[141] F. Cesari, L. Esposito, F. M. Furgiuele, C. Maletta, A. Tucci, Fracture toughness of alumina-zirconia composites, Ceram. Int. 32(2006) 249-255, http://dx.doi.org/10.1016/j.ceramint.2005.02.012.

[142] B.Basu, J.Vleugels, O.VanDerBiest, ZrO_2-Al_2O_3 composites with tailored toughness, J.Alloys Compd. 372 (2004) 278–284, http://dx.doi.org/ 10.1016/j.jallcom.2003.09.157.

[143] Piconi C., Maccauro, G., "ZrO_2 as a Ceramic Biomaterial" Biometrials, Volume 20, Issue 1, pp. 1-25,1999.

[144] Podzorova, L.I., Shvorneva, L.I., Il'icheva, A.A., et al., Microstructure and phase composition of ZrO_2-CeO_2-Al_2O_3 materials modified with MgO and Y_2O_3, Inorg. Mater., 2013, vol. 49, no. 4, pp. 376-381.

[145] C. Domínguez, J. Chevalier, R. Torrecillas, G. Fantozzi, Microstructure development in calcium hexa- aluminate, J. Eur. Ceram. Soc. 21 (2001) 381-387.

[146] A. Arab, Z.D.I Sktani, Q. Zhou, Z. A. Ahmad and P. Chen, 'Effect of MgO Addition on the Mechanical and Dynamic Properties of Zirconia Toughened Alumina (ZTA) Ceramics', Materials 2019, 12, 2440; doi:10.3390/ma12152440

[147] N. P. Bansal, S. R. Choi "Processing of Alumina-Toughened ZrO_2 Composite", NASA/TM -212451, 2003.

[148] M.L. Hu, M.H. Fang, S. Sen Chen, T. Yang, Z.H. Huang, Y.G. Liu, Effects of Calcium Hexa-aluminate Addition on the Mechanical Properties of Zirconia-Toughened-Alumina, Key Eng. Mater. 544 (2013) 286-290.

[149] D. Asmi, I. Low, Processing of an in-situ layered and graded alumina/calcium hexa-aluminate composite: Physical characteristics, J. Eur. Ceram. Soc. 2219 (1998).

[150] N.A. Rejab, A.Z.A. Azhar, K.S. Kian, M.M. Ratnam, Z.A. Ahmad, Effects of MgO addition on the phase, mechanical properties, and microstructure of zirconia-toughened alumina added with CeO2 (ZTA-CeO_2) ceramic composite, Materials Science and Engineering A595, (2014) 18-24.

[151] Della Bona A, Benetti P, Borba M, Cecchetti D, "Flexural and diametral tensile strength of composite resins". Braz Oral Res 2008; 22(1):84-9

[152] S. Abbas, S. Maleksaeedi, E. Kolos, A. Ruys, Processing and properties of zirconia-toughened alumina prepared by gel-casting, Materials 8 (2015) 4344-4362.

[153] A. Rittidech, R. Somrit, and T. Tunkasiri, "Effect of adding Y_2O_3 on structural and mechanical properties of Al_2O_3-ZrO_2 ceramics," Ceram. Int., vol. 39, no. SUPPL.1, pp. S433-S436, 2013.

[154] X. Song, Z. Lui, M. Kong and Y. Zeng. "Thermal stability of yttria-stabilized zirconia (YSZ) and YSZ-Al_2O_3 coatings," Ceram. Int., vol. 43, no. 16, pp. 14321-14325, 2017.

[155] D. F. Zambrano, A. Barrios and L. Tobon, "Thermal properties and phase stability of Yttria-Stabilized Zirconia (YSZ) coating deposited by Air Plasma Spray onto a Ni-base superalloy," Ceram. Int., vol. 44, no. 4, pp. 3625-3635, 2018.

[156] F. Sommer, R. Landfried, F. Kern, and R. Gadow, "Mechanical properties of zirconia toughened alumina with 10-24 vol.% 1.5 mol% Y-TZP reinforcement," J. Eur. Ceram. Soc., vol. 32, no. 15, pp. 3905-3910, 2012.

[157] T. Nagaoka, T. Tsugoshi, Y. Hotta, M. Yasuoka, K. Watari, Forming and sintering of porous calcium-hexa-aluminate ceramics with hydraulic alumina, J. Mater. Sci. 41 (2006) 7401-7405.

[158] N. Bhaskar, D. Sarkar, B. Basu, Probing cytocompatibility, hemocompatibility, and quantitative inflammatory response in Mus musculus toward oxide bio-ceramic wear particulates and a comparison with CoCr, ACS Biomater. Sci. Eng. 4 (2018) 3194-3210.

[159] D. Sarkar, S. Mandal, B. Reddy, N. Bhaskar, D. Sundaresh, B. Basu, ZrO_2-toughened Al_2O_3-based near-net shaped femoral head: unique fabrication approach, 3D Microstruct., Burst Strength Muscle Cell Response Mater. Sci. Eng.: Chimia 77 (2017) 1216-1227.

List of Recent Publications

In Peer-reviewed International Scientific Journals:

1. Md. Al-Amin; Saugata Sarker; Homayra Tabassum Mumu; Dipa Islam; Md. Zahangir Alam; M. A. Gafur. **'**The effect of sintering temperature and zirconia content on the mechanical and micro-structural properties of MgO, TiO_2 and CeO_2 doped alumina-zirconia (ZTA) ceramic'. J. Korean Ceramic Society, 2022.
2. Md. Abdul Gafur; Md. Al-Amin; Md. Saifur Rahman Sarker; Md. Zahangir Alam. Structural and mechanical properties of alumina-zirconia (ZTA) composites with unstabilized zirconia modulation, J. Materials sciences and applications, 12, 542-560, 2021.
3. Saugata Sarker; Homayra Tabassum Mumu; Md. Al-Amin; Md. Zahangir Alam; M. A. Gafur. Impacts of inclusion of additives on physical, microstructural, and mechanical properties of Alumina and Zirconia toughened alumina (ZTA) ceramic composite: A review, J. Materials Today proceedings, 62, 2892-2918, 2022.

In International Conference Presentation:

Md. Al-Amin; Md. Zahangir Alam; M. A. Gafur. 'XRD investigation of the Effect of CaO and CeO_2 Additives on ZTA-5TiO_2-5MgO Ceramic Composites.' ICSTB-2021, BCSIR, Dhaka-1205, Bangladesh.

Under Review in International Scientific Journal:

Md. Al-Amin; Saugata Sarker; Homayra Tabassum Mumu; Dipa Islam; Md. Zahangir Alam; M. A. Gafur. 'Effects of sintering temperature on the microstructural and mechanical properties of MgO and TiO_2 simultaneously doped zirconia toughened alumina ceramics [xYSZ-(90-x)Al_2O_3-5MgO-5TiO_2, where x=5 and 15]' (Under review, J. Materials Today Communication, 2021).